Aus dem

Zentrum für Neurologie der Universitätsklinik Tübingen

Neurologische Klinik und Hertie Institut

für klinische Hirnforschung

Abteilung Neurologie mit Schwerpunkt Epileptologie

Functional Characterization of novel *GABRB1* Gene Defects associated with Developmental and Epileptic Encephalopathies

Inaugural-Dissertation
zur Erlangung des Doktorgrades
der Medizin

der Medizinischen Fakultät
der Eberhard Karls Universität
zu Tübingen

vorgelegt von

Hanke, Moritz Sebastian

2025

Dekan: Professor Dr. B. Pichler

1. Berichterstatter: Professor Dr. H. Lerche
2. Berichterstatter: Professor Dr. O. Rieß

Tag der Disputation: 06.08.2025

Dedicated To:

The 6th of November, 2020.

Table of Contents

List of Figures

List of Tables

List of Abbreviations

ASM: Antiseizure Medication

bp: Base Pair

CAE: Childhood Absence Epilepsy

CBZ: Carbamazepine

CI: Confidence Interval

CLB: Clobazam

CNS: Central Nervous System

CZP: Clonazepam

DEE: Developmental and Epileptic Encephalopathy

DRC: Dose-Response Curve

DS: Dravet Syndrome

DZP: Diazepam

EE: Epileptic Encephalopathy

EEG: Electroencephalogram

eGFP: Enhanced Green Fluorescent Protein

EGTS: Epilepsy with Generalized Tonic-Clonic Seizures

EIEE: Early Infantile Epileptic Encephalopathy

EME: Early Myoclonic Encephalopathy

EOEE: Early Onset Epileptic Encephalopathy

FS: Febrile Seizures

GABA: Gamma-Aminobutyric Acid

$GABA_AR$: Gamma-Aminobutyric Acid Type A Receptor

GEFS+: Genetic Epilepsy with Febrile Seizures Plus

GGE: Generalized Genetic Epilepsy

GoF: Gain of Function

HEK: Human Embryonic Kidney

IED: Interictal Epileptic Discharge

IGE: Idiopathic Generalized Epilepsy

IPSP: Inhibitory Postsynaptic Potential

IS: Infantile Spasms

JAE: Juvenile Absence Epilepsy

JME: Juvenile Myoclonic Epilepsy

LEV: Levetiracetam

LGS: Lennox-Gastaut Syndrome

LoF: Loss of Function

M1-4: Transmembrane Segment 1-4

MAF: Minor Allele Frequency

MRI: Magnetic Resonance Imaging

N/A: Not Applicable

NAFE: Non-Acquired Focal Epilepsy

ns: Non-significant

ORF: Original Reading Frame

PB: Phenobarbital

PCR: Polymerase Chain Reaction

PHT: Phenytoin

SNP: Single Nucleotide Polymorphism

TEVC: Two-Electrode Voltage Clamp

TPM: Topiramate

VGB: Vigabatrin

VPA: Valproate

VUS: Variant of Uncertain Significance

WT: Wild-Type

X. laevis: *Xenopus laevis*

1 Introduction

1.1 Epilepsy

1.1.1 Definition, Epidemiology, and Classification

Epilepsy is a neurological disease characterized by pathologically increased neuronal excitability of a particular brain region or the whole brain that causes epileptic seizures. Affected individuals present with a heterogeneous clinical appearance, for instance, displaying motor, sensory, or vegetative seizures with or without loss of awareness. Seizures are caused by sudden, abnormal, synchronous, high-frequency electrical discharge of groups of cortical neurons that may either affect a limited focal brain region or spread to adjacent regions or even to the whole brain. The function of the affected brain region determines the symptoms that people with epilepsy experience. For instance, a seizure originating from the motor cortex will primarily result in motor symptoms. One can distinguish between focal-, unknown- and generalized onset seizure types, where focal seizures originate within networks of one hemisphere and generalized seizures originate from a point between rapidly communicating bilateral networks. It is also possible for focal seizures to originate from subcortical structures.

Seizures can be divided into unprovoked and provoked seizures. Provocation factors cause a transient reduction of the seizure threshold. Some examples of provocation factors include alcohol-withdrawal, concussion, or fever. The definition of an epilepsy diagnosis (Fisher et al. 2014) is met when either:

a) At least two unprovoked seizures occur >24 hours apart.
b) An unprovoked seizure with a probability of further seizures exceeding 60% occurs.
c) An epilepsy syndrome is diagnosed.

Based on the clinical presentation in combination with electroencephalogram (EEG) findings, it is possible to distinguish between focal, generalized, combined generalized & focal, and unknown epilepsy types (Scheffer et al. 2017).

An epilepsy syndrome is determined through a particular phenotype and a pattern of features occurring together. These features include seizure types and triggers,

EEG findings, imaging features, diurnal features, etiology, prognosis comorbidities, as well as age at seizure onset and remission (Scheffer et al. 2017). For instance, a typical epilepsy syndrome is Childhood Absence Epilepsy (CAE), which typically manifests with brief, daily absence seizures with 3Hz spike-and-wave EEG discharges, normal imaging, an onset between 3-8 years, and often remittance by adolescence (Crunelli and Leresche 2002).

The median prevalence of active epilepsy in high-income countries is currently 0.55%, whereas the life-time prevalence of a person experiencing a one-time provoked or unprovoked epileptic seizure is up to 5% (Beghi 2020).

The etiology of epilepsy is currently classified into structural, infectious, genetic, immune, metabolic, or unknown. An epilepsy diagnosis can include more than one etiology. For example, tuberous sclerosis comprises both a structural and a genetic etiology (Scheffer et al. 2017).

1.1.2 Genetic Epilepsies

Genetic epilepsies are defined as epilepsies in which one or more presumed or known genetic germline alterations directly cause the disorder. This results in a heterogeneous clinical spectrum from mild or self-limiting to severe or even lethal forms (Scheffer et al. 2017).

Within generalized epilepsy syndromes, the four most common and well-established syndromes CAE, Juvenile Absence Epilepsy (JAE), Juvenile Myoclonic Epilepsy (JME), and Epilepsy with Generalized Tonic-Clonic Seizures (EGTC) are subsumed under the term Genetic Generalized Epilepsies (GGE), which can also still be referred to as Idiopathic Generalized Epilepsies (IGE) (Scheffer et al. 2017). Affected individuals exhibit a comparatively mild phenotype with no severe developmental impairment. Another syndrome is the autosomal dominantly inherited Genetic Epilepsy with Febrile Seizures Plus (GEFS+), presenting with a range of mostly mild phenotypes ranging from simple febrile seizures to rare severe syndromes with developmental problems.

Epileptic syndromes where the seizures cause severe cognitive and behavioral impairments are referred to as epileptic encephalopathies (EE). They often have

a genetic etiology, mainly, but not exclusively, beginning in infancy or childhood. The epileptiform activity then interferes with brain development, resulting in slowing, plateauing, or regression. Treating epileptic activity is crucial to reducing the severity of the consequences of the developmental syndrome. However, various epilepsy syndromes display developmental delay even prior to epileptiform activity, suggesting crucial neurodevelopmental mechanisms that explain the clinical presentation independently from the epileptiform activity. These severe epilepsy syndromes with developmental delay are called developmental and epileptic encephalopathies (DEE). Many severe epilepsy syndromes like Dravet Syndrome (DS), Lennox-Gastaut Syndrome (LGS), or Infantile Spasms (IS, formerly known as West Syndrome) are examples of common and well-defined DEE subtypes (Guerrini et al. 2023; Scheffer et al. 2017).

One can infer a genetic etiology either from the family history of autosomal dominant disorders, clinical research on cohorts suffering from the same syndrome, e.g., through twin- or familial aggregation studies, or by finding a causative genetic variant with a proven epileptic pathomechanism. The research to date suggests a mixed picture with monogenic and polygenic inheritance patterns. For instance, 70-80% of DS cases are caused by monogenic variants in the *SCNA1* gene, encoding the $Na_V1.1$ sodium channel (Marini et al. 2011). Monogenic epilepsies account for up to 40% of known severe genetic epilepsies, suggesting the majority to be polygenic disorders (Guerrini et al. 2021). This complex inheritance pattern is underpinned by monozygotic twins reaching high rates of epilepsy concordance (across all syndromes) of 62%, compared to 18% for dizygotic twins (Berkovic et al. 1998). However, different variants or even the same variant within a single gene can also cause a broad clinical spectrum, a phenomenon called pleiotropy. For example, a pathogenic variant in *SCN1A* can be associated with mild and severe cases of GEFS+ within the same family (Mullen and Scheffer 2009).

Genetic epilepsies follow different inheritance patterns, for instance, recessive, dominant, or polygenic, notably with a significant amount of genetic epilepsies arising from *de novo* variants. For instance, in infants with severe DEEs, the vast

majority of found variants occur *de novo*, with the causal variant being determined in 30-50% of cases (McTague et al. 2016). The sustained scientific effort within the field of genetic epilepsies (DEEs, GGEs, and non-acquired focal epilepsy (NAFE)) has led to an increasingly large number of identified genes and variants, showing that missense ultra-rare variants were enriched in neuron-specific and developmental genes compared to genes not expressed in the brain (Koko et al. 2021).

1.2 Monogenetic Epilepsies

Monogenetic epilepsies are often caused by variants in genes encoding voltage- or ligand-gated ion channels (Guerrini et al. 2021). The latter are activated by specific neurotransmitters (the ligands). These variants typically cause alterations in the neuron's conductive properties, leading to network hyperexcitability. There are also known epilepsy-associated genetic defects unrelated to ion channels, e.g., metabolic malfunctions related to the glucose transporter GLUT-1, which is expressed in endothelium and glial cells and responsible for the glucose transport across the blood-brain barrier (De Vivo et al. 1991). Other proteins that have prominently been identified as causally related to epilepsy include a wide range from potassium channels to transmembrane binding receptors and transcriptional modifiers, e.g., encoded by the *KCNQ2, KCNA2, STXBP1* or *CHD2* genes (Saitsu et al. 2008; Singh et al. 1998; Suls et al. 2013; Syrbe et al. 2015). A precise functional characterization of the epileptogenic pathomechanism is important, as it may enable a personalized therapy, for instance, by blocking an overactive ion channel or pursuing a specific diet circumventing a metabolic defect (Catterall 2018; Hedrich et al. 2021; Meira et al. 2019).

Various epilepsy-associated variants affecting the γ-aminobutyric acid receptor A ($GABA_AR$) have been described (see 1.4 Epilepsy-related $GABA_A$ Receptor Variants) (Maljevic et al. 2019b) Apart from epilepsy, defects in $GABA_AR$ have been linked to several other pathologies, like anxiety disorders, insomnia, schizophrenia, and alcoholism (Anstee et al. 2013; Möhler 2006).

1.3 $GABA_A$ Receptors

$GABA_A$ receptors are ligand-gated ionotropic channels belonging to the superfamily of Cys-loop-ligand-gated-ion channels. They open upon the binding of γ-aminobutyric acid (GABA) (Sieghart 1995). GABA functions as the primary inhibitory neurotransmitter of the mammalian central nervous system (CNS), and $GABA_ARs$ display nearly ubiquitous cerebral and spinal expression (Luscher et al. 2011). A conformational change upon GABA binding opens an anion transmembrane pore, mainly selective to chloride ions under physiological conditions, and drives the cell's membrane potential to the Cl^- -reversal potential of, for instance, around -70 mV in neurons (Mueller et al. 1983; Sigel and Steinmann 2012). However, the important role of excitatory $GABA_ARs$ ('GABA Switch') in brain development has also been pronounced (Ben-Ari 2002). $GABA_ARs$ are primarily located at synapses, usually resulting in fast (phasic) or slow (tonic) inhibitory currents (Sallard et al. 2021). Regarding epilepsy, it seems pathomechanistically plausible that $GABA_AR$ impairment leads to disinhibition, resulting in an overexcitability of neuronal networks.

There are eight different $GABA_AR$ subunit subtypes (α, β, γ, δ, ε, θ, π, and ρ) encoded by 19 different genes (*GABRA1-6*, *GABRB1-3*, *GABRG1-3*, *GABRD*, *GABRE*, *GABRQ*, *GABRP* und *GABRR1-3*). Each $GABA_AR$ subunit is composed of four transmembrane domains, referred to as M1-4, with an outward-facing N-terminus and an outward-facing C-terminus (Figure 1A). The former mediates GABA binding and the assembly of the multimeric, functional $GABA_AR$ (Miller and Aricescu 2014). Functional $GABA_ARs$ are usually heteropentamers, i.e., composed of a total of five subunits, with the M2 segment aligning the anion pore (Figure 1 B) (Olsen and Sieghart 2008). The most common $GABA_ARs$ are composed of two α, two β, and one γ or δ subunits, with an α1β2γ2 composition being the predominant isoform in the adult brain (Nemecz et al. 2016). Viewed from the synaptic cleft, the subunits are arranged β2-α1-β2-α1-γ2 in a counter-clockwise orientation. The two N-terminal ends of the two β2-α1 interfaces mediate GABA binding (Zhu et al. 2018). The molecular structure is exemplified in Figure 1 C and D. Homopentameric assemblies have also been described.

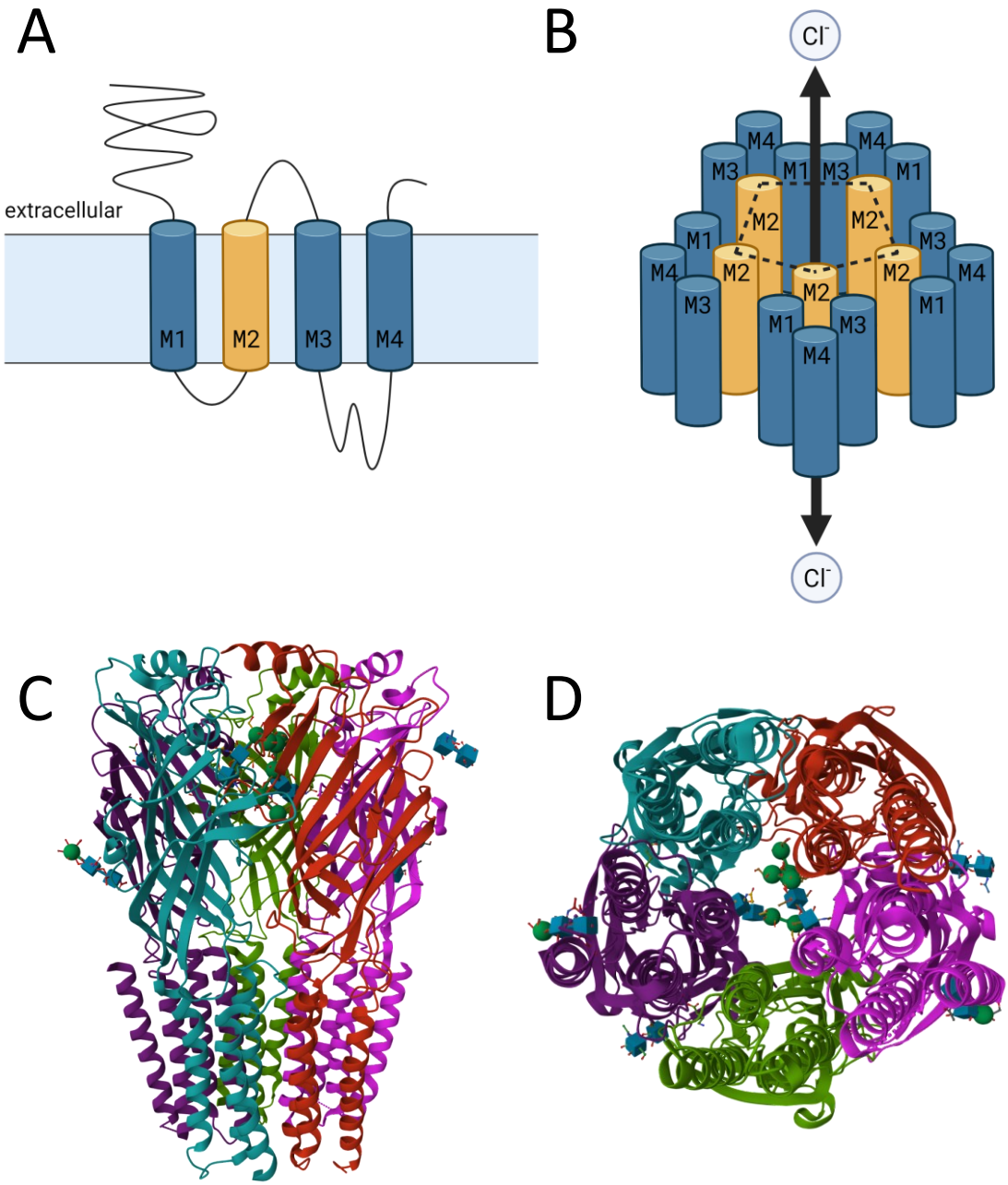

Figure 1. Schematic and molecular structure of GABA$_A$ receptor subunits and their heteropentameric assembly. **A.** Schematic representation of a GABA$_A$R subunit with four transmembrane segments (M1-4) and the extracellular long N- and short C-terminus. The N-terminus mediates GABA binding and subunit assembly. The M2 segment is marked in yellow to highlight its pore-aligning role in all subunit types. **B.** Schematic representation of heteropentameric GABA$_A$R assembly from five subunits. It is most common for a GABA$_A$R to contain two α, two β, and one γ or δ subunit. The M2 segments (highlighted in yellow) of the five subunits align the pore (marked as a dashed pentagon). This allows for anions, typically Cl^-, to flow in both directions upon GABA binding. Physiological membrane potentials typically cause a

Cl^- influx. Figures A. and B. were created with BioRender.com. **C. & D.**Cryo-electron microscope structure of a β1-α1-β1-α1-γ2 $GABA_AR$ in complex with GABA. The two β1 subunits are depicted in turquoise/green, the two α1 subunits in purple/pink, and the γ2 subunit in red. The figure was extracted from the RCSB Protein Data Bank, PDB ID: 6DW0 (Berman et al. 2000; Phulera et al. 2018). **C.** Side-view from outside. The four transmembrane alpha-helices (bottom) are located in the cell membrane. The extracellular segment (top) mediates GABA binding. **D.** View from the synaptic cleft. The β1-α1-β1-α1-γ2 counter-clockwise orientationis clearly visible. The channel pore flanked by the M2 transmembrane segment of each subunit appears closed due to glycosylation.

The heterogeneity in $GABA_AR$ compositions results from the immense number of theoretical (but much lower number of physiologically expressed) combination possibilities of subunits, which, in turn, result in diverging channel kinetics, expression patterns, and pharmacological interactions. Drawing from studies of human brain $GABA_AR$ subunit transcriptome analyses, one can conclude that 95% of expressed subunits are made up of α, β, γ, or δ, with the respective order of α1> α2 > α5 > α6 > α3 ≈ α4, β2 > β3 > β1 and γ2> γ1 being most expressed (Sequeira et al. 2019).

Some functional cassettes of all $GABA_AR$ subunits remain highly conserved concerning amino acid position and composition across different species and subunits. M1-4, as well as specific N-terminal segments, are particularly conserved. Conservation implies high functional importance of the given regions, as variants are likely highly detrimental to the receptor function, resulting in a strong selection pressure against variants (also see section 3.2). Conserved regions can be determined by examining sequence alignments from different channel subunits and different species. Some regions are highly conserved among all subunits; others are conserved among smaller groups of subunits with some variation among subgroups. For instance, $GABA_AR$ α and γ subunits share considerable sequence similarity, whereas β and δ subunits are phylogenetically closer (Sigel and Steinmann 2012). Mutation burden analysis, i.e., examining the frequency and nature of specific changes, e.g., missense mutations, between affected individuals and controls or in the general population, helps to delineate sub-regions critical for normal channel function that are enriched for pathogenic variants (Maljevic et al. 2019b).

A particular subclass of ionotropic GABA receptors is the $GABA_A$-ρ receptor, previously known as the $GABA_C$ receptor. It is composed exclusively of ρ-subunits, physiologically found in the retina of vertebrate species and insensitive to allosteric modulators like benzodiazepines. When referring to the $GABA_AR$ in this thesis, the canonical version described above is implied. The other main class of GABA receptors are the G-protein-coupled $GABA_B$ receptors. Whereas the ionotropic $GABA_ARs$ are primarily responsible for fast inhibitory neurotransmission, metabotropic $GABA_B$ receptors mediate slow inhibition.

1.4 Epilepsy-related $GABA_A$ Receptor Variants

1.4.1 GABRAx, GABRGx, and GABRD Variants

Recently, increased interest has evolved in monogenic or presumed polygenic $GABA_AR$ variants related to epilepsies (Maljevic et al. 2019b; May et al. 2018; Mefford 2018). Recent studies stressed the enrichment of ultra-rare $GABA_AR$ missense and deleterious variants, particularly in DEEs, but also GGEs and NAFEs (Epi25 2019; Koko et al. 2021). The first $GABA_AR$ variants related to epilepsy were found in 2001 in *GABRG2* in large families of individuals with mild phenotypes: GEFS+, CAE, and febrile seizures (FS) (Baulac et al. 2001; Wallace et al. 2001). Shortly afterward, a *GABRA1* variant was found in individuals from a large family with autosomal dominant JME (Cossette et al. 2002). Consecutively, numerous variants have been identified in *GABRG2* and *GABRA1* that are linked to severe DEEs, suggesting a high variance in clinical manifestation. Other variants discovered in *GABRA2*, *GABRA3*, *GABRA5,* and *GABRA6* were associated partly with DEEs and partly with milder epilepsy forms like CAE (Hernandez and Macdonald 2019). Notably, individuals carrying X-chromosome-linked *GABRA3* variants, besides showing a clinical presentation ranging from DEEs to GGEs, also displayed dysmorphic features like micrognathia, cleft palate, and short stature (Niturad 2016; Niturad et al. 2017; Scheuber 2023). Subsequently, also *GABRD* and *GABRG1* variants were linked to epilepsy (Dibbens 2004; Williams et al. 2022).

1.4.2 GABRB Variants

The first β-subunit variant linked to epilepsy was described in *GABRB3* in 2008 in individuals with CAE (Tanaka et al. 2008). Consecutively, various other variants in *GABRB2* and *GABRB3* have been linked to a broad clinical spectrum ranging from GGEs to DEEs. Only a handful of *GABRB1* variants linked to epilepsy have been described to date.

The human *GABRB1* gene is located on the short arm of chromosome four close to the centromere (Dean et al. 1991). The first reported epilepsy-related variant was the *de novo* F246S variant (NM_000812.4:c.737T>C:p.Phe246Ser) located in the M1 region, which was found in a male carrier with IS that represents the only *GABRB1* variant functionally characterized hitherto. The electrophysiological results showed complex alterations in channel kinetics (see section 4.4.1) (Allen et al. 2013; Janve et al. 2016). Later, a second *de novo* T287I (c.860C>T:p.Thr287Ile) variant in the M2 region was identified in a treatment-resistant male Norwegian individual with early onset epileptic encephalopathy (EOEE) with a severe developmental delay (Lien et al. 2016). Two other variants have since been described. One is a K339N (c.1017G>C:p.Lys339Asn) variant linked to severe DEE with an unclear inheritance pattern (Fernández-Marmiesse et al. 2019). The other is a paternally inherited V349I (c.1075G>A:p.Val359Ile) variant found in JME and represents the first *GABRB1* variant linked to IGE (Z.-J. Lin et al. 2023). All variants are thoroughly discussed in section 4.4.

Due to the high conservation rate across critical functional regions of subunits, it is possible to compare variants in certain subunits to their corresponding position in other subunits. For instance, the threonine at 287 in *GABRB1* corresponds to the threonine at 287 in *GABRB3*. Interestingly, the same T287I variant described by Lien et al. in 2016 in *GABRB1* was also described in an affected *GABRB3* individual with early infantile epileptic encephalopathy (EIEE) in 2016 (Papandreou et al. 2016).

1.4.3 Methods for Functional Characterization

The broad clinical spectrum found in individuals with $GABA_AR$ subunit variants called for a more thorough analysis of underlying pathomechanisms and their

influence on receptor function. A variety of electrophysiological cellular expression systems, as well as mouse models, have been utilized as experimental systems. Cellular expression systems include heterologous models like human embryonic kidney (HEK) cells or *Xenopus laevis* (subsequently called *X. laevis*) oocytes and homologous models like murine hippocampal neurons. Patch clamp studies in mammalian cell lines and two-micro-electrode voltage clamp (TEVC) in oocytes allow for a characterization of the functional deficits and their consequences on receptor function.

For patch-clamp studies, gating parameters recorded in response to GABA application include the time and current change for the activation, desensitization, and deactivation phase. Activation describes the time and current change from the begin of GABA application until the peak current amplitude is reached. Desensitization describes the time and current decay in the presence of GABA, and deactivation refers to the time and current decay after GABA has been removed until the current reaches the resting level again before the GABA stimulus was originally applied (Figure 2 A). These parameters are usually determined upon subsequent application of GABA in different concentrations to determine the GABA sensitivity (also referred to as potency, Figure 2 B). For TEVC recordings, analyzed parameters are mostly limited to a concentration-dependent analysis of peak current amplitudes since the application of GABA to the whole oocyte is relatively slow and can be highly variable.

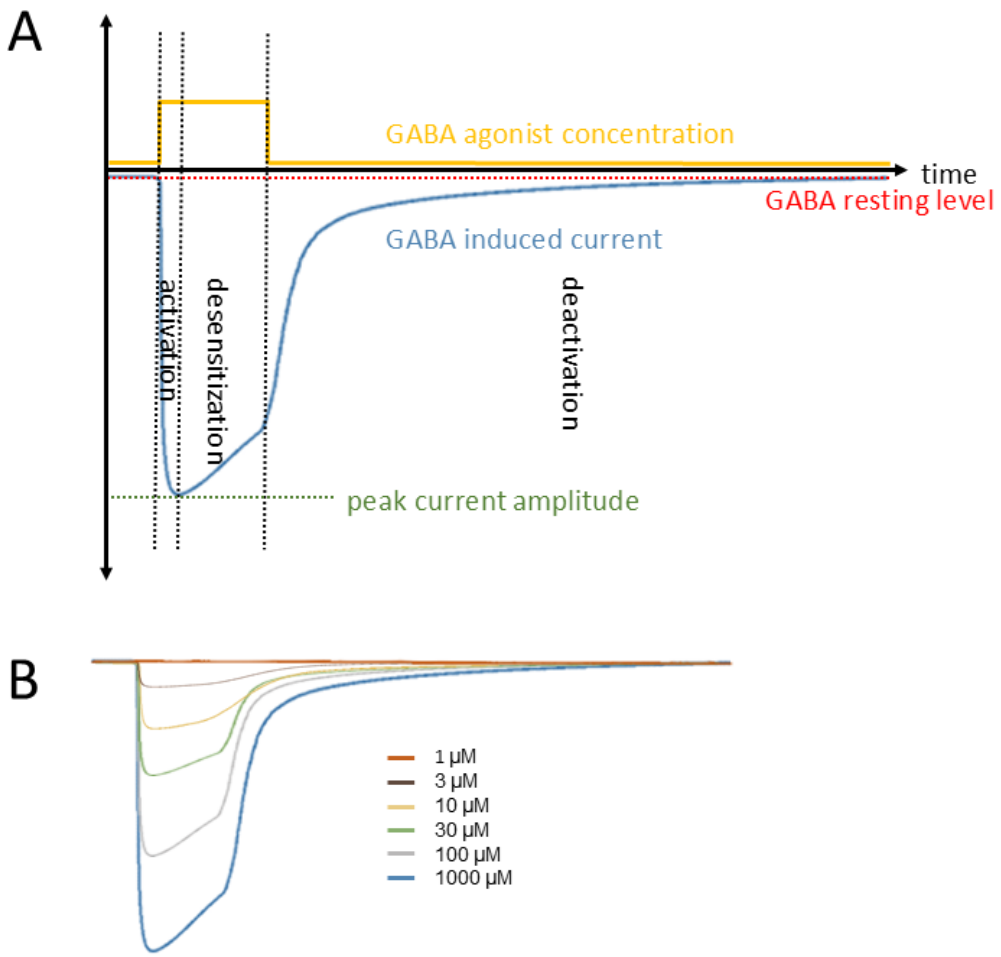

Figure 2. Schematic representation of electrophysiological parameters in GABA-induced currents. **A.** The blue line exemplifies a typical GABA current response upon GABA application, which causes a change in GABA concentration (yellow line). The vertical lines divide the current response into the activation, desensitization, and deactivation phases. These respectively describe the time and current change; for activation from begin of GABA application to peak current amplitude (green line); for desensitization from peak current amplitude to the end of GABA application; and for deactivation from the end of GABA application to return to GABA resting level (red line). **B.** Comparing peak current amplitudes for subsequent application of GABA in different concentrations (for instance, from 1 µM to 1000 µM, exemplified by current traces in different colors) allows for determining GABA sensitivity (and, more generally, other concentration-dependent parameters).

Another important parameter to be investigated is the surface expression of mutated receptors compared to wild-type (WT) receptors, which might be altered through protein trafficking to the cell membrane. One method to investigate this as another cause for $GABA_AR$ impairment are immunostainings.

The most prominent mechanism for functional deficits identified in mutated $GABA_AR$s has been the loss of receptor function (LoF) (Maljevic et al. 2019b; Oyrer et al. 2018). This implies reduced or abolished receptor functionality that can result from various cellular mechanisms. Misfolded proteins can disrupt the receptor's structure, which can diminish GABA binding efficacy, hinder channel opening, or affect the receptor's conformational stability, potentially resulting in insufficient current response upon GABA binding, reduced activation, faster desensitization, and deactivation or lower GABA sensitivity. Additionally, variants might interfere with receptor turnover and degradation processes, alter interaction with intracellular modulatory proteins, or impair receptor trafficking to the cell membrane, reducing the number of functional receptors. Recently and so far less commonly, it has been described that a gain of receptor function (GoF) can also be linked to severe early-onset DEE. These variants augment and increase receptor function by mechanisms opposite to those laid out for LoF. For instance, tonically open $GABA_AR$s in the absence of GABA have been linked to genetic epilepsies (Butler et al. 2018). Also, *GABRD* GoF variants in individuals with DEE increase GABA sensitivity, but due to the receptors' extrasynaptic location and role in tonic inhibition, this is still mechanistically plausible (Ahring et al. 2022a). While LoF variants can lead to a decrease in inhibitory GABA-mediated signaling, potentially tipping the balance towards neuronal network hyperexcitability causing epileptic seizures (Baulac et al. 2001; Wei et al. 2017), epileptogenic mechanisms of GoF variants are less clear yet, as discussed later in section 4.6.

1.4.4 Treatment Options

No standardized therapy exists for individuals with $GABA_AR$ variants, and most conditions are refractory. Due to studies of *GABRA1* and *GABRG2* variants in mouse models, treatment options based on the functional alterations have been suggested in the form of antiseizure medications (ASM), like vigabatrin (VGB), valproate (VPA), ethosuximide or benzodiazepines (Oyrer et al. 2018). VGB and VPA have been shown to control seizures in individuals with *GABRA1* variants (Kodera et al. 2016). Due to the role of GABAergic transmission during brain development, the studies stress the importance of treating individuals very early.

No therapy suggestions based on molecular findings have been proposed for variants linked to the β-subunit, and treatment of $GABA_AR$-linked epilepsies generally remains challenging, requiring physicians to rely on empirical treatments.

Understanding the exact molecular and electrophysiological pathogenic mechanisms regarding LoF or GoF is crucial to developing personalized therapies, as, due to the nature of receptor function, a targeted therapy might also be at risk of aggravating a preexisting condition, e.g., if GABAergic drugs are used in individuals carrying GoF variants (Absalom et al. 2020).

1.5 Novel *GABRB1* Variants

Upon the inception of this study, only one pathogenic *GABRB1* variant (F246S) was functionally characterized, whereas the functional consequences of a second variant (T287I) were not studied (see section 1.4.2). In the context of an international collaboration, our research group at the Hertie Institute for Clinical Brain Research (Tübingen, Germany) collected information on four individuals with novel missense variants in *GABRB1*. This includes one individual with c.740T>C:p.Ile247Thr, one with c.841A>T:p.Thr281Ser and two with c.854C>A:p.Thr285Lys variants (henceforth referred to as I247T, T281S, and T285K; the coding positions are given with respect to the canonical RefSeq transcript of *GABRB1,* NM_ 000812.3). All variants occurred *de novo*. Seizure onset was between the age of two and four months for all individuals, who all displayed a severe developmental delay. Thus, all individuals can be classified as suffering from a severe genetic DEE. More information is provided in section 3.1, and the key aspects are summarized in Table 1.

Table 1. Overview of novel GABRB1 variants and the associated clinical epileptic phenotypes. Details are found in section 3.1.

Variants	Sex	Age at seizure onset	Seizure phenotypes	Neurological development
c.740T>C: p.Ile247Thr	Female	4 months	tonic, focal clonic, multifocal epileptic activity / migrating ictal activity	Severe delay
c.841A>T: p.Thr281Ser	Male	2 months	spasms, tonic - multifocal epileptic activity	Severe delay
c.854C>A: p.Thr285Lys	Female	2 months	focal tonic, focal clonic, spasms, multifocal epileptic activity	Severe delay
c.854C>A: p.Thr285Lys	N/A	2 months	focal clonic, myoclonic, spasms, multifocal epileptic activity	Severe delay

The I247 variant is located in the M1 domain, while the T281S and T285K variants are located in the M2 domain. The sequence of amino acids between position 281 and 288 of *GABRB1* is known to be highly conserved among different species and $GABA_AR$ subunits (also see section 3.2). This extremely high grade of conservation suggests a vital role of this motif in ensuring proper functionality of the $GABA_AR$ and suggests that variants in this region are likely detrimental. This is also underlined by the low variety within this domain in healthy control populations (Maljevic et al. 2019b). Notably, the T287I variant introduced previously is also found in this domain. A schematic overview is provided in Figure 3. The color coding for the variants from this figure is used throughout the thesis.

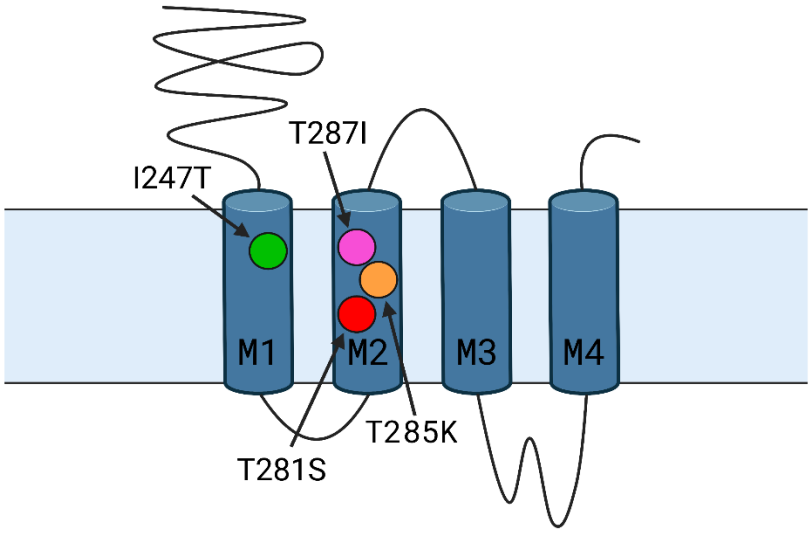

Figure 3. Schematic representation of the $GABA_A$ receptor β1 subunit and variant positions. The Ile247Thr variant is located at the beginning of the first transmembrane domain (M1), while Thr281Ser, Thr285Lys, and Thr287Ile variants are clustered around the center of the second transmembrane domain (M2). The color coding for the variants is used throughout the thesis. The figure was created with BioRender.com.

1.6 Research Hypothesis and Aims

This thesis aimed to functionally study *GABRB1* as a gene associated with genetic epilepsies. While functional data have been proposed in the context of the F246S variant, the phenotype (IS) deviated from the four novel individuals, and the functional alterations showed a mix of GoF and LoF features with complex changes in channel kinetics (Janve et al. 2016). Moreover, no functional analysis has been provided for the published T287I variant, which displayed a DEE phenotype largely similar to the one found in the newly identified individuals (Lien et al. 2016), nor any other epilepsy-associated *GABRB1* variant.

By providing the electrophysiological data causally linking the I247T, T281S, T285K, and T287I variants to their phenotypes and outlining the disease mechanism on a functional level, this thesis aimed to assess their molecular pathogenicity. Furthermore, it was of interest to examine whether genotype-phenotype correlations between the variants' functional results and their clinical presentations could be delineated. This includes features within the four DEE

variants, as well as a comparison to the IS variant and other reported *GABRB1* variants. It was also of interest to understand whether diverging electrophysiological mechanisms linked to DEEs, i.e., LoF versus GoF, could be found. Lastly, this thesis aimed to compare the electrophysiological findings to corresponding variants in other $GABA_AR$ subunits.

Ultimately, the research hypothesis to be rejected for each variant is that the electrophysiological data do not suggest a plausible functional mechanism linking the suggested genetic variant to the observable phenotype.

To test this hypothesis, two sets of analyses were planned:

a) *In silico* analysis of genetic conservation, constraint, and recurrence in $GABA_AR$ paralogs to predict the functional outcomes of these variants.
b) TEVC analysis of the WT $GABA_AR$ and $GABA_AR$ channels carrying the I247T, T281S, T285K, and T287I variants expressed in *X. laevis* oocytes to compare the current amplitudes in response to different concentrations of GABA.

Initially, patch-clamp analysis was also planned in HEK 293 cells and murine neurons to investigate the effects of the given variants on channel kinetics under representative physiological circumstances. While the required vectors were successfully constructed, recordings were ultimately not conducted due to time constraints.

It should be noted that a manuscript featuring various key methods, results, and discussion aspects of this study was submitted to *Brain* on the 19th of December 2024 in collaboration with C. Millevert and A. Kan (shared first co-authorship).

2 Materials and Methods

2.1 Clinical Phenotypes

Several collaborators (named in parentheses) provided the clinical data for the individuals carrying the investigated variants. This included physicians examining and treating the patients at, for I247T, the Child Neurology and Psychiatric Unit, G. Salesi Pediatric Hospital; United Hospitals of Ancona; Ancona, Italy (C. Marini), for T281S, the University Hospital Center Zagreb and University of Zagreb School of Medicine, Dept. of Paediatrics, Zagreb, Croatia (N. Barišić), the University Hospital of Antwerp, Dept. of Neurology, and the VIB Center for Molecular Neurology, Applied & Translational Neurogenomics Group, VIB, Antwerp, Belgium (S. Weckhuysen), for T285K, first individual, the Pediatric Neurology Unit, Dept. Woman-Mother-Child, Lausanne University Hospital and University of Lausanne, Lausanne, Switzerland (S. Lebon), and for T285K, second individual, the Dept. of Paediatrics, Helios Klinikum, Berlin, Germany (E.-M. Niehoff).

The clinical information on the individual with the T287I variant was taken from the respective publication (Lien et al. 2016). Though unpublished at the time of starting this work, more information on the I247T individual was published in 2019 in a paper on migrating focal seizures (Burgess et al. 2019). One T285K individual was mentioned in a paper on exome sequencing (Jauss et al. 2022). The other two cases (T281S and T285K – second individual) have not yet been published. The clinical data was collated by collaborators at the VIB Center for Molecular Neurology, Applied & Translational Neurogenomics Group, VIB, Antwerp, Belgium (S. Weckhuysen, personal communication), and the Child Neurology and Psychiatric Unit, G. Salesi Pediatric Hospital; United Hospitals of Ancona; Ancona, Italy (C. Marini, personal communication).

2.2 *In silico* Variant Evaluation

To assess their potential pathogenicity, the allele frequencies of the respective variants in several population databases, namely, gnomAD Release 2.1 (Karczewski et al. 2020), TOPMed Release Freeze 8 (Taliun et al. 2021), and DiscovEHR Release Freeze 50 (Dewey et al. 2016) were examined.

An *in silico* evaluation for potential pathogenicity using several conservation, deleteriousness, and constraint metrics (CADD (Rentzsch et al. 2019), GERP++ RS (Davydov et al. 2010), Para-Z-Score (Lal et al. 2020), PPh2 (Adzhubei et al. 2010), REVEL (Ioannidis et al. 2016), MPC (Samocha et al. 2017) and MTR (Traynelis et al. 2017)) was also performed.

Ortholog conservation among different species and paralog conservation among $GABA_AR$ subunits (*GABRA1-6*, *GABRB1-3*, *GABRG1-3*, *GABRD*) using Ensembl and the associated archives (Cunningham et al. 2022) and UniProt (The UniProt Consortium 2019) were additionally evaluated. Alignments were visualized using CLC Sequence Viewer 8.0 (QIAGEN Bioinformatics, Venlo, Netherlands).

To predict the potential function outcomes, the location of these variants in *GABRB1* protein structure in UniProt (The UniProt Consortium 2019) and the Protein Data Bank (Berman et al. 2000) and their location in the $GABA_AR$ channel structure were examined. Structure visualization was done using ChimeraX (Pettersen et al. 2021) based on published α1β1γ2 channel structure (Phulera et al. 2018). Consecutively, the occurrence of pathogenic variants in similar locations in other paralog $GABA_AR$ subunits and their reported functional outcomes using the same tools as above, as well as the Mastermind Genomic Search Engine and ClinVar (Chunn et al. 2020; Landrum et al. 2018) were evaluated.

The variants were classified using the American College of Medical Genetics and Genomics (ACMG) classification for variant pathogenicity (Richards et al. 2015), and the classification was re-visited following electrophysiological characterization of the variants.

2.3 Molecular Biology

As introduced in section 1.6, this study planned to express WT and mutant $GABA_ARs$ in *X. laevis* oocytes, HEK293 cells, and murine neurons. While the required vectors were successfully constructed, experiments in HEK293 cells and murine neurons were ultimately not carried out. Expression in HEK293 cells requires the preparation of suitable plasmids (carrying a CMV promotor) with appropriate tags. Also, to transcribe the respective RNA for the

electrophysiological recordings of the variants in oocytes, cloning a *GABRB1* cDNA construct in a suitable plasmid vector was required. Ultimately, the target variants in the WT channel in all these vectors needed to be introduced. These constructs were not available in-house or from collaborators.

The *GABRB1* cDNA (based on NM_000812) was bought from OriGene Technologies, Inc. (Rockville, USA). It was provided as ORF Clone in OriGene's pCMV6-Entry vector with a Myc-DDK-tag (CAT#: RC205166).

Brief testing of RNA *in vitro* transcription and expression in *X. laevis* oocytes as α1β1γ2 did not result in measurable GABA-induced currents. It was decided to prepare new expression vectors optimized for expression in *X. laevis* oocytes and eukaryotic cells as follows:

a) *In vitro* transcript plasmid (T7 promotor-based) containing β1 subunit cDNA only with *X. laevis* globin 3'UTR cassette, where RNA preparations are pre-mixed with α1 or α5 and γ2 before injection (established standard in-house approach).
b) *In vitro* transcript plasmid (T7 promotor-based) containing concatenated pentameric α1β1γ2 cDNA as described by collaborators (Liao et al. 2019) to ensure structural conformity during subunit assembly and receptor formation in oocytes.
c) Eukaryotic expression plasmid (CMV promotor-based) containing β1 subunit cDNA with an N-terminal eGFP tag suited for eukaryotic expression.

2.3.1 Constructing pGEMHE-β1 Vector

2.3.1.1 Setup pGEMHE-*GABRB1* Overlap PCR

A suitable oocyte vector identified was pGEMHE, which was available in-house containing a *KCND2* sequence. Conducting an overlap extension polymerase chain reaction (PCR) of a *GABRB1* PCR product from the pCMV6-Entry vector and a pGEMHE PCR product from the pGEMHE-*KCND2* vector by introducing a 22 bp overlap between the two PCR products allowed the creation of a pGEMHE-*GABRB1* product while removing *KCND2* in the same step.

The two initial PCRs were conducted as follows in accordance with the respective product information sheet. The DNA templates were the PGEMHE-*KNCD2* construct and pCMV6-Entry-*GABRB1,* respectively. Matching primers are found in Table 2 and Table 3. It contained the following components and was topped up to 20 µl with distilled water. The final concentration is given in brackets.

- 0.2 µl Phusion™ High-Fidelity DNA Polymerase (0.02 U/µl), Thermo Fisher Scientific, Waltham, USA.
- 4 µl Phusion™ HF Buffer, Thermo Fisher Scientific.
- 4 µl 10mM dNTPs (500 µM), Thermo Fisher Scientific.
- 0.6 µl DMSO, Thermo Fisher Scientific.
- 1 µl 10 µM of forward and reverse primer, respectively (0.5 µM per primer).
- 1 µl 100 ng/µl template DNA (5 ng/µl).

All primers used in this project were ordered from Integrated DNA Technologies, Inc. (IDT, Coralville, USA). The nomenclature given for the primer name corresponds to the name used for ordering at IDT. “F” refers to a forward primer, and “R” to a reverse primer.

Table 2. Primer sequences for pGEMHE backbone amplification PCR introducing overlap sequence.

Name	Sequence
pGEM-F-TAA-Ovh	5'- TAA GAA TTC TCT AGA GCA AGC TTG ATC TGG TTA -3'
pGEMHE-EcoRI-R	5'- TAT GAA TTC GGA TCC GAA TTG ATC TGC CAA AGT TGA GCG TTT ATT C -3'

Table 3. Primer sequences for GABRB1 product amplification introducing overlap sequence.

Name	Sequence
pCMV6-kzc-F	5'- GGG AAT TCG TCG ACT GGA TCC -3'
GABRB1-R-pGEM-Ovh	5'- AGA TCT CCT CGA TGA ATT GAT CTG CCA AAG TTG AGC GTT TAT TC -3'

The following settings were used for the Thermocycler (TurboCycler 2 Thermal Cycler, Blue-Ray Biotech, New Taipei City, Taiwan):

1. Initial Denaturation: 30 s at 98 °C.
2. Denaturation: 10 s at 98 °C.
3. Annealing: 20 s at 68°C for pGEMHE-*KCND2* and 63 °C for pCMV6-Entry-*GABRB1.*
4. Extension: 60 s for pGEMHE-*KCND2* and 30 s for pCMV6-Entry-*GABRB1* at 72 °C.
5. Steps 2.-4. were repeated 29 times.
6. Final extension: 5 min at 72 °C.

2.3.1.2 Agarose Gel Electrophoresis

A 2 µl aliquot of the PCR product with 20.000 x Red Safe Dye was loaded and run on a 1 % agarose gel containing ethidium bromide (final concentration 0.5 µg/mL) in Tris/Borate/EDTA buffer using gel electrophoresis. A Quick-Load® Purple Format DNA Ladder (NEB) was also loaded on the gel to have a DNA length reference. An in-house fluorescent light gel documentation system was used to visualize the DNA bands, displaying the expected PCR product sizes.

2.3.1.3 pGEMHE-*GABRB1* Overlap PCR

Subsequently, the overlap PCR was performed. 5 µl of the respective PCR products, added 1 µl 10mM dNTPs and 0.2 µl Phusion™ High-Fidelity DNA Polymerase (2 U/µl) were combined. The Thermocycler protocol given above was repeated, with the adjustments of annealing at 60 °C and extension for 90 s, for a total of 25 cycles. As described above, the PCR product results were checked via gel electrophoresis. In addition to the bands showing the initial PCR products, it also depicted a larger band of the correct size, indicating the successful merger of the pGEMHE and *GABRB1* PCR products.

2.3.1.4 Restriction Enzyme Digestion

Restriction enzyme digestion of the overlap PCR product was set up, serving a dual purpose. Firstly, DpnI only digests methylated DNA, which removes the vector remnants that might still be present from the first two PCRs. Secondly,

BamHI sites were inserted in the overlap PCR, allowing the construct to recirculate fully upon transformation after BamHI digestion. The digestion consisted of:

- 9 µl overlap PCR product.
- 2 µl CutSmart® Buffer, New England BioLabs (NEB), Inc., Ipswich, USA.
- 1 µl BamHI-HF®, NEB, (20.000 U/ml).
- 1 µl DpnI, NEB, (20.000 U/ml).

It was topped up to 20 µl with distilled water and digested at 37 °C for 2.5 h. Restriction enzymes were deactivated by heat at 80 °C for 15 min.

2.3.1.5 Transformation of Overlap PCR Product

After that, 5 µl of the digested PCR product was transformed into competent Top10 bacteria (in-house) following the protocol described in section 2.3.5. Respectively, 100 µl of the SOC Outgrowth Medium (NEB) containing bacteria were plated on two agar plates containing Ampicillin using a sterile glass spatula. Agar plates were produced in-house with 100 µg/ml Ampicillin from LB medium with 1.5% agar. Plates were incubated at 37 °C for 12 h. Incubation yielded five colonies in total, who were screened for the *GABRB1* insert using a colony PCR.

2.3.1.6 Colony PCR

Colony PCR was conducted as follows to screen clones for the *GABRB1* insert:

- 0.5 µl MyTaq™ DNA Polymerase, Bioline by Meridian Bioscience®, Columbia, USA.
- 4 µl MyTaq Reaction Buffer (contains 5 mM dNTPs and 15 mM $MgCl_2$).
- Bacterial colony picked with a pipet tip and diluted in 5 µl SOC Outgrowth Medium, NEB, 1.5 µl used for PCR. The remaining 3.5 µl were stored at 4 °C.
- 1 µl forward and reverse primer, respectively (0.5 µM final concentration per primer).

Reactions were topped up to 20 µl with distilled water. The primers used are found in Table 4.

Table 4. Primer sequences used for colony PCR screening of pGEMHE-GABRB1.

Name	Sequence
M13 pUC Fwd	5'- CCC AGT CAC GAC GTT GTA AAA CG -3'
M13 pUC Rev	5'- AGC GGA TAA CAA TTT CAC ACA GG -3'

The following settings were used for the Thermocycler:

1. Initial Denaturation: 60 s at 95 °C.
2. Denaturation: 15 s at 95 °C.
3. Annealing: 15 s at 53 °C.
4. Extension: 15 s at 72 °C.
5. Steps 2.-4. were repeated 30 times.
6. Final extension: 60 s at 72 °C.

PCR results were checked for expected DNA fragment length via gel electrophoresis as described above, and a clone carrying the desired *GABRB1* insert was successfully identified. Figure 4 shows a map of the pGEMHE-*GABRB1* construct.

2.3.1.7 Mini Preparation and Glycerol Stocking

Consecutively, 2 µl of the stored bacterial colony was inoculated in 5 ml LB medium (5 g/l Bactoyeast, 10 g/l B-tryptone, 10 g/l NaCl, pH 7.0, autoclaved), which contained 100 µg/ml Ampicillin and was cultured in a shaking incubator at 170 rpm for 16 h at 37 °C.

500 µl of bacteria containing LB medium was carefully mixed through pipetting with 500 µl 50% glycerol to create a glycerol stock stored at -80 °C. The remaining 4.5 ml were used to extract the desired plasmid DNA by performing a mini preparation (Extractme Plasmid Mini Kit, BLIRT S.A., Gdańsk, Poland) according to the manufacturer's instructions: Initially, the bacterial cells were centrifuged at 4,000 g for 5 min. The supernatant was subsequently removed, and the remaining pellet was resuspended in 250 µl of Suspension Buffer. Following this, 250 µl of Lysis Buffer was added to disintegrate the cell membranes, and the mixture was left to incubate for 2 min. 350 µl of Neutralization Buffer was

introduced, with the tube being gently inverted multiple times. The mixture was then centrifuged at 11,000 g for 10 min. The supernatant was carefully pipetted onto a filter situated on a tube, followed by centrifugation at 11,000 g for one min. For DNA purification, 750 µl of Wash Buffer was added to the filtered product, and the mixture was centrifuged once more at 11,000 g for one min. After discarding the liquid, another round of centrifugation was carried out for 2 min. Subsequently, a new collection tube was used, and 25 µl of Elution Buffer was added to the filter containing the purified DNA. The mixture was incubated for 60 s at room temperature. Finally, a 60 s centrifugation at 11,000 g allowed for collecting the extracted DNA product in the tube. The concentration of the isolated product was determined to be sufficient with a NanoDrop ND-1000 spectrophotometer (Thermo Fisher Scientific).

Consecutively, two methods were employed to verify *GABRB1* presence in pGEMHE: restriction enzyme digestion and Sanger sequencing.

2.3.1.8 Construct Verification via Restriction Enzyme Digestion

Two separate digestions, one single-site and one multi-site cleavage, were set up to compare if the resulting DNA band lengths would match the expected ones for the construct. Digestions used 2 µl of the construct (1236 ng total) and respectively 1 µl EcoRV (single-site, NEB), 1 µl SalI (multi-site, Thermo Fisher Scientific), and 2 µl of their respective buffer (CutSmart® Buffer, NEB for EcoRV and Tango Buffer, Thermo Fisher Scientific for SalI). Digestions were topped up to 20 µl using Ampuwa water (Fresenius Kabi AG, Bad Homburg, Germany) and left at 37 °C for 2.5 h. Enzymes were deactivated for 15 min at 80 °C. DNA bands depicted the correct respective expected lengths when loaded on the gel, as described above.

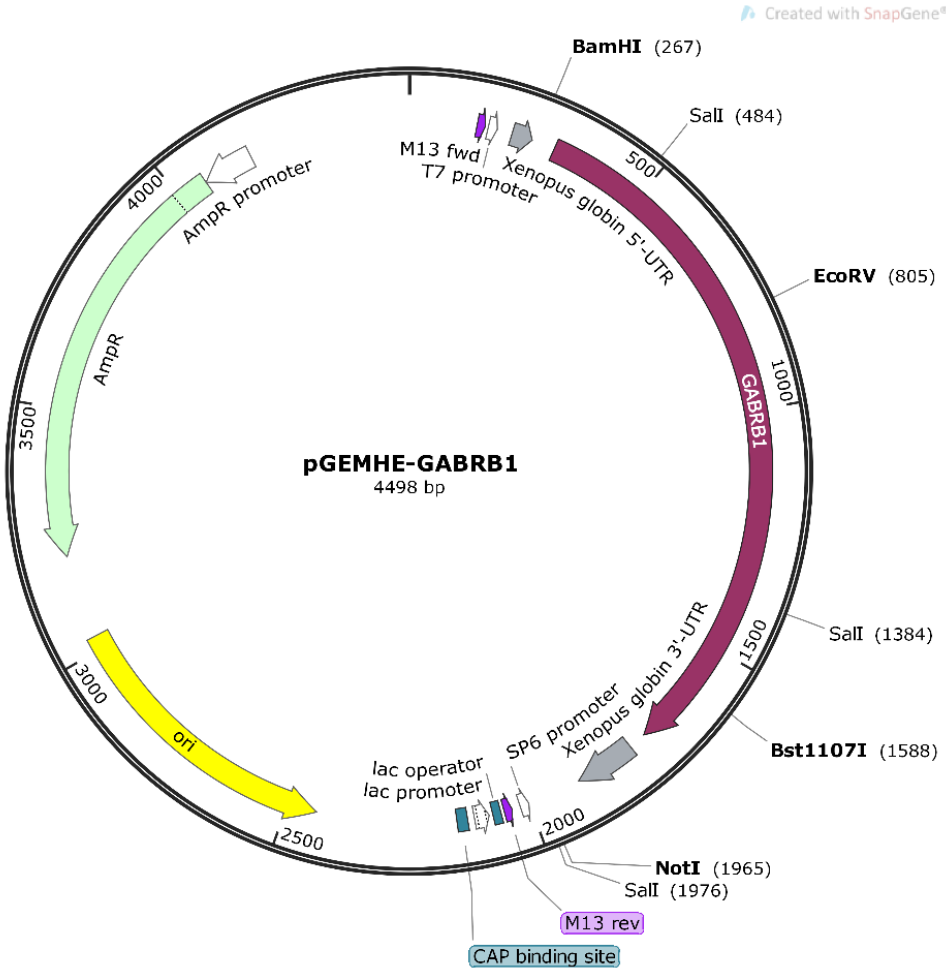

Figure 4. Vector map of pGEMHE with GABRB1 insert used in the final experiments. Functional elements are marked respectively. Relevant restriction enzyme sites are labeled (single-site cleavage in bold). This and subsequent vector maps were visualized with SnapGene® Viewer (GSL Biotech LLC).

2.3.2 Constructing pSGEM-γ2-β1-α1-β1-α1 Vector

Collaborators (V. W. Y. Liao, H. C. Chua, N. M. Kowal, M. Chebib, T. Balle, P. Ahring, N. Absalom, University of Sydney, Australia) successfully used γ2-βx-αx-βx-αx constructs for controlling the conformation and assembly of $GABA_AR$s in oocytes. Their work used these linker amino acids: $\gamma2^{first}$-βx^{second}: $(AGS)_5$, βx^{second}-αx^{third}: $(AGS)_5LGS(AGS)_3$, αx^{third}-βx^{fourth}: $AGT(AGS)_5$, βx^{fourth}-αx^{fifth}: $(AGS)_4ATG(AGS)_4$, where the subscript numbers imply the number of repetitions of the same amino acid block. They kindly provided our group with the backbone vector pNS3h-γ2-X-α1-X-α1 where X is a cloning site (see Figure 5 A.). This trimer contained unique linker sequences, encoding the linker amino acids as

detailed above, and restriction sites between the different subunits. This construct was used by subcloning β1 subunit cDNA with the aim of creating a pentameric construct in pSGEM. As this vector was not used for the final experiments presented in this thesis (see section 4.8.1), the methods of its construction will not be presented in detail. Briefly, the γ2-X-α1-X-α1 trimer from the original pNS3h vector with hygromycin B resistance was subcloned into an in-house pSGEM oocyte vector with ampicillin resistance and oocyte globin 3UTR (see Figure 5 B.). Concomitantly, β1 cDNA from the commercial pCMV-Entry vector was subcloned into two established in-house intermediate donor vectors with cloning sites and linker sequences matching the pentameric design (pMini2 for $\beta1^{second}$ and pUC19 for $\beta1^{fourth}$, referring to pentamer nomenclature – see Figure 6). Subsequently, the two β1 subunits were subcloned into the trimer via a γ2-β1-α1-X-α1 tetramer to create the final pSGEM-γ2-β1-α1-β1-α1 pentamer construct (see Figure 7).

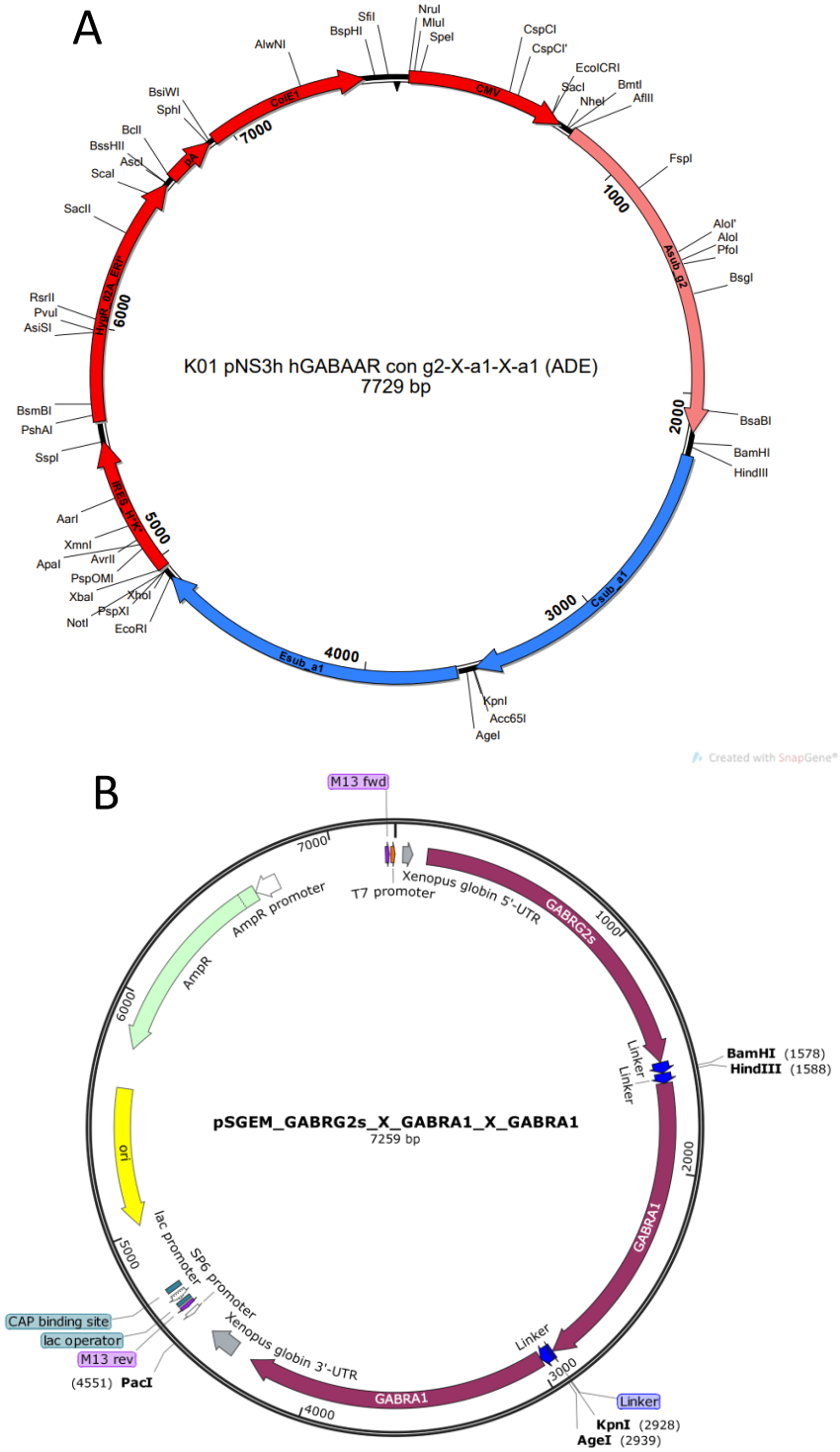

Figure 5. Vector maps of pNs3h and pSGEM γ2-X-α1-X-α1 trimer constructs. **A.** pNs3h-γ2-X-α1-X-α1 (g2-X-a1-X-a1) vector provided by Prof. P. Ahring et al. X represents the cloning site for the β1. The black inter-subunit sequences encode the unique amino acid linker sequences. **B.** pSGEM- γ2-X-α1-X-α1 trimer vector. The pNs3h-trimer + linker segment was cloned into an established in-house pSGEM oocyte backbone. Amino acid linker segments are marked in blue.

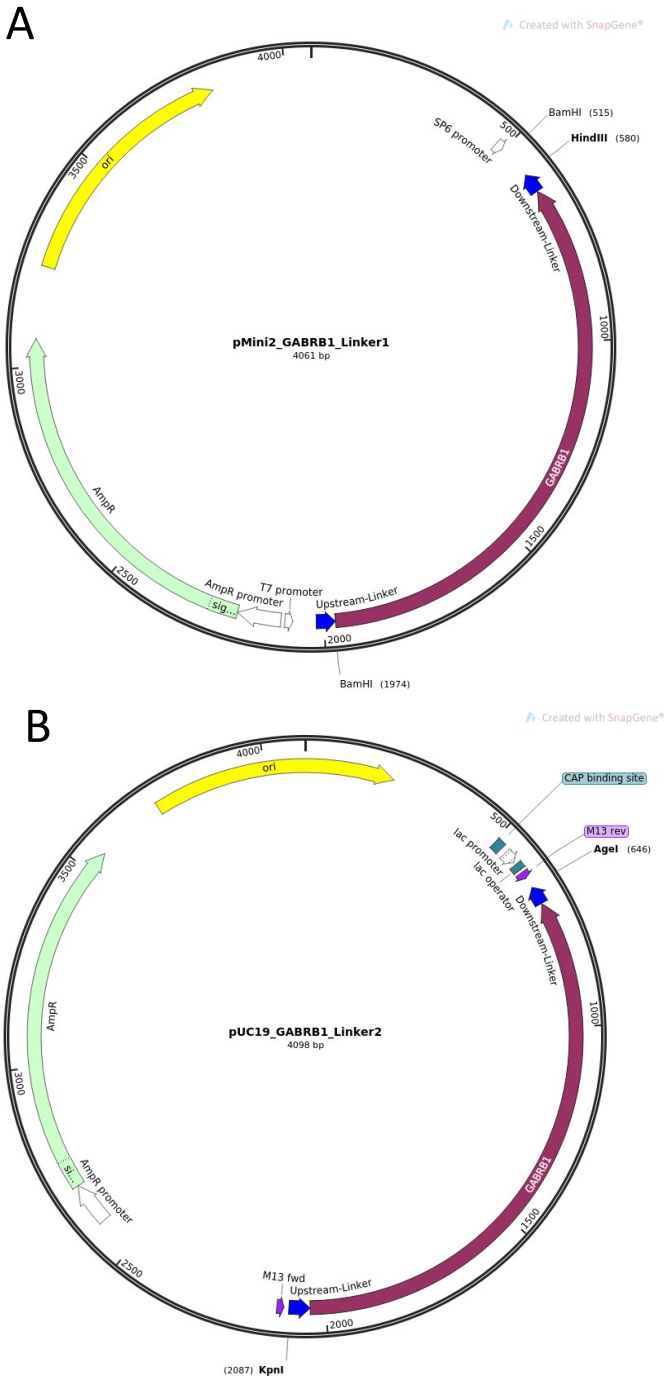

Figure 6. Vector maps of intermediate β1 pMini and pUC19 GABRB1 donor vectors. **A.** pMini2-*GABRB1* vector. **B.** pUC19-*GABRB1* vector. Both vectors contain linker segments (marked blue), resulting in the desired amino acid linker segments when digested and ligated into the trimer with the respective restriction enzymes (BamHI & HindIII for pMini2 and KpnI & AgeI for pUC19). Restriction enzyme sites are marked in bold.

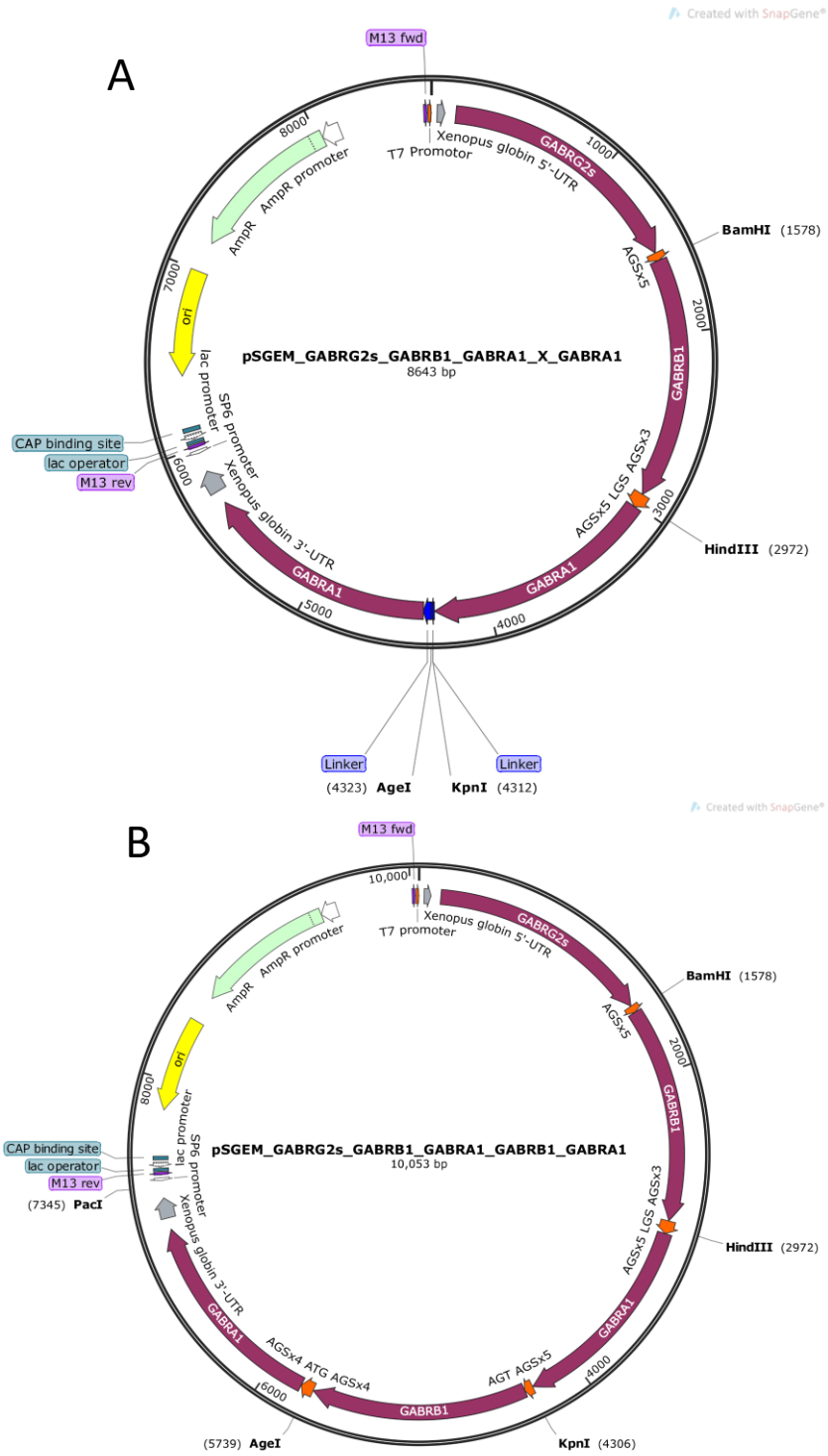

Figure 7. Vector maps of pSGEM γ2-β1-α1-X/β1-α1 tetramer and pentamer constructs. **A.** pSGEM-γ2- β1-α1-X-α1 tetramer construct. Note that this construct exists in the correct C117W + N429I version. **B.** The final pSGEM-γ2-β1-α1-β1-α1 pentamer construct attained by cloning two β1 subunits in the trimer. BamHI and HindIII restriction enzyme sites were used to clone $\beta1^{second}$ and KpnI and AgeI for $\beta1^{fourth}$. Restriction enzyme sites are marked in bold. Final amino acid linker segments are marked orange, and pre-final-cloning linker segments in blue.

2.3.3 Constructing pCMV-β1-eGFP Vector

The original pCMV-Entry vector contained a Myc-DDK tag that does not allow immediate visualization upon transfection. Therefore, an enhanced green fluorescent protein (eGFP) coding sequence was cloned that would result in a C-terminal *GABRB1* eGFP tag to visualize successfully transfected cells. Briefly, compatible cloning sites were introduced in eGFP using PCR using pcDNA3.1-eGFP as a template and sub-cloned these fragments in pCMV6-GABRB1-Myc-DDK, thus replacing the C-terminus tag. The details of these experiments are not provided as this vector was ultimately not used for recordings (see sections 1.6 and 4.9). The construct is depicted in Figure 8.

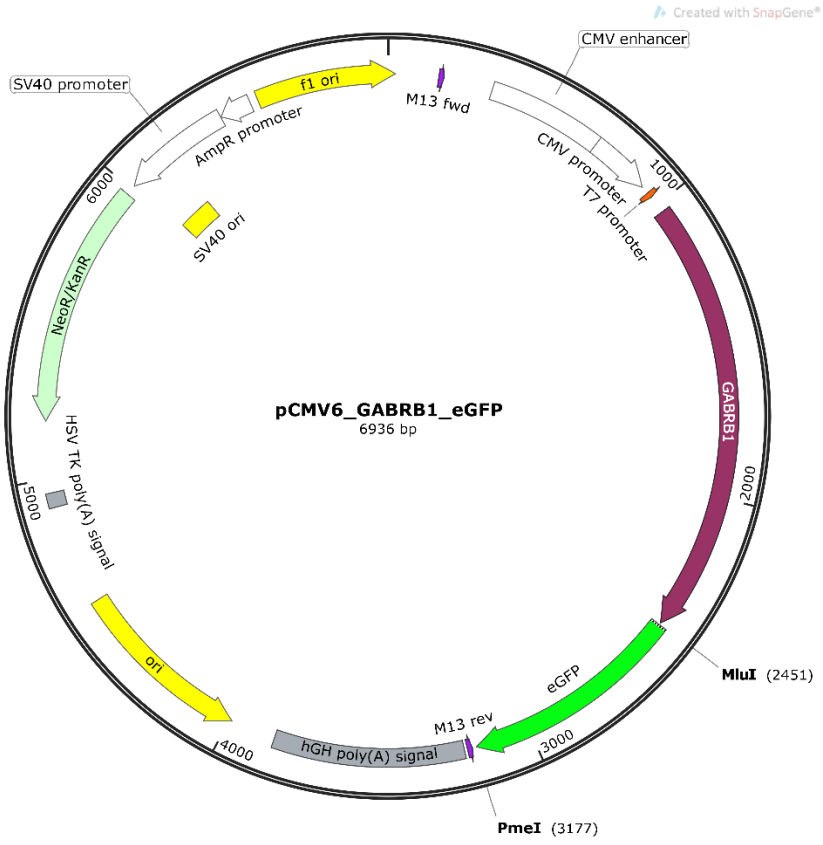

Figure 8. Vector map of pCMV6 vector containing GABRB1 and eGFP intended for patch clamp recordings in neurons or HEK 293 cells. eGFP (green) was cloned via PmeI and MluI restriction enzyme sites (bold) from a pcDNA3.1-eGFP template to replace the Myc-DDK tag at the C-Terminus of a pCMV6-GABRB1 construct resulting in a pCMV6-GABRB1-eGFP vector. Patch clamp recordings in neurons and HEK 293 cells were ultimately not carried out.

2.3.4 Sequence Verification and Error Correction

2.3.4.1 pGEMHE-*GABRB1* Construct Verification via Sanger Sequencing

In addition to restriction digestion, the sequence of the pGEMHE-β1 plasmid was validated using Sanger sequencing with two separate primers, together covering the entire *GABRB1* cDNA sequence. All sequencing was provided as “Ready 2 Run” by LGC Genomics (Berlin, Germany), and samples were prepared in accordance with their instructions: 10 µl 100 ng/µl plasmid + 4 µl 5 µM primer. The primers used can be found in Table 5. “T7_F” was used over “M13 pUC Fwd”, as it is also used for RNA synthesis, and I wanted to assess primer binding by its suitability to generate clean sequencing.

Table 5. Primer sequences used for GABRB1 Sanger sequencing.

Name	Sequence
T7_F	5’- TAA TAC GAC TCA CTA TAG GG -3’
M13 pUC Rev	5'- AGC GGA TAA CAA TTT CAC ACA GG -3'

SnapGene® Viewer 5.2.4 (GSL Biotech LLC, Boston, USA) and CLC Sequence Viewer 8 (QIAGEN) were utilized to align the sequencing results with *GABRB1* RefSeq NM_000812.3 (NCBI Nucleotide Database 2019).

The comparison showed two variants on the amino acid level in the construct:

1. W117C variant, caused by a T to G point mutation at nucleotide position 351 (inducing a TGT to TGG codon change).
2. I429N variant, caused by an A to T point mutation at nucleotide position 1287 (inducing an AAC to ATC codon change).

To investigate whether the W117C and I429N mutations were inherent to the original *GABRB1* OriGene construct or got inadvertently introduced during cloning, The *GABRB1* NM_000812.3 sequence, the sequenced *GABRB1*-pGEMHE construct and the original *GABRB1*-pCMV6-Entry Original Reading Frame (ORF) sequence given by OriGene (OriGene 2020) were aligned using the same software given above. This showed that the two variants given above were already contained in the original plasmid provided by OriGene.

One of the collaborators (P. Ahring, personal communication) noted that W117 is a highly conserved amino acid essential for supporting the 3D structure of the GABA binding site. I429 is in the less conserved M3-M4 loop. Ultimately, the two variants needed to be substituted with a codon for the original amino acid via site-directed mutagenesis to obtain the canonical *GABRB1* sequence. This canonical *GABRB1* sequence could then be used to introduce the four potentially pathogenic variants of interest via site-directed mutagenesis.

2.3.4.2 Mutagenesis for C117W

Reversing the W117C variant was done first by performing the following PCR according to the manufacturer's instructions (final concentration in brackets):

- 0.5 µl *Pfu* DNA Polymerase (Promega, Walldorf, Germany) (0.075 U/µl).
- 2 µl 10x *Pfu* Buffer (Promega), 20mM $MgSO_4$.
- 1 µl 10mM dNTPs (Thermo Fisher Scientific) (500 µM).
- 0.6 µl DMSO.
- 1 µl µM forward and reverse primer (see Table 6), respectively (0.5 µM per primer).
- 1 µl100 ng/µl pGEMHE-*GABRB1* plasmid, sequenced (5 ng/µl).
- Volume was topped up to 20 µl using distilled water.

Table 6. Primer sequences for mutagenesis PCR correcting the W117C GABRB1 variant.

Name	Sequence
*GABRB1*_p.C117W_F	5'- CCA GCT GTG GGT TCC AGA CAC CTA CTT TCT GA -3'
*GABRB1*_p.C117W_R	5'- AAC CCA CAG CTG GTC AGC TAC CCT ATT GTC T -3'

The following settings were used for the Thermocycler:

1. Initial Denaturation: 5 min at 95 °C.
2. Denaturation: 30 s at 95 °C.
3. Annealing: 30 s at 67 °C.
4. Extension: 5 min & 10 s at 72 °C.

5. Steps 2.-4. were repeated 19 times.
6. Final extension: 10 min at 72 °C.

2.3.4.3 Further C117W Preparation

Subsequently, the PCR was checked via gel electrophoresis, as previously described, which displayed a DNA band of the expected size.

A DpnI digestion of this PCR product was set up as previously described (without BamHI). 1.5 µl of this digestion was transformed into competent Top10 bacteria (in-house) following the protocol described in section 2.3.5. Respectively, 100 µl of the SOC Outgrowth Medium (NEB) containing bacteria were plated at 37 °C for 12 h on an Ampicillin agar plate with the same specifications as previously described. Incubation yielded several clones. Four were picked, incubated, glycerol stocked, and used for a mini preparation as described previously.

The isolated plasmid DNA of the four clones was sequenced and analyzed as previously described. The "*GABRB1*_I247T_R" (see Table 9) primer was used for this, as it was well-positioned to yield a clean sequence of the region of interest. Three clones carried the (canonical) C117W sequence. The last one was discarded.

2.3.4.4 Mutagenesis for N429I

The site-directed mutagenesis was repeated, this time reversing the I429N variant. A mixture of clones with sequenced plasmids carrying the C117W variant was used as template DNA. *Pfu* PCR was conducted as previously described with primers from Table 7. The annealing temperature was changed to 70 °C.

Table 7. Primer sequences for mutagenesis PCR correcting the I429N GABRB1 variant.

Name	Sequence
*GABRB1*_p.N429I_F	5'- GCG TAT ACG CAG GCG TGC CTC CCA GCT C -3'
*GABRB1*_p.N429I_R	5'- CTG CGT ATA CGC CCC TTG CTG GGA ACC -3'

2.3.4.5 Further N429I Preparation

The steps above were repeated for the (canonical) N429I variant, including gel electrophoresis, DpnI digestion, transformation, glycerol stocking, and mini preparation.

Prior to sequencing, a restriction enzyme digestion was performed to assess if site-directed N429I mutagenesis had worked, as primers were designed to introduce a novel Bst1107I (BstZ17I) single-site cleavage. 0.5 µl Bst1107I (BstZ17I) (10U/ µl), 2 µl 10x Buffer Orange (both Thermo Fisher Scientific), and 200-400 ng of DNA plasmid from respective four mini-preparations were used and topped up to 20 µl with Ampuwa water (Fresenius Kabi AG), digested for 1 h at 37 °C and heat deactivated for 15 min at 80 °C. In gel electrophoresis, two clones had been correctly linearized. The others were discarded.

2.3.4.6 Correct pGEMHE-*GABRB1* Verification Sequencing

As this construct posed the template for the site-directed mutagenesis of all the novel *GABRB1* variants, it was thoroughly sequenced, as previously described. Primers in Table 8 were used to ensure the presence of all crucial sites, i.e., T7 Promoter, Xenopus globin 5'-UTR, Xenopus globin 3'-UTR, and a canonical *GABRB1* sequence that aligns to the amino acid sequence of RefSeq NM_000812.3. Figure 4 shows a map of the final construct.

Table 8. Primer sequences used for Sanger sequencing of final pGEMHE-GABRB1 construct.

Name	Sequence
T7_F	5'- TAA TAC GAC TCA CTA TAG GG -3'
pSGEM_3UTR_R	5'- ATT AGG AGC AGA TAC GAA TGG CTA C -3'
M13 pUC Fwd	5'- CCC AGT CAC GAC GTT GTA AAA CG -3'
M13 pUC Rev	5'- AGC GGA TAA CAA TTT CAC ACA GG -3'
*GABRB1*_T287I_F	5'- GTG CTT ACA ATG ATA ACC ATC AGC ACC -3'

2.3.4.7 Sequence Verification and Error Correction in Other Vectors

The full pentameric cDNA sequence cloned in pSGEM (Figure 7 B.) and the eGFP-tagged β1 sequence cloned in pCMV6 (Figure 8) were sequenced. Both vectors contained the W117C and I429N variants. This was expected as all constructs were cloned from the same commercially obtained pCMV6-Entry vector with the alleged WT *GABRB1*.

It was attempted to assemble a corrected pSGEM pentamer and subsequently successfully conducted a C117W and N429I mutagenesis, transformation, and sequencing confirmation of a γ2-β1-α1-X-α1 tetramer and the corresponding + pUC19-GABRB1 vector (see Figure 6 B. and Figure 7 A.). Unfortunately, repeated T4 DNA ligation efforts of cloning the final β1 into the tetramer to achieve a corrected pentamer failed. All vectors are available upon request.

Ultimately, it was decided to use the standard approach of pre-mixed RNA injections of non-concatenated subunits in *X. laevis* oocytes.

Correction of W117C and I429N in pCMV6-*GABRB1*-eGFP was not attempted, and HEK 293 cells were not recorded via patch clamp.

2.3.5 Mutagenesis for I247T, T281S, T285K and T287I

To characterize the four identified novel missense variants, the variants were introduced into the previously assembled pGEMHE-*GABRB1* construct via site-directed mutagenesis. The variants c.740T>C:p.Ile247Thr, c.841A>T:p.Thr281Ser, c.854C>A:p.Thr285Lys and c.860C>T:p.Thr287Ile were introduced via *Pfu* PCR using the Primers from Table 9.

Table 9. Primer sequences for site-directed mutagenesis to introduce I247T, T281S, T285K, and T287I variants in pGEMHE-GABRB1.

Name	Sequence
*GABRB1*_I247T_F	5'- ATT GGT TAC TTC ACT TTG CAA ACC TAC A -3'
*GABRB1*_I247T_R	5'- TGT AGG TTT GCA AAG TGA AGT AAC CAA T -3'
*GABRB1*_T281S_F	5'- GCA CTA GGA ATC TCG ACA GTG CTT A -3'
*GABRB1*_T281S_R	5'- TAA GCA CTG TCG AGA TTC CTA GTG C -3'
*GABRB1*_T285K_F	5'- ACG ACA GTG CTT AAA ATG ACA ACC ATC -3'
*GABRB1*_T285K_R	5'- GAT GGT TGT CAT TTT AAG CAC TGT CGT -3'
*GABRB1*_T287I_F	5'- GTG CTT ACA ATG ATA ACC ATC AGC ACC -3'
*GABRB1*_T287I_R	5'- GGT GCT GAT GGT TAT CAT TGT AAG CAC -3'

Pfu PCR was conducted as previously described. The annealing temperature was set to a gradient of 62, 64, and 66 °C for three respective aliquots. The extension time was adjusted to 5 min and 30 s. PCR products were controlled via gel electrophoresis as previously described. 64 °C showed the highest yield for all PCR products, apart from T285K, where 62 °C yielded the most product. The respective products were digested with DpnI at 37 °C for 1 h, followed by a DpnI heat-inactivation as previously described.

The four PCR products were transformed into competent Top 10 *E. coli* bacteria (in-house) with the following protocol: The *E. coli* cells were retrieved from storage at -80 °C and placed on ice for 15 min. Subsequently, 1 µl (10 ng) of DNA was introduced, and the mixture was incubated on ice for 30 min. The bacterial cells were then exposed to a heat shock at 42 °C for 30 s before being returned to the ice for 2-5 min. The bacteria were then mixed with 250 µl of SOC medium (NEB) and incubated at 300 rpm at 37 °C for 1 h. 150 µl of SOC Medium containing the transformed cells was subsequently plated onto Ampicillin agar plates as previously described for each variant and incubated at 37 °C for 12 h. The following day, five individual colonies per variant were selected, treated with Ampicillin, and incubated in a shaking incubator as described in section 2.3.1.7.

Glycerol stocks were taken, and a mini-preparation of all clones was performed as described in section 2.3.1.7. DNA concentrations for the plasmid DNA carrying variants ranged from 200-600 ng/µl.

The plasmid DNA from the respective clones was sequenced to verify the correct mutagenesis of the four variants. Sequencing data was visualized using SnapGene® Viewer (GSL Biotech LLC). The "*GABRB1*_KpnI5_F" primer was first used to control the area of interest where I expected the variant to be. If the variant was properly in place, the entire *GABRB1* section was sequenced using "T7_F" and "pSGEM_3UTR_R" primers to exclude accidental mutations. See Table 10 for used primers and section 3.3.1 for results

Table 10. Primer sequences for verifying correct mutagenesis and ensuring correct GABRB1 sequence via Sanger sequencing.

Name	Sequence
T7_F	5'- TAA TAC GAC TCA CTA TAG GG -3'
pSGEM_3UTR_R	5'- ATT AGG AGC AGA TAC GAA TGG CTA C -3'
*GABRB1*_KpnI5_F	5'- GAC CAA CTC TGG GTG CCC GAC ACC TAC TTT CT -3'

2.4 Electrophysiological Recordings in *X. laevis* Oocytes

2.4.1 RNA in vitro Transcription

In order to synthesize the RNA encoding the $GABA_AR$ subunits, the circular plasmid DNA posing the RNA synthesis template needed to be linearized and purified. This was required for the β1-subunits, encoded by the canonical *GABRB1* WT, or one of the four *GABRB1* variants, the α5-subunit (encoded by *GABRA5*) and the γ2s-subunit (encoded by *GABRG2*). γ2s (S=short) represents a splice variant that lacks an eight-amino acid stretch compared to γ2L (L=large) (Olsen and Sieghart 2008). γ2s is physiologically expressed in the brain and commonly used in *X. laevis* oocyte experiments (Gutierrez et al. 1994; Karim et al. 2013). Generally, when referring to γ2 or *GABRG2*, this thesis refers to γ2s and the sequence encoding the short version, respectively. *GABRA5* and

GABRG2 were available in a pcDNA3.1 vector from previous in-house experiments. Plasmids were linearized using single-site restriction enzyme cleavage in a non-functionally relevant section downstream of the Xenopus globin 3'-UTR. NotI-FD was used for pGEMHE-*GABRB1* and BamHI-FD (both NEB) for pcDNA3.1-*GABRA5* and pcDNA3.1-*GABRG2*. 4 µg of plasmid DNA was mixed with 4 µl CutSmart® Buffer (10x, NEB), 1 µl restriction enzyme (20.000 units/ml), topped up to 40 µl with distilled water, and left to digest for 2 h at 37 °C. Restriction enzymes were heat-inactivated at 80 °C for 15 min.

When stocks of DNA plasmids were depleted, new mini-preparations were performed from available glycerol stocks. These were available for *GABRA5* and *GABRG2* from previous in-house experiments. 5 µl from the glycerol stock were inoculated in 5 ml LB medium, and the following preparation was performed as previously described.

The linearized DNA was purified to reduce the presence of RNAse and increase the chance of successful RNA preparation using a phenol/chloroform extraction. For this, 60 µl of DEPC-treated H_2O and 150 µl of phenol/chloroform were added to the digestion. The mixture was transferred to a Phase Lock Gel Eppendorf tube. The tube was centrifuged at 14.000 g for 2 min. Hereafter, 100 µl of Chloroform/Isoamyl alcohol was added, and the tube was centrifuged once more for 2 min at 14.000 g. The resulting supernatant (roughly 125 µl) was carefully moved to a fresh tube and briefly combined with 1/10 volume (12.5 µl) of ammonium acetate (3M, pH 5.3) and three times the volume (375 µl) of 100% ethanol. The tube was mixed via pipetting and briefly centrifuged. Following an overnight incubation (8-12 h) at -80 °C, the tube underwent centrifugation at 4 °C for 15 min, with the supernatant subsequently discarded. Next, 300 µl of 70% ethanol was introduced, followed by centrifugation and supernatant disposal like in the previous iteration. Residual liquid was removed via careful pipetting. The residual pellet was left for 15 min of air drying and then dissolved in 20 µl of DEPC-treated H_2O. The concentration was determined using a Nanodrop ND-1000 spectrophotometer (Thermo Fisher Scientific). DNA linearization was confirmed by gel electrophoresis as previously described, and the product was stored at -20 °C until further usage.

The linearized DNA encoding the respective subunits was transcribed into RNA starting from the T7 Promoter region. All mentioned reagents were purchased from Roche, Basel, Switzerland. 1 µg of the desired subunit plasmid DNA was mixed with 1 µl rNTPs, 1 µl RNAse Inhibitor, 2.5 µl 10x buffer, 2.5 µl, m^7G Cap-Analogon, and 1 µl T7 RNA polymerase. The reaction was topped up to 25 µl using DEPC H_2O and incubated at 37 °C for 2 h. Afterward, 10 U of DNAse (1 µl) was added, and the reaction was incubated for another 30 min at 37 °C to remove the linearized template DNA.

Hereafter, RNA was isolated by performing a phenol/chloroform extraction. Initially, 75 µl of DEPC-treated H_2O and 150 µl of phenol/chloroform were added, and the protocol was subsequently performed as described previously. RNA Concentration was determined via Nanodrop and controlled via gel electrophoresis as previously described. It was stored at -80 °C.

2.4.2 Preparation of X. laevis Oocytes

Two sources for mature *X. laevis* oocytes (stage V-VI) were used throughout the experiments. When available, untreated oocytes were provided by the Department for Animal Physiology, University of Tübingen. To prepare them for RNA injection, the following protocol was conducted: Firstly, the batch was bathed in OR-2 solution (produced in-house: 82.5 mM NaCl, 2.5 mM KCl, 1.0 mM $MgCl_2$, 5 mM Hepes buffer, pH = 7.6) treated with 1 mg/ml CLS II collagenase (Biochrom AG, Berlin, Germany) and gently rotated for 1-1.5 h. This was done to remove the external layer carrying follicular cells. Afterward, the oocytes were washed in Petri dishes with Barth's solution (produced in-house: 88 mM NaCl, 2.4 mM $NaHCO_3$, 1 mM KCl, 0.41 mM $CaCl_2$, 0.82 mM $MgSO_4$, and 5 mM Tris/HCl, pH was titrated to 7.4 via NaOH). The washing step was repeated twice. Subsequently, single oocytes were selected under a microscope and transferred via a Pasteur pipette into a Nunc™ Microwell™ 96-well plate (Thermo Fisher Scientific), prefilled with 200 µl Barth's solution with 50 µg/ml Gentamicin. When not available from the Department for Animal Physiology, defolliculated and washed oocytes were ordered from Dr. Lohmann Diaclean GmbH – EcoCyte Bioscience, Dortmund, Germany, which were delivered refrigerated on ice within

24 h. Preparation steps were skipped, and the oocytes were directly transferred to the 96-well plate. Oocytes were incubated for 1-2 h prior to RNA injection at 16 °C.

2.4.3 RNA injection of X. laevis Oocytes

RNA mixes encoding the respective subunits for $GABA_AR$ formation were injected into the prepared oocytes using the automated Roboinject injection system (see Figure 9, Multi Channel Systems MCS GmbH, Reutlingen, Germany) according to the manufacturer's instructions. Firstly, the glass capillary injection needle was filled with mineral oil. Afterward, the 96-well plate was inserted and calibrated to the center of the needle. Subsequently, using the Roboinject software, oocytes were assigned to their injection liquid, and respective tubes were placed in the bracket. Injection settings were confirmed, and the automated injection started via the software. 70 nl of the respective sample was injected into the oocytes. Between injections of different liquids, the needle was thoroughly washed with DEPC H_2O by the system.

Figure 9. Picture of Roboinject setup as it was used for RNA injection of X. laevis oocytes. The picture was taken from the official Roboinject manual with kind permission from Multi Channel Systems MCS GmbH.

Mixes of the α5β1γ2 subunits for homozygous conditions were created in a ratio of 5:1:5 or 1:1:2, indicating the relative amount of α5, β1, and γ2, respectively. The mixes were adjusted to a total (all subunits combined) RNA concentration of 1 µg/µl, with some 1:1:2 mixes being adjusted to 0.25 µg/µl. More information and the rationale for this can be found in sections 3.4.2 and 4.2.2. Mixes were topped up to 8 µl with DEPC H_2O. For the heterozygous condition, 50% of β1 RNA amount was WT and the other 50% variant. Only the T285K variant was tested in the heterozygous condition, as it was the only one exhibiting a total LoF in the homozygous condition.

Some oocytes were injected and recorded with H_2O for every well as a control condition.

After injection, plates were sealed with parafilm and incubated at 16 °C for 4-6 days to allow for translation of injected subunit RNA, pentameric $GABA_AR$ formation, and its expression in the cell membrane.

2.4.4 Two-Electrode Voltage Clamp Recordings

GABA-evoked currents in the oocytes were recorded via fully automated two-electrode voltage clamp (TEVC) using the Roboocyte2 system (Multi Channel Systems, see Figure 10). Recording data was stored on Microsoft Access Databases (Microsoft Corporation, Redmond, USA).

For TEVC recordings, two low-resistance glass microelectrodes are inserted into the oocyte. One electrode measures the cell's membrane potential, while the other can inject current to control the membrane potential. During GABA application, ion channels open, and this current can be measured indirectly via the change in injected current required to uphold the given membrane potential. This holding potential was set to -70 mV. Currents were sampled at 1 kHz. All recordings were conducted at room temperature (20-23 °C).

Firstly, the 96-well plate containing the injected oocytes was inserted, and the glass microelectrodes were calibrated to the plate. The two glass microelectrodes were acquired from Multi Channel Systems, had a resistance of 0.1-2 MΩ, and were filled with 1 M KCl and 1.5 M KAc. Consecutively, oocytes were selected for

recording, and the recording script (Javascript) was loaded into the Roboocyte2 software. The script was modified from a previous version that was available in-house. Oocytes that displayed macroscopic signs of necrosis (i.e., deformed shape or cloudy liquid) were not selected for recording. During the recording, when no GABA agonist was applied, the recorded oocyte was continuously washed with ND 96 solution (in mM: 93.5 NaCl, 2 KCl, 1.8 CaCl2, 2 MgCl2, 5 HEPES, titrated with NaOH to pH 7.5) at a flowrate of 5000 µl/min. A waste pump suctioned the surplus liquid from the well at the same flowrate.

GABA solutions were prepared from ND 96 at concentrations of (in µM) 1, 3, 10, 30, 100, 300, and 1000. Initially, the oocyte was impaled by the TEVC electrodes. If the initial resting membrane potential of the cell was below -14 mV or the leak current was above 500 nA or below -500 nA, the cell was not recorded. Then, an initial $GABA_AR$ expression and response test was conducted by doing a 5 s baseline recording, applying 300 µM GABA solution for 15 s, followed by a 90 s recorded washout and a 180 s non-recorded washout. The cell was not recorded if the current response (peak response compared to baseline current before agonist application) was above -100 nA. Subsequently, the previously mentioned GABA solutions were recorded in an ascending order of previously mentioned concentrations to allow for calculating a dose-response curve (DRC). Each recording consisted of a recorded 5 s pre-agonist application washout, a 15 s recorded agonist application, a 90 s recorded washout, and a 180 s non-recorded washout. All agonists were also applied with a flowrate of 5000 µl/min. Leak currents were assessed before each recording with cutoff values similar to those above.

Note that the first two agonist applications after the 300 µM expression and response test were conducted with ND 96 solution to achieve a >10 min washout period eventually. This was done as early pilot experiments had suggested a GABA carryover from the 300 µM to the 1 µM solution, with the 1 µM application yielding higher GABA responses than 3 µM or 10 µM (data not shown).

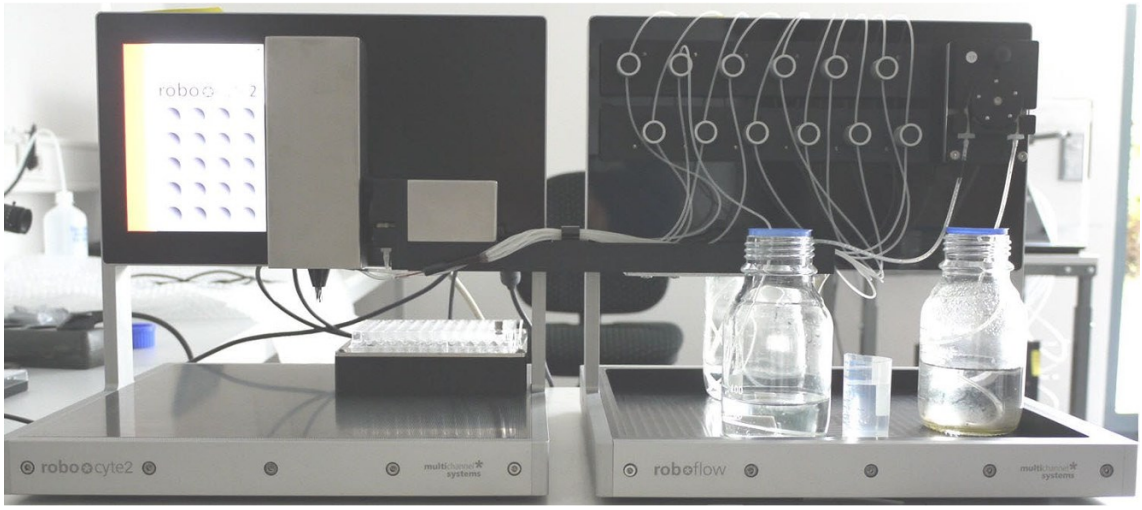

Figure 10. Picture with representative setup of the automated Roboocyte2 TEVC system. To the left: 96-well plate and recording electrodes. To the right: Valve system (Roboflow) with space for various solutions that can be applied. Just the washing solution and waste are displayed here. The picture was taken from the official Roboocyte2 manual with kind permission from Multi Channel Systems MCS GmbH.

2.5 Data Analysis

Roboocyte2+ software was used to automatically visualize GABA response curves and apply a built-in leak baseline subtraction and current drift correction to each cell. Peak minimum current values were exported for each GABA agonist concentration for each cell as a DAT file and accessed via Microsoft Editor (Microsoft). Data were initially analyzed in Microsoft Excel 2019 (Microsoft).

Minimum peak current values for 1 mM GABA responses were normalized to the mean of the WT minimum peak current values for 1 mM GABA responses from that recording batch. This ensured comparability of the maximum relative GABA response for the four variants from different batches. Cells were excluded if the minimum current response at 1 mM GABA application was above -100 nA or the alleged response was attributed to noise. For the final analysis of the normalized 1 mM GABA application response, cells were split into three groups containing the following:

1. Pooled cells from all three conditions:
    a. α5β1γ2 1:1:2 composition with 0.25 µg/µl total RNA injected.
    b. α5β1γ2 1:1:2 composition with 1 µg/µl total RNA injected.

c. α5β1γ2 5:1:5 composition with 1 µg/µl total RNA injected.

2. Only cells with an α5β1γ2 1:1:2 composition with 0.25 µg/µl total RNA injected.
3. Only cells with an α5β1γ2 5:1:5 composition with 1 µg/µl total RNA injected.

For the first set of DRCs, minimum peak current values for all GABA concentrations were normalized to the peak minimum current value for each cell to allow for analysis independent of the absolute peak minimum current. This peak minimum current was usually reached at 1 mM but occasionally at 300 or 100 µM. 300 µM GABA application in the expression test was excluded as the peak minimum current setpoint. Albeit mathematically representing a minimum, this peak minimum value will subsequently be referred to as a maximum current response to increase its intuitiveness. To account for inherent noise in the recording, measured minimum responses were set to 0 for 1 µM GABA applications. Several oocyte plates were excluded from the analysis as the WT and all variant conditions consistently showed <10% normalized GABA responses at 30 µM GABA application, which was in stark contrast to all other plates and systematically produced severe outliers. Empirically, this was likely not due to the inherent functional properties of the cells but to erroneous 30 µM GABA application for the respective plates. This required the final analysis to include cells from all three previously described RNA injection conditions to allow for suitable plotting.

For the second set of DRCs, minimum peak current values for all GABA concentrations were normalized to the average of the peak minima recorded from WT condition cells of the corresponding well. These peak minima were met at 1 mM GABA application. All other analysis characteristics correspond to the previously described approach for DRCs.

Data was exported to GraphPad Prism 7 (GraphPad Software, Boston, USA) for data visualization, plotting of DRCs, and statistical analysis.

For the DRCs, the following four-parameter logistic equation was used to fit the normalized GABA responses for each cell:

$$Y = \min + \frac{\max - \min}{1 + 10^{(log_{EC50} - X) \times nH}}$$

Y represents the normalized current response, and X the GABA concentration. “min” and “max” refer to the bottom and top plateaus of the sigmoidal curve given as normalized current. EC_{50} is the concentration where 50% of the maximum current is met. nH is the HillSlope coefficient, which describes the steepness of the curve. The data was visualized on a logarithmic scale. Statistical differences in the fitted EC_{50} value were evaluated via non-parametric one-way ANOVA on ranks (Kruskal Wallis test) and Dunn’s *post hoc* test.

To test the significance of differences in normalized responses of the minimum peak current values, the normal-distribution of the data was initially assessed via a Shapiro-Wilk normality test. Subsequently, a Kruskal-Wallis-test (non-parametric ANOVA on ranks) with Dunn’s *post hoc* multiple comparisons test relative to the WT was performed.

3 Results

3.1 Clinical Data

3.1.1 General

As introduced in section 1.5, this thesis aimed to investigate four *de novo* missense variants in *GABRB1* (I247T, T281S, T285K, T287I). All clinical information was collected by our collaborators C. Marini (Child Neurology and Psychiatric Unit, G. Salesi Pediatric Hospital; United Hospitals of Ancona; Ancona, Italy) and S. Weckhuysen (University Hospital of Antwerp, Dept. of Neurology, and the VIB Center for Molecular Neurology, Applied & Translational Neurogenomics Group, VIB, Antwerp, Belgium). See section 2.1 for more details. The T285K variant was found in two non-related individuals from different countries. For each of the other variants, only one individual is known. Seizure onset was between the age of two and four months for all four individuals. They all showed daily seizure frequency at onset. None of them showed specific provoking factors. The neurodevelopmental outcome can be described as severely delayed for all affected individuals. Overall, they can all be classified as DEE.

3.1.2 Individual Carrying the I247T Variant

The I247T variant was found in a female from Italy who displayed seizure onset at the age of four months. She presented with tonic seizures accompanied by vibratory/focal clonic components and cyanosis. EEG findings at onset revealed asynchronous paroxysmal epileptiform activity in the temporo-occipital regions of both the left and right hemispheres, with ictal discharges exhibiting migratory characteristics in the same areas. The individual exhibited delays in psychomotor development, characterized by hypotonia, lack of eye fixation, and an absence of smiling. VPA, VGB, Phenobarbital (PB), and nitrazepam were prescribed to her without clinical improvement. Magnetic Resonance Imaging (MRI) revealed very mild enlargement of the frontal spaces.

Two years after seizure onset, treatment with VPA, nitrazepam continued and was supplemented with carbamazepine (CBZ), which successfully achieved a

seizure-free state. Still, the follow-up EEG revealed temporo-occipital paroxysmal activity. Despite the cessation of seizures, the individual continued to exhibit severe delays in psychomotor development. Further clinical manifestations included hypotonia, quadriplegia, and disrupted sleep patterns with frequent arousals. Additionally, she displayed low-set and enlarged ears and repetitive and stereotyped movements. At this point, MRI revealed a thin *corpus callosum*, cortical atrophy, and a mild delay in myelination. Magnetic resonance spectroscopy demonstrated a reduced N-acetyl aspartate/creatine (Na/Cr) ratio, a lactate peak, and hypoperfusion in the frontal lobes.

Five years post-onset, the clinical picture prevailed.

3.1.3 Individual Carrying the T281S Variant

The T281S variant was found in a male individual in Croatia who displayed seizure onset at the age of two months. He presented with a diverse range of seizure types, including spasms, tonic seizures, and dystonic upper body movements characterized by the extension of the right side of the body and flexion of the left. Additionally, during sleep, the individual experienced periods of central apnea. EEG findings at onset showed multifocal discharges without seizures or slow wave activity and right parietal-temporal activity during seizures and episodes of cyanosis. He displayed developmental delay, hypotonia, difficulties with swallowing, and a weak cry. Phenytoin (PHT) was initially prescribed, with VPA and clobazam (CLB) added to the treatment regimen a few months later. A brain MRI revealed no abnormalities.

Two years after seizure onset, tonic seizures and spasms occurred persistently. The ASM regimen was adjusted to levetiracetam (LEV) with no clinical improvement. Follow-up EEG revealed bilateral continuous polyspikes and slow discharges. The individual continued to show severe delays in psychomotor development. Further clinical manifestations included fluctuating muscle tone with hypotonia and an inability to track objects visually. MRI imaging remained normal. The seizure type and neuropsychiatric features persisted, and the LEV therapy continued after five years post-onset. Additionally, EEG findings revealed

continuous, generalized spike-and-wave discharges at a frequency of 2-2.5 Hz, with a predominance in the frontal lobe.

In contrast to previous MRI findings, the five-year follow-up revealed bilateral mesial temporal sclerosis with a reduced volume of hippocampal structures bilaterally.

3.1.4 Individuals Carrying the T285K Variant

The first identified individual with the T285K variant was a female from Switzerland who displayed seizure onset at the age of two months. She presented with focal seizures, characterized by vocalization, staring, loss of reaction, and hemibody tonic or clonic asymmetric movements on the right or left side. EEG findings at onset revealed multifocal asynchronous paroxysmal epileptiform activity, with ictal discharges demonstrating focal onset on both hemispheres and secondary bilateral propagation. The psychomotor development was characterized by poor visual contact and poor feeding, and the motor development by mild hypotonia. The individual was prescribed a comprehensive treatment regimen with pyridoxal phosphate, PHT, LEV, topiramate (TPM), diazepam (DZP), and clonazepam (CZP). Furthermore, she was placed on a ketogenic diet. Brain MRI revealed no abnormalities.

Two years post-onset, the individual continued to have daily seizures of various types, including focal tonic, focal clonic, staring, myoclonus, and spasms. The condition was resistant to the previous treatment regimen and adjusted to VGB, steroids, potassium bromide (KBr), TPM, and DZP, which did not yield clinical improvements. The follow-up EEG revealed multifocal abundant epileptiform activity and a suppression-burst pattern characterized by bursts of diffuse paroxysmal high-voltage theta-delta activity alternating with low-voltage periods. Myoclonus was found to correlate with burst activity. No developmental progress could be observed. Additional neuropsychiatric features included axial hypotonia, limb hypertonia, pyramidal signs, and microcephaly measuring -3 standard deviations from the mean population.

No five-year follow-up data or additional MRI data is available.

The second individual carrying the T285K variant was a female from Germany, with less clinical information available. Seizure onset was at two months, with seizures characterized as focal clonic, including myoclonic elements and spasms. The EEG displayed multifocal epileptic activity. The neurodevelopmental outcome is severely delayed, and the condition is treatment-resistant (ASM not known).

3.1.5 Individual Carrying the T287I Variant

Clinical information on the individual carrying the T287I variant has been previously reported (Lien et al. 2016). The following quote summarizes their findings:

> "Our patient is a 32-months old hypotonic non-dysmorphic boy with treatment resistant epilepsy from age 3 months and severe developmental delay. He was recently started on a ketogenic diet that so far seems to have a positive effect. Results from cerebral MRI, ophthalmology, metabolic screening and a genomic copy number array (Affymetrix CytoScan HD) were all normal."

3.2 *In silico* Variant Evaluation

3.2.1 Minor Allele Frequency, Deleteriousness, Conservation, and Constraint

For *in silico* assessment of minor allele frequency (MAF), deleteriousness, conservation, and constraint, the four variants or variant positions were analyzed with common and widely established databases and scores, as described in the methods section. The results, including cut-off values, are displayed in Table 11, Table 12, Table 13 and Table 14.

None of the four variants was found in three population databases typically chosen as controls (gnomAD r2.1, TOPMed, DiscovEHR), indicated by the MAF of 0 in all three databases, showing that all are ultra-rare variants. T281S, T285K, and T287I were all predicted to be deleterious (PPh2 HDIV, CADD, REVEL), which means they were predicted to be harmful and adversely affect protein function. The T281, T285, and T287 positions were all predicted to be conserved

across different species (GERP++, Para-Z-Score), indicating their biological importance for protein functionality. The three positions were also all constrained (MPC, MTR), which means they tolerate mutations poorly with negative effects on organismal fitness. I247T was predicted to be deleterious by CADD and REVEL scores but not by the PPh2 HDIV score. I247 was predicted to be conserved by both employed scores. It was predicted to be constrained by the MPC score but not the MTR score. All variants were predicted to be pathogenic, with the highest uncertainty for the I247T variant.

Table 11. Minor allele frequencies of respective variants in three common population databases. Variants are typically considered ultra-rare variants if their MAF is less than 0.01% in a database.

cDNA Change	Amino Acid Change	gnomAD r2.1	TOPMed	DiscovEHR
c.740T>C	I247T	0	0	0
c.841A>T	T281S	0	0	0
c.854C>A	T285K	0	0	0
c.860C>T	T287I	0	0	0

Table 12. Deleteriousness of respective variants using three common evaluation tools. The typical cutoff values for a deleterious, pathogenic variant are CADD ≥ 20, PPh2 HDIV ≥ 0.85, and REVEL ≥ 0.50.

cDNA Change	Amino Acid Change	PPh2 HDIV	CADD	REVEL
c.740T>C	I247T	0.5	23.8	0.6
c.841A>T	T281S	1	23.9	0.9
c.854C>A	T285K	1	25	0.9
c.860C>T	T287I	1	25.2	1

Table 13. Conservation of respective variant positions using two common evaluation tools.
The typical cutoff values for conserved variant positions are GERP++ ≥ 2 and Para-Z-score ≥ 0.

cDNA Position	Amino Acid Position	GERP++	Para-Z-score
c.740T	I247	5.4	0.9
c.841A	T281	4.5	0.4
c.854C	T285	4.7	0.1
c.860C	T287	4.7	0.7

Table 14. Constraint of respective variant positions using two common evaluation tools.
The typical cutoff values for highly constrained variant positions are MTR ≤ 0.565 and MPC ≥ 2.

cDNA Position	Amino Acid Position	MPC	MTR
c.740T	I247	2.6	0.6
c.841A	T281	2.4	0.4
c.854C	T285	2.8	0.3
c.860C	T287	2.6	0.3

3.2.2 Ortholog Conservation

To approximate the importance of the amino acids affected by the identified missense variants, ortholog conservation from nematodes to humans for selected species was additionally evaluated. All four affected amino acids, I247, T281, T285, and T287, proved fully preserved from nematodes to humans, underpinning their high degree of conservation. This is also congruent with their high scores for deleteriousness.

The motif surrounding the amino acids also proved largely conserved, potentially implying high functional relevance. Figure 11 shows orthologs for the entire first transmembrane segment (M1, containing I247) and some positions immediately upstream. Figure 12 shows the entire second transmembrane segment (M2) containing T281, T285, and T287.

```
H. sapiens      241  RNIGYF I LQTYMPSTLITILSWVSFWI
P. troglodytes  241  RNIGYF I LQTYMPSTLITILSWVSFWI
M. mulatta      241  RNIGYF I LQTYMPSTLITILSWVSFWI
L. africana     241  RNIGYF I LQTYMPSTLITILSWVSFWI
C. lupus        241  RNIGYF I LQTYMPSTLITILSWVSFWI
B. taurus       241  RNIGYF I LQTYMPSTLITILSWVSFWI
M. musculus     241  RNIGYF I LQTYMPSTLITILSWVSFWI
R. norvegicus   241  RNIGYF I LQTYMPSTLITILSWVSFWI
G. gallus       240  RNIGYF I LQTYMPSILITILSWVSFWI
D. rerio        248  RNIGYF I LQTYMPSTLITILSWVSFWI
X. tropicalis   241  RNIGYF I LQTYMPSTLITILSWVSFWI
C. elegans      259  RSVGYF I FQTYLPCVLIVMLSWVSFWI
```

Figure 11. GABRB1 orthologs of different species, from nematodes to humans, before and in the M1 segment. The position of I247 is marked in green. The number gives the amino acid position of the first displayed letter (R).

```
H. sapiens      271  ASAARVALGI T TVL T M T TISTHL
P. troglodytes  271  ASAARVALGI T TVL T M T TISTHL
M. mulatta      271  ASAARVALGI T TVL T M T TISTHL
L. africana     271  ASAARVALGI T TVL T M T TISTHL
C. lupus        271  ASAARVALGI T TVL T M T TISTHL
B. taurus       271  ASAARVALGI T TVL T M T TISTHL
M. musculus     271  ASAARVALGI T TVL T M T TISTHL
R. norvegicus   271  ASAARVALGI T TVL T M T TISTHL
G. gallus       270  ASAARVALGV T TVL T M T TINTHL
D. rerio        278  ASAARVALGI T TVL T M T TINTHL
X. tropicalis   271  ASAARVALGI T TVL T M T TISTHL
C. elegans      289  ATSARVALGI T TVL T M T TISTGV
```

Figure 12. GABRB1 orthologs of different species, from nematodes to humans, in the M2 segment. The positions of T281, T285, and T287 are marked in red, orange, and pink, respectively. The number gives the amino acid position of the first displayed letter (A).

3.2.3 Paralog Conservation

To further evaluate the conservation of the amino acids affected by the identified missense variants, paralog conservation between *GABRA1-6*, *GABRB1-3*, *GABRG1-3,* and *GABRD* for *homo sapiens* was also evaluated. While I247 is positioned in a highly conserved region, this amino acid is weakly conserved and can only be found in *GABRB2*, *GABRB3,* and *GABRD*. It is notable here that β and δ subunits overall show a higher degree of sequence similarity while α and γ

are phylogenetically closer. Additionally, three alternative amino acids are found at its position, i.e., valine for *GABRA1*-3 and *GABRA5*, methionine for *GABRA4* and *GABRA6*, and threonine for *GABRG1*-3. In contrast, T281, T285, and T287 show full conversation across all paralogs. Notably, they all belong to a TTVLTMTT motif, which is fully conserved in all paralogs. Figure 13 and Figure 14 show the paralog conservation alignments of the respective regions around I247 or T281, T285, and T287, respectively.

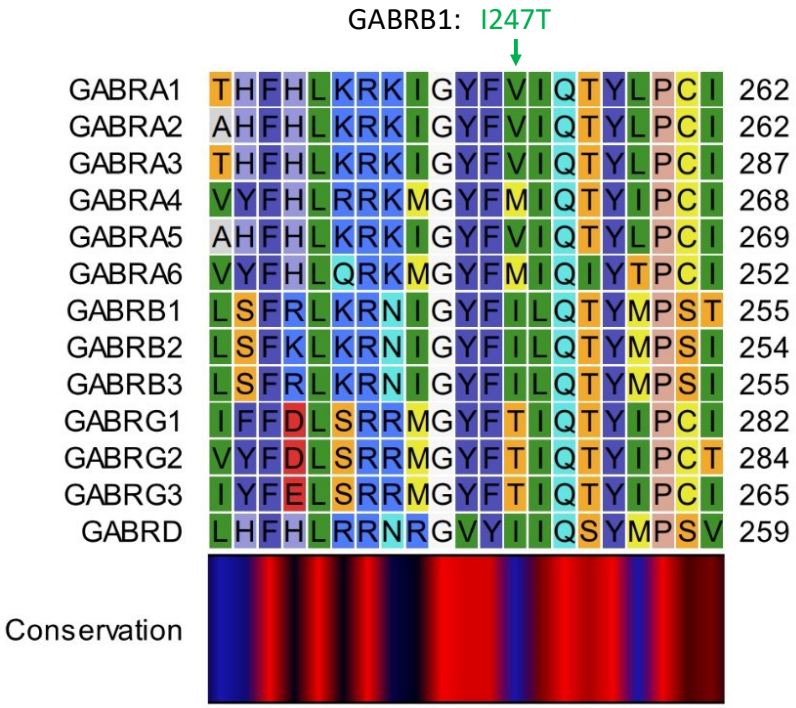

Figure 13. Paralog conservation of selected homo sapiens GABA$_A$R subunits around the I247T variant before and in the M1 segment. The RasMol color scheme was used to highlight amino acids based on their polarity (bright indicates polar and dark non-polar). The number gives the amino acid position of the last displayed letter (I, T, or V). The section encompasses 21 amino acid positions. The conservation bar indicates the conservation from fully conserved (red) over decently conserved (black) to weakly conserved (blue).

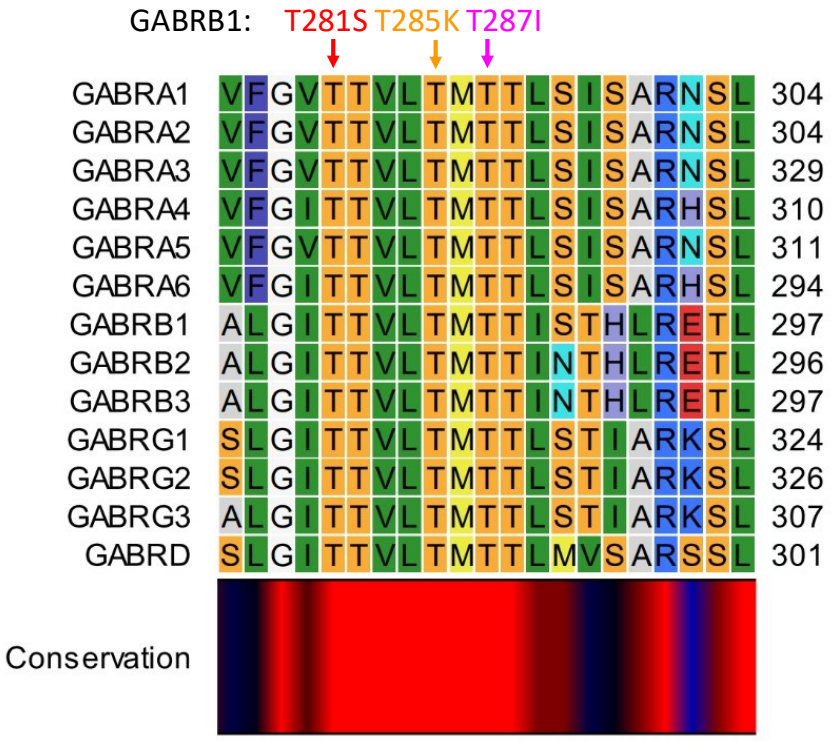

Figure 14. Paralog conservation of selected homo sapiens GABA$_A$R subunits around T281S, T285K, and T287I variants in the M2 segment. The RasMol color scheme was used to highlight amino acids based on their polarity (bright indicates polar and dark non-polar). The number gives the amino acid position of the last displayed letter (L). The section encompasses 21 amino acid positions. The conservation bar indicates the degree of conservation from fully conserved (red) over decently conserved (black) to weakly conserved (blue).

3.2.4 Correspondence to Known Variants in Paralogs

Several point missense variants linked to epilepsy in other GABA$_A$R subunits than β1 have hitherto been clinically described and functionally characterized. Information on the variants was collected as previously described for the amino acid section surrounding this study's four variants for the identical subunits that were previously used to align paralogs. This is of interest, as it can be used to compare functional findings for surrounding variants, variants affecting the corresponding amino acid with a different amino acid change, or variants affecting the corresponding amino acid with a similar amino acid change. Specifically, identical changes were used to approximate the variants' clinical relevance and functional outcomes. Figure 15 and Table 15, as well as Figure 16 and Table 16, give an overview of these results for the I247 section and the T281, T285, and

T287 sections, respectively. The tables also include the references for the variants mentioned in the following section.

Corresponding in amino acid position, the following variants were previously reported. One similar variant was reported for I247T (*GABRB2*: I246T). For T281S, three corresponding variants have been reported from two genes (*GABRB3*: T281A, T281I; *GABRG2*: T310I). For T285K, five corresponding variants have been described from four genes (*GABRA1*: T292I, T292S; *GABRA2*: T292K; *GABRA5*: T299I; *GABRB2*: T284K). Two of these also had the identical threonine to lysine change. For T287I, five corresponding variants have been reported from five genes, four of which had the identical threonine to isoleucine change (*GABRA1*: T294I; *GABRA4*: T300I; *GABRB3*: T287I; *GABRG1*: T314K; *GABRD*: T291I).

GABRA1	251	GYFVIQTY	258
GABRA2	251	GYFVIQTY	258
GABRA3	276	GYFVIQTY	283
GABRA4	257	GYFMIQTY	264
GABRA5	258	GYFVIQTY	265
GABRA6	261	GYFMIQIY	268
GABRB1	244	GYFILQTY	251
GABRB2	243	GYFILQTY	250
GABRB3	244	GYFILQTY	251
GABRG1	271	GYFTIQTY	278
GABRG2	273	GYFTIQTY	280
GABRG3	254	GYFTIQTY	261
GABRD	248	GVYIIQSY	255

Figure 15. $GABA_AR$ subunit paralog corresponding alignment showing known epilepsy-associated point missense variants before and in the M1 segment. The location of the I247T variant is highlighted in green. Reported neighboring variants are marked in red. Bold font indicates that more than one variant for this locus has been reported. Underscore indicates the exact amino acid change as the one in this study was reported. The numbers give the amino acid position of the first and last displayed letters, respectively (G and Y).

Table 15. Overview of known $GABA_AR$ subunit point missense variants marked in Figure 15. Information was assembled from the given references. Detailed context on the phenotype, where relevant, is given in the discussion. DEE: Developmental and Epileptic Encephalopathies DS: Dravet Syndrome, EE: Epileptic Encephalopathy, GoF: Gain-of-Function, IESS: Infantile Epileptic Spasms Syndrome, IS: Infantile Spasms, LoF: Loss-of-Function, N/A: not applicable.

$GABA_AR$ subunit gene	*Variant (cDNA)*	*Variant (amino acid)*	*Corresponding position in GABRB1*	*Epilepsy/ Syndrome*	*Functional Findings*	*Reference*
GABRA1	c.751G>A	G251S	G244	DS	LoF	(Carvill et al. 2014; Johannesen et al. 2016)
GABRA1	c.752G>A	G251D	G244	"Mild EE"	N/A	(Johannesen et al. 2016)
GABRA1	c.770C>G	T257R	T250	IESS	N/A	(Zhang and Liu 2022)
GABRB1	c.737T>C	F246S	F246	IS	LoF + GoF elements	(Allen et al. 2013; Janve et al. 2016; Wei et al. 2017)
GABRB2	c.730T>C	Y244H	Y245	DEE	N/A	(Hamdan et al. 2017)
GABRB2	735T>A	F245L	F246	DEE	N/A	(el Achkar et al. 2021)
GABRB2	c.734T>C	F245S	F246	IS	N/A	(Yang et al. 2020)
GABRB2	737T>C	I246T	I247	DEE	LoF + GoF elements	(el Achkar et al. 2021)
GABRB3	c.733T>C	Y245H	Y245	DEE	GoF	(Absalom et al. 2022)
GABRB3	c.745C>A	Q249K	Q249	DEE	LoF	(Absalom et al. 2022)
GABRG2	c.821A>G	Y274C	Y245	"Generalized epilepsy"	N/A	(Parrini et al. 2017)

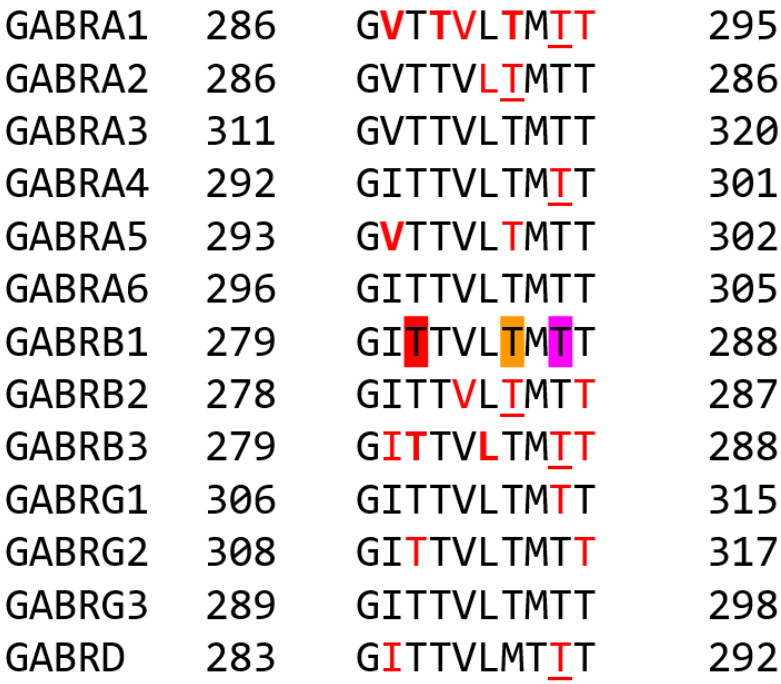

Figure 16. $GABA_AR$ subunit paralog corresponding alignment showing known epilepsy-associated point missense variants, including the highly conserved TTVLTMTT motif in the M2 segment. The locations of the T281S, T285K, and T287I variants are highlighted in red, orange, and pink, respectively. Reported variants are marked in red. Bold font indicates that more than one variant for this locus has been reported. The underscore indicates that the same variant as the one in this study was reported. The numbers give the amino acid position of the first and last displayed letters, respectively (G and T).

Table 16. Overview of known $GABA_AR$ subunit point missense variants marked in Figure 16. Information was assembled from the given references. Detailed context on the phenotype, where relevant, is given in the Discussion. DD: Developmental Delay, DS: Dravet Syndrome, EE: Epileptic Encephalopathy, EIEE: Early Infantile Epileptic Encephalopathy, EOEE: Early Onset Epileptic Encephalopathy, FS+: Febrile Seizures Plus, GGE: Generalized Genetic Epilepsy, GoF: Gain of Function, LGS: Lennox-Gastaut Syndrome, LoF: Loss of Function, N/A: Not Applicable, VUS: Variant of Uncertain Significance.

$GABA_AR$ subunit gene	*Variant (DNA)*	*Variant (amino acid)*	*Corresponding position in GABRB1*	*Epilepsy/ Syndrome*	*Functional Findings*	*Reference*
GABRA1	c.859G>T	V287L	I280	EE	N/A	(Kodera et al. 2016)
GABRA1	c.859G>A	V287I	I280	"Epilepsy and neurodevelopmental disorder"	N/A	(Lindy et al. 2018)
GABRA1	c.865A>C	T289P	T282	EIEE	N/A	(Johannesen et al. 2016)

GABRA1	c.865A>G	T289A	T282	EIEE	N/A	(Johannesen et al. 2016)
GABRA1	c.868G>A	V290M	V283	From "Epilepsy panel"	N/A	(ClinVar 2023)
GABRA1	c.875C>T	T292I	T285	DS, LGS (two individuals)	LoF	(Allen et al. 2013; Chen et al. 2022; Johannesen et al. 2016)
GABRA1	c.875C>G	T292S	T285	DEE	GoF	(Chen et al. 2022; Reyes-Nava et al. 2020)
GABRA1	c.881C>T	T294I	T287	"Epilepsy and neurodevelopmental disorder"	N/A	(Lindy et al. 2018)
GABRA1	c.884C>T	T295I	T288	"Epilepsy and neurodevelopmental disorder"	N/A	(Lindy et al. 2018)
GABRA2	c.871C>G	L291V	L284	EOEE	LoF	(Maljevic et al. 2019a)
GABRA2	c.875C>A	T292K	T285	EOEE	LoF	(Butler et al. 2018)
GABRA4	c.899C>T	T300I	T287	DEE	GoF	(Ahring et al. 2022b; Vogel et al. 2022)
GABRA5	c.880G > C	V294L	V280	DEE	GoF + LoF elements	(Butler et al. 2018)
GABRA5	c.880G>T	V294F	V280	EOEE	LoF	(Hernandez et al. 2019)
GABRA5	c.896C>T	T299I	T285	"Epileptic seizures", classified as VUS	N/A	(Charzewska et al. 2023)
GABRB2	845T>C	V282A	V283	"Generalized epilepsy with DD"	LoF + GoF elements	(el Achkar et al. 2021)
GABRB2	c.851C>A	T284K	T285	DEE	N/A	(Hamdan et al. 2017)
GABRB2	c.859A>C	T287P	T288	EE	LoF	(Ishii et al. 2017)
GABRB3	c.838A>T	I280F	I280	DEE	GoF	(Absalom et al. 2022)
GABRB3	c.841A>G	T281A	T281	DEE	GoF	(Absalom et al. 2022)
GABRB3	c.842C>T	T281I	T281	DEE	LoF	(Absalom et al. 2022)

GABRB3	c.850C>A	L284M	L284	DEE	GoF	(Absalom et al. 2022)
GABRB3	c.851T>G	L284R	L284	DEE	GoF	(Absalom et al. 2022)
GABRB3	c.596T>C	L284P	L284	DEE	GoF	(Absalom et al. 2022)
GABRB3	c.860C>T	T287I	T287	DEE	GoF	(Absalom et al. 2020; Absalom et al. 2022; Papandreou et al. 2016)
GABRB3	c.863C>A	T288N	T288	DEE	GoF	(Absalom et al. 2022)
GABRG1	c.941C>A	T314K	T287	DEE	N/A	(Williams et al. 2022)
GABRG2	c.929C>T	T310I	T281	"Epilepsy"	N/A	(Yang et al. 2022)
GABRG2	c.950C>T	T317I	T288	FS+	N/A	(Yang et al. 2022)
GABRD	c.860T>C	I284T	I280	DEE	GoF	(Ahring et al. 2022a)
GABRD	c.872C>T	T291I	T287	GGE	GoF	(Ahring et al. 2022a)

3.2.5 Variant Location in the $GABA_AR$ Quaternary Structure

The location of the variants in a 3D-model of the $GABA_AR$ consisting of a β1-α1-β1-α1-γ2 composition was predicted as described in section 2.2. Results are shown in Figure 17. I247 is located at the start of the M1 segment alpha-helix and faces outwards, as viewed from the pore. T281, T285, and T287 are located towards the end of the M2 segment alpha-helix. All three amino acids face directly inwards towards the pore. The pore is primarily constituted by the five M2 segments of the respective subunits.

To summarize, the *in silico* analysis showed evidence that the variants would likely disrupt normal channel function and were considered likely pathogenic based on the following ACMG criteria (Richards et al. 2015):

a) *De novo* in a patient with the disease and no family history (Pathogenic Strong 2).
b) Located in a mutational hot spot and/or critical and well-established functional domain (Pathogenic Moderate 1).

c) Absent from controls in several population databases (Pathogenic Moderate 2).
d) Multiple lines of computational evidence support a deleterious effect on the gene or gene product (Pathogenic Supporting 3).

Extrapolating from previously functionally characterized variants in other $GABA_AR$ subunits that exactly correspond in position and amino acid change, I247T would be expected to show a mixed LoF + GoF effect, T285K to show a LoF effect, and T287I to show a GoF effect. As a $GABA_AR$ subunit variant analogous to T281S has not yet been observed, it is not possible to extrapolate from that. Nonetheless, previous functional results show a mixed picture with a change to Ala at the same position in β3, equivalent to T281A in β1, resulting in a GoF, while a change to Ile at the same position in β3, equivalent to T281I in β1 resulting in a LoF (Absalom et al. 2022).

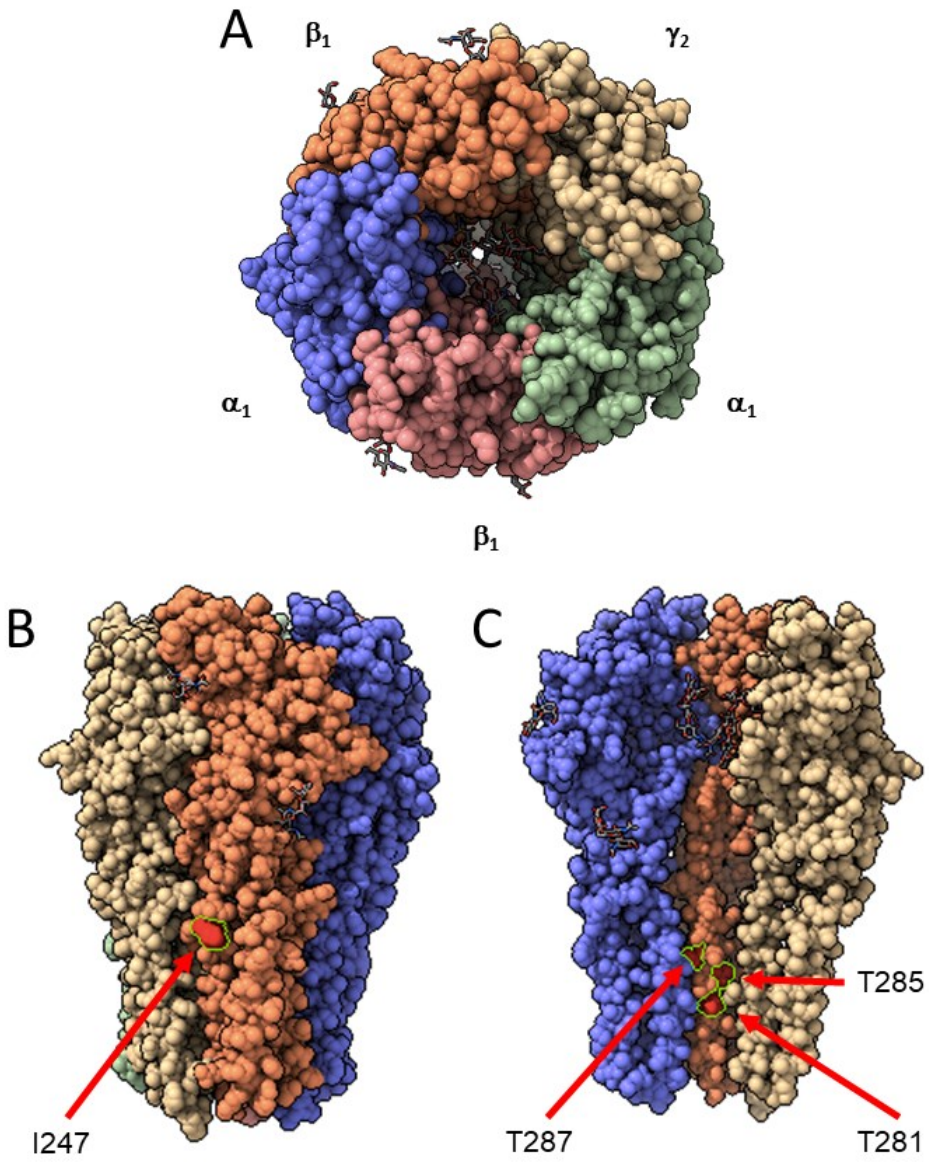

Figure 17. Predicted location of variant locations I247, T281, T285, and T287 in a 3D GABA$_A$R model. **A.** Arrangement of a GABA$_A$R consisting of a β1-α1-β1-α1-γ2 composition in a counter-clockwise orientation viewed from the synaptic cleft. **B.** Side view from the outside, i.e., the cell membrane. Green α1 and red β1 largely hidden by shown subunits. I247 is located in the outwards facing β1 M1 segment. **C.** Side view from inside the pore. Green α1 and red β1 not shown. The loci of the three variants, T281, T285, and T287, are located in the β1 M2 segment and face inwards towards the pore.

3.3 Molecular Biology

3.3.1 Mutagenesis Sequencing Results for I247T, T281S, T285K and T287I Variants

Figure 18 shows exemplary Sanger sequencing results that verify clones carry the desired variants in the respective pGEMHE-GABRB1 vector; see section 2.3.5 for methodological details. The changes successfully introduced to the respective codons were: I247T: ATT to ACT; T281S: ACG to TCG; T285K: ACA to AAA; and T287I: ACA to ATA.

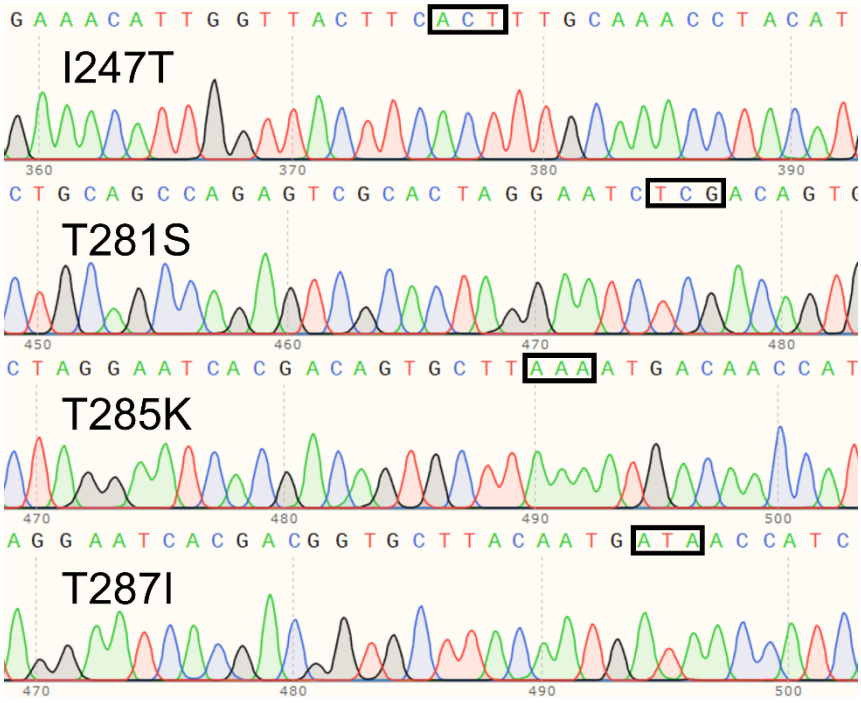

Figure 18. Sanger sequencing results from site-directed mutagenesis for selected I247T, T281S, T285K, and T287I clones. Clones were sequenced using the "*GABRB1*_KpnI5_F" primer. The relevant codon successfully altered during the mutagenesis is framed in black. Three-digit numbers give the nucleic acid position starting from the beginning of the sequencing and are not relevant here. Visualized via SnapGene® Viewer.

3.4 Electrophysiological Recordings

3.4.1 Exemplary Currents

To functionally analyze the potentially pathogenic variants, they were recorded via two-electrode voltage clamp (TEVC) in *X. laevis* oocytes. The I247T, T281S, T285K, and T287I variants were recorded in homozygous conditions. T285K was

additionally recorded in the heterozygous condition (see section 4.2.2 for rationale). Heterozygous conditions for variants other than T285K were not recorded. Representative current responses to 1 mM GABA application of the respective conditions are depicted in Figure 19.

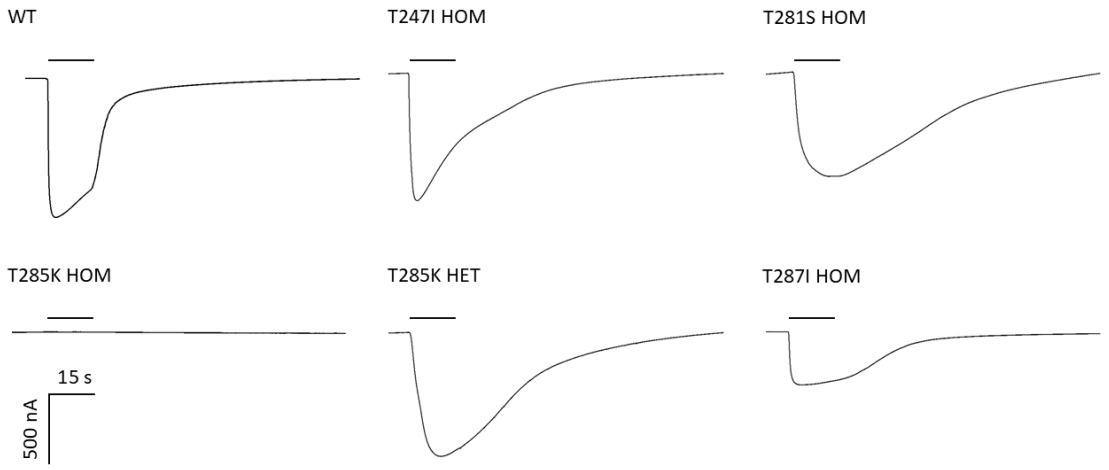

Figure 19. Exemplary TEVC current traces of X. laevis oocytes' response to 1 mM GABA application for WT and variant conditions. TEVC current response traces of $GABA_AR$s expressed in *X. laevis* oocytes to 1 mM GABA application were recorded automatically by Roboocyte2 for the homozygous (HOM, i.e., all injected β1 RNA carried the variant) I247T, T281S, T285K, T287I, and heterozygous (HET, i.e., half of the injected β1 RNA carried the variant). All exemplary traces were recorded from an α5β1γ2 1:1:2 composition with 0.25 µg/µl total RNA injected. There was an initial 5 s resting baseline recording, 15 s GABA application, and 90 s recorded washout with ND 96 solution. The 15s GABA application is shown via the horizontal bar above the trace.

3.4.2 Normalized Minimum Responses

As described in the methods section, three distinct analyses were performed to evaluate the normalized peak current amplitude response to 1 mM GABA application. The first analysis included a total of 208 cells pooled from several different RNA injection conditions. Namely, these were 88 cells recorded from an α5β1γ2 1:1:2 composition with 0.25 µg/µl total RNA injected, 110 cells recorded from an α5β1γ2 5:1:5 composition with 1 µg/µl total RNA injected, and 10 cells from an α5β1γ2 1:1:2 composition with 1 µg/µl total RNA injected. These compositions and concentrations were chosen as they were established in-house and are generally common in $GABA_AR$ TEVC recordings. The two other analyses

were separately conducted from the 88 and 110 cells with their according RNA injection condition, respectively. Detailed information can be found in Figure 20, Figure 21, and Figure 22. Table 17, Table 18, and Table 19 provide additional statistical information on the analyses.

In essence, when comparing the differences in normalized responses pairwise between the WT and the other conditions via Dunn's *post hoc* significance testing, there were no statistically significant differences between the WT and any tested variant conditions in all three analyses, except for the homozygous T285K condition, which showed a strongly significant reduction ($p<0.0001$) in all analyses. Notably, the homozygous T287I condition showed a recognizable, albeit non-significant reduction in the pooled analysis ($p=0.164$) and analysis of the 1:1:2 composition with 0.25 µg/µl total RNA injected ($p=0.0861$) when compared to the WT. The control condition (H_2O) also always showed a significant ($p<0.0001$) reduction when compared to the WT.

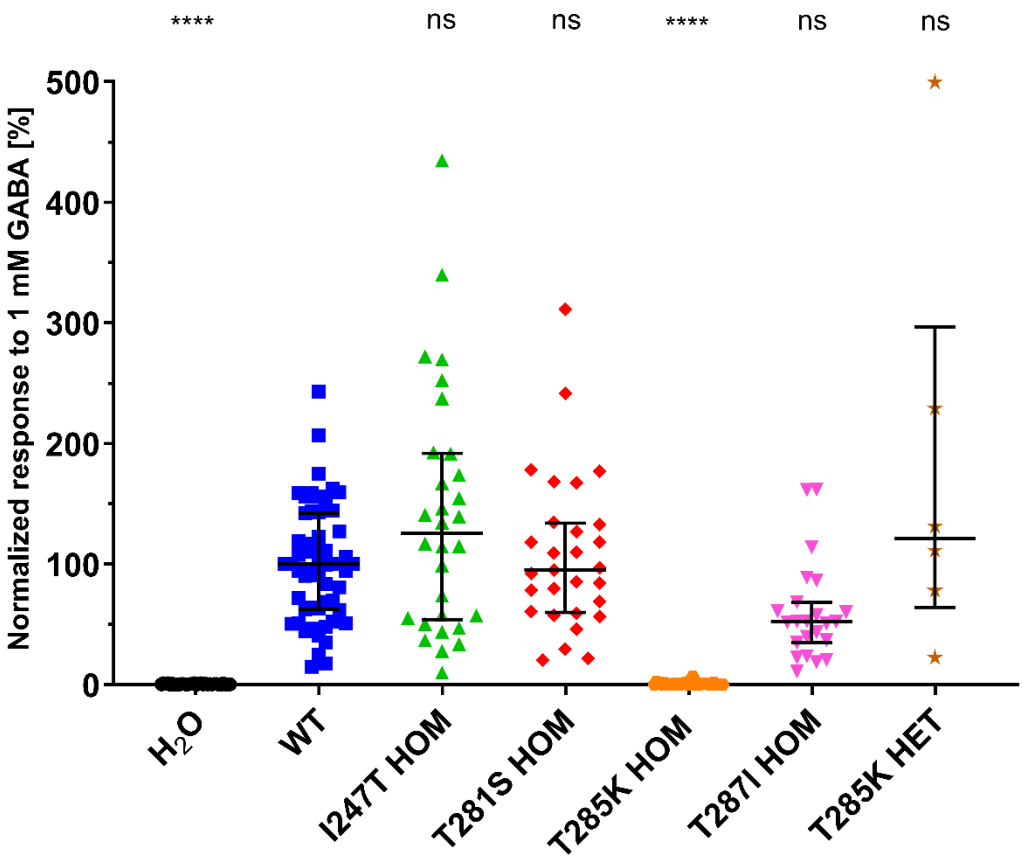

Figure 20. Scatter plot showing variants' peak current amplitude response to 1 mM GABA application normalized against WT in a pooled analysis for varying injected α5β1γ2 RNA composition and concentration conditions. TEVC peak current amplitude response of $GABA_A$Rs expressed in *X. laevis* oocytes to 1 mM GABA application for the homozygous (HOM, i.e., all injected β1 RNA carried the variant) I247T, T281S, T285K, T287I, and heterozygous (HET, i.e., half of the injected β1 RNA carried the variant) T285K variant conditions normalized as percentage to the average peak current amplitude response of WT recordings of each batch and a H_2O control. This is a pooled analysis of different α5β1γ2 RNA composition and concentration conditions, namely 88 cells recorded from a 1:1:2 composition with 0.25 µg/µl total RNA injected, 110 cells from a 5:1:5 composition with 1 µg/µl total RNA injected and 10 cells from a 1:1:2 composition with 1 µg/µl total RNA injected. Each dot represents a normalized peak current amplitude response datapoint of one cell. Bars indicate the median and interquartile range. Differences in normalized responses were tested pairwise between the WT and the respective other conditions via Dunn's *post hoc* statistical significance testing and indicated as ns (non-significant) or **** ($p<0.0001$). Detailed information is found in Table 17.

Table 17. Statistical parameters for Figure 20. P-value and Significance refer to pairwise Dunn's *post hoc* significance testing with the WT.

	H_2O	**WT**	**I247T HOM**	**T281S HOM**	**T285K HOM**	**T287I HOM**	**T285K HET**
n	32	55	30	29	33	23	6
Minimum [%]	0	14.86	10.05	20.38	0	10.86	22.44
Maximum [%]	1.4	242.8	434.8	311.3	6.84	162	499.6
Mean [%]	0.5519	100	139.5	107.8	0.8855	59.6	178.7
Standard Deviation [±%]	0.3873	48.21	101.2	64.82	1.29	40.32	171.4
Standard Error of Mean [±%]	0.0684	6.501	18.47	12.04	0.2246	8.408	69.96
Median [%]	0.45	100	125.8	95.03	0.49	52.17	121.3
25% Percentile [%]	0.29	62.39	54.03	60.05	0	34.85	64.24
75% Percentile [%]	0.8575	142.5	191.9	133.9	1.3	68.41	296.8
P value (relative to WT)	<0.0001	N/A	>0.9999	>0.9999	<0.0001	0.164	>0.9999
Significance	****	N/A	ns	ns	****	ns	****

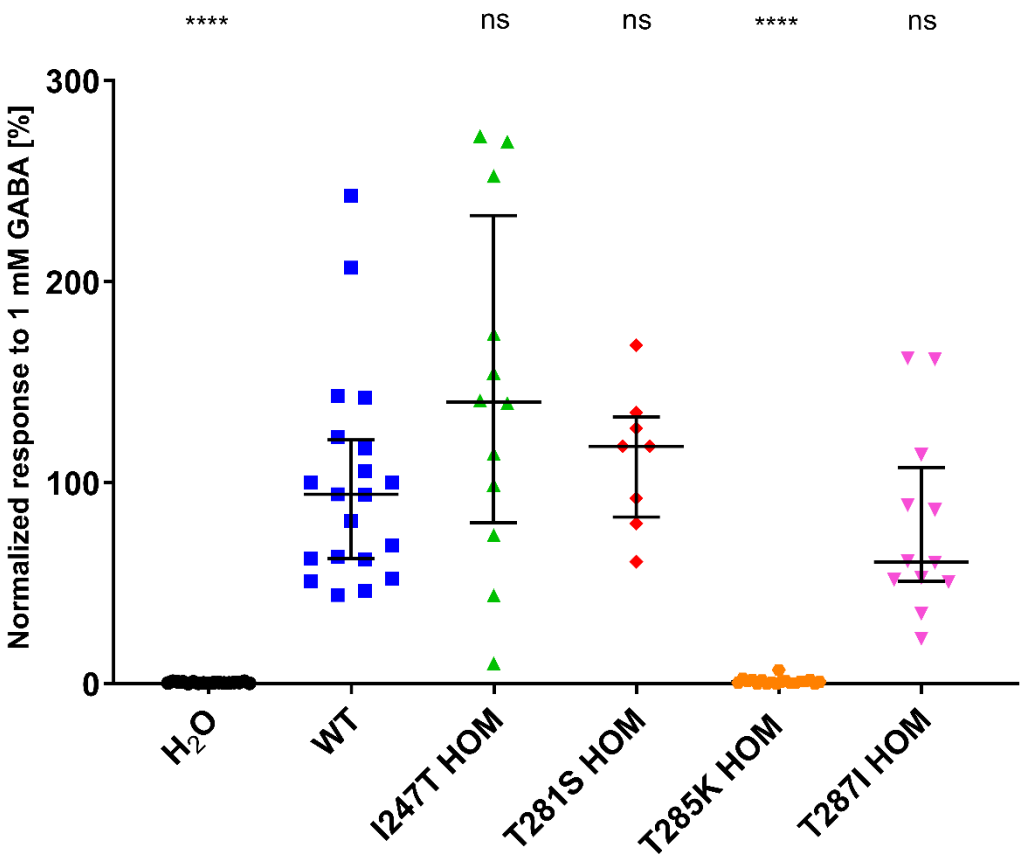

Figure 21. Scatter plot showing variants' peak current amplitude response to 1 mM GABA application normalized against WT exclusively for cells injected with an α5β1γ2 1:1:2 composition adjusted to 0.25 µg/µl total RNA. TEVC peak current amplitude response of $GABA_AR$s expressed in X. laevis oocytes to 1 mM GABA application for the homozygous (HOM, i.e., all injected β1 RNA carried the variant) I247T, T281S, T285K, T287I variant conditions normalized as percentage to the average peak current amplitude response of WT recordings of each batch and a H_2O control. This is exclusively an analysis of the 88 cells recorded from an α5β1γ2 1:1:2 composition with 0.25 µg/µl total RNA injected. Each dot represents a normalized response datapoint of one cell. Bars indicate the median and interquartile range. Differences in normalized responses were tested pairwise between the WT and the other conditions via Dunn's *post hoc* statistical significance testing and are indicated as ns (non-significant) or **** ($p<0.0001$). Detailed information is found in Table 18.

Table 18. Statistical parameters for Figure 21. P-value and Significance refer to pairwise Dunn's *post hoc* significance testing with the WT.

	H_2O	**WT**	**I247T HOM**	**T281S HOM**	**T285K HOM**	**T287I HOM**
n	17	20	12	8	19	12
Minimum [%]	0	44.21	10.05	60.75	0	22.4
Maximum [%]	1.24	242.8	272.3	168.5	6.84	162
Mean [%]	0.5712	100	145.4	112.4	1.243	78.84
Standard Deviation [±%]	0.3718	52.63	85.73	33.92	1.56	45.84
Standard Error of Mean [±%]	0.09018	11.77	24.75	11.99	0.3578	13.23
Median [%]	0.49	94.2	140.1	118.1	0.97	60.61
25% Percentile [%]	0.29	62.14	80.07	82.95	0.23	50.95
75% Percentile [%]	0.91	121.2	232.9	132.8	1.79	107.6
P value (relative to WT)	<0.0001	N/A	>0.9999	>0.9999	<0.0001	>0.9999
Significance	****	N/A	ns	ns	****	ns

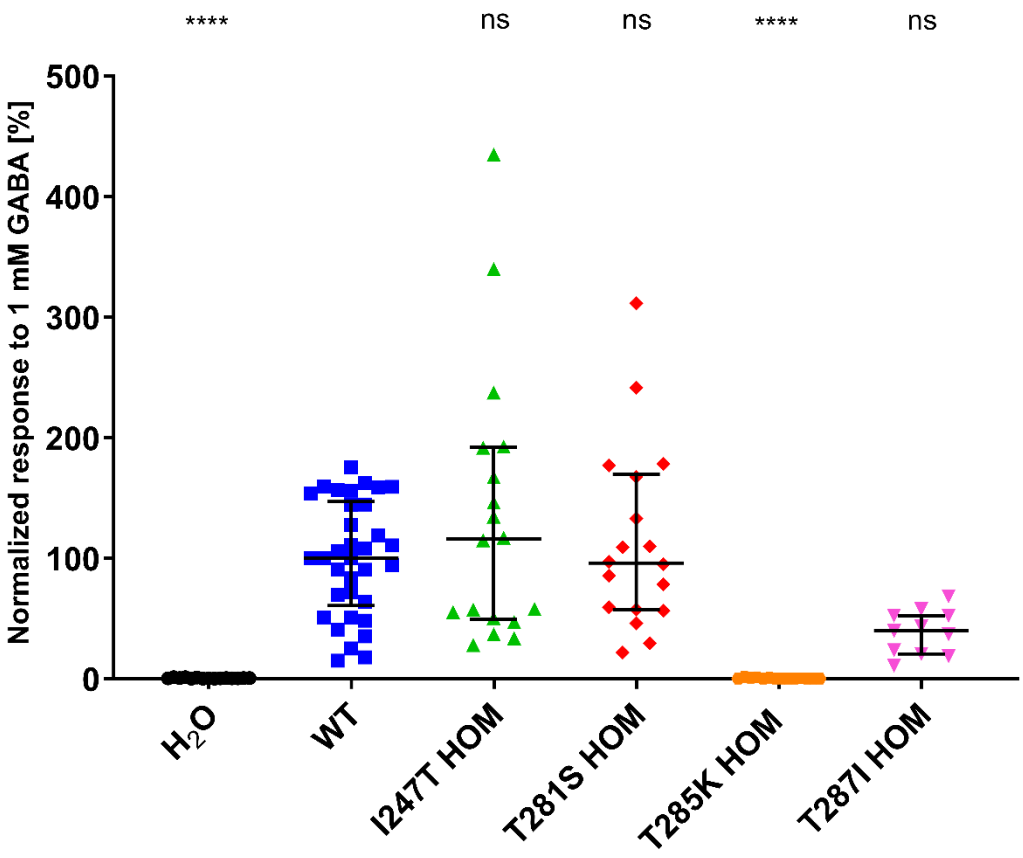

Figure 22. Scatter plot showing variants' peak current amplitude response to 1 mM GABA application normalized against WT exclusively for cells injected with an α5β1γ2 5:1:5 composition adjusted to 1 µg/µl total RNA. TEVC peak current amplitude response of $GABA_ARs$ expressed in X. laevis oocytes to 1 mM GABA application for the homozygous (HOM, i.e., all injected β1 RNA carried the variant) I247T, T281S, T285K, T287I variant conditions normalized as percentage to the average peak current amplitude response of WT recordings of each batch and a H_2O control. This is exclusively an analysis of the 110 cells recorded from an α5β1γ2 5:1:5 composition with 1 µg/µl total RNA injected. Each dot represents a normalized response datapoint of one cell. Bars indicate the median and interquartile range. Differences in normalized responses were tested pairwise between the WT and the other conditions via Dunn's *post hoc* statistical significance testing and are indicated as ns (non-significant) or **** ($p<0.0001$). Detailed information is found in Table 19.

Table 19. Statistical parameters for Figure 22. P-value and Significance refer to pairwise Dunn's *post hoc* significance testing with the WT.

	H_2O	**WT**	**I247T HOM**	**T281S HOM**	**T285K HOM**	**T287I HOM**
n	15	34	18	18	14	11
Minimum [%]	0	14.86	27.95	21.76	0	10.86
Maximum [%]	1.4	175.1	434.8	311.3	1.54	68.41
Mean [%]	0.53	100	135.7	114.1	0.4007	38.61
Standard Deviation [± %]	0.4161	47	112.6	76.32	0.5377	18.36
Standard Error of Mean [±%]	0.1074	8.06	26.53	17.99	0.1437	5.537
Median [%]	0.42	100.1	115.9	96.05	0.165	39.67
25% Percentile [%]	0.29	60.58	49.46	57.24	0	20.67
75% Percentile [%]	0.7	146.8	191.9	169.8	0.86	52.43
P value (relative to WT)	<0.0001	N/A	>0.9999	>0.9999	<0.0001	0.0861
Significance	****	N/A	ns	ns	****	ns

3.4.3 Dose-Response Curves

To assess the GABA sensitivity, i.e., the GABA response dependent on applications of a range of increasing GABA concentrations, dose-response curves (DRCs) were calculated and plotted. This was done for α5β1γ2 compositions pooled across all three previously described RNA injection conditions of the WT and the homozygous conditions of the I247T, T281S, and T287I, as well as the heterozygous condition of the T285K variant. No DRC could be plotted for the homozygous condition of the T285K variant, as the threshold for recording multiple GABA concentrations was not met for any cells during the initial 1 mM expression test application. The DRCs from GABA response normalization to the maximum current value for each cell are shown in Figure 23.

The homozygous condition of the I247T, T281S, and T287I variants show a highly significant ($p<0.0001$) increase in GABA sensitivity. This is measured by comparing the best-fit EC_{50} values of the four-parameter logistic fits to the EC_{50} of the WT fit using a non-parametric one-way ANOVA Kruskal-Wallis test with Dunn's *post hoc* multiple comparisons test. The standard error of the mean is

respectively given in parentheses. The EC_{50} of the WT was 66.52 µM (± 0.88). The one of I247T was 5.57 µM (± 1.11), corresponding to an 11.9-fold increase in GABA sensitivity. The one for T281S was 4.29 µM (± 0.17), corresponding to a 15.5-fold increase in GABA sensitivity. The one for T287I was 9.58 µM (± 0.30), corresponding to a 6.9-fold increase in GABA sensitivity. Maximum GABA responses plateaued at 100 µM for T281S and T287I and 300 µM for I247T compared to 1 mM for the WT. The strong increase in GABA sensitivity for these three variants can also be inferred from the fact that the 95% confidence intervals (CI) of the EC_{50} do not overlap between these variants and the WT. The best-fit EC_{50} for the heterozygous T285K fit was 81.18 µM (± 5.60) and did not differ significantly ($p>0.9999$) from the one of the WT. No factor in GABA sensitivity decrease was thus calculated). Also, their 95% EC_{50} CIs partly overlap. These and other statistical parameters can be found in Table 20 and Table 21.

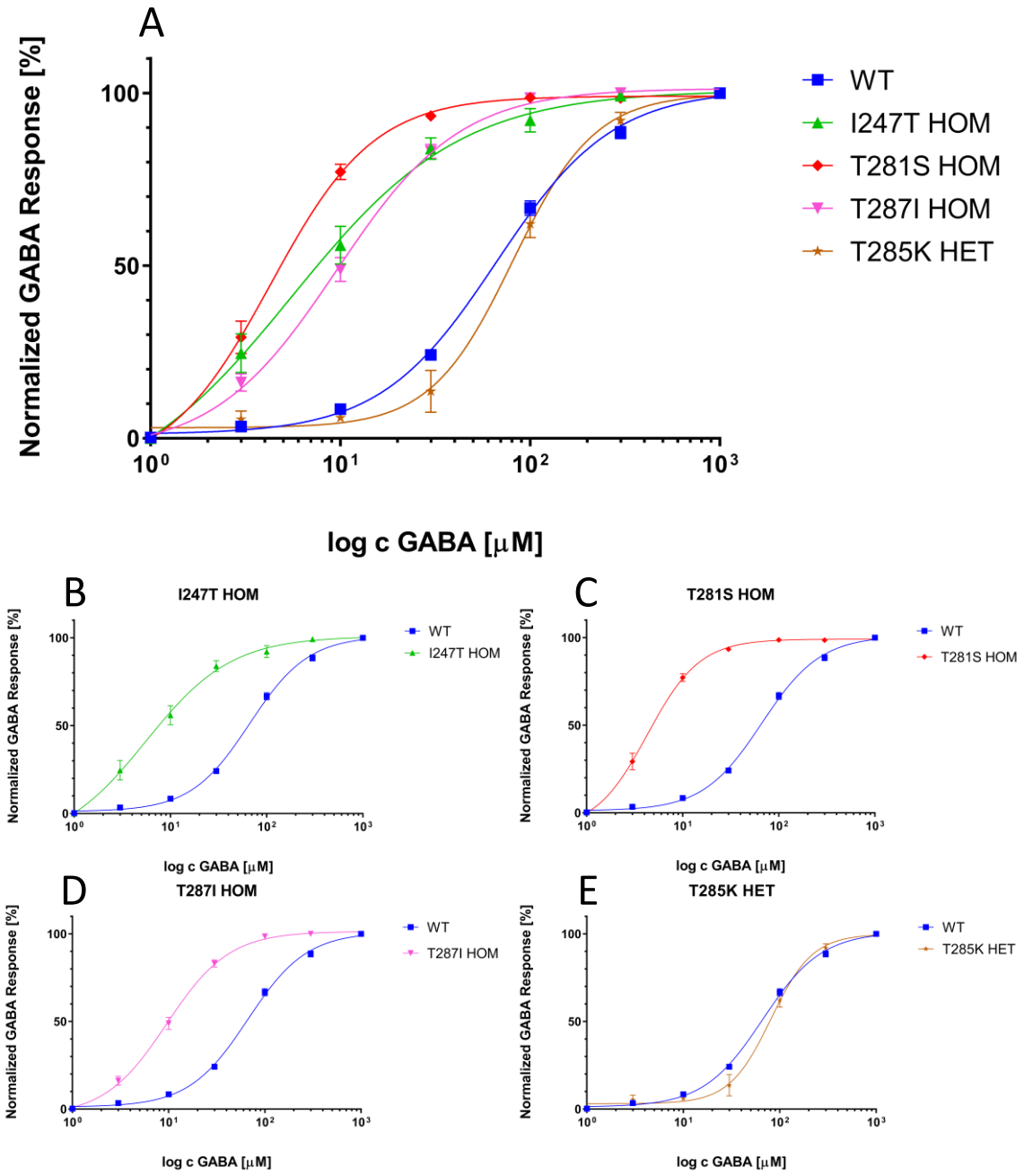

Figure 23. GABA sensitivity DRCs calculated from current responses to subsequent GABA application normalized to each cell's maximum current response for all variants. TEVC peak current amplitude response of $GABA_AR$s expressed in X. laevis oocytes to subsequent application of 1, 3, 10, 30, 100, 300, and 1000 µM (logarithmic representation) normalized to each cell's maximum peak current amplitude response for the homozygous (HOM, i.e., all injected β1 RNA carried the variant) I247T, T281S, T285K, T287I, and heterozygous (HET, i.e., half of the injected β1 RNA carried the variant) T285K variant conditions. This is a pooled analysis across different α5β1γ2 RNA composition and concentration conditions (1:1:2 with 0.25 µg/µl, 1:1:2 with 1 µg/µl and 5:1:5 with 1 µg/µl total RNA injected). Mean responses are shown as datapoints with

error bars indicating SEMs. To account for inherent noise, measured minimum responses were set to 0 for 1 µM GABA applications. **A.** shows all DRCs and **B.-E.** the respective DRCs for the homozygous (HOM) I247T, T281S, T287I and heterozygous (HET) T285K conditions compared to the WT. The exact statistical parameters can be found in Table 20.

Table 20. GABA sensitivity statistical parameters for Figure 23. EC_{50} with a 95% confidence interval (CI) was determined from a four-parameter logistic fit. P value refers to the statistical differences of the EC_{50} values calculated from a non-parametric one-way ANOVA (Kruskal Wallis test) with Dunn's *post hoc* multiple comparison test between the variant and the WT. 1:1:2, 5:1:5, 0.25 µg/µl and 1 µg/µl refer to the α5β1γ2 composition and total amount of RNA injected in the cells, respectively.

Sensitivity analysis	**WT**	**I247T HOM**	**T281S HOM**	**T287I HOM**	**T285K HET**
n	40	9	18	21	5
Thereof 1:1:2, 0.25 µg/µl	18	6	5	11	2
Thereof 5:1:5, 1 µg/µl	21	3	10	10	0
Thereof 1:1:2, 1 µg/µl	1	0	3	0	3
EC_{50} (Best-fit) in µM GABA	66.52	5.57	4.29	9.58	81.18
95% CI EC_{50} in µM GABA	61.27 to 72.38	1.90 to 8.53	3.53 to 5.01	8.21 to 10.94	69.55 to 94.58
Standard Error of the Mean (SEM)	0.88	1.11	0.17	0.30	5.60
P value EC_{50} (relative to WT)	<0.0001	<0.0001	<0.0001	<0.0001	>0.9999
Significance	****	****	****	****	ns

DRCs were calculated using a four-parameter logistic fit for the four variants from normalizing their concentration-dependent current responses to the average of the 1 mM GABA response of the WT for the corresponding well. Thus, the plots integrate GABA sensitivity and total response. Figure 24 gives an overview of the DRCs. It also compares the DRCs resulting from normalization to the average WT maximum response of that plate to the DRCs resulting from normalization to each cell's maximum response for the four conditions. In this comparison, I247T displayed an even stronger increase in GABA sensitivity than T281S, which stayed almost completely equal, while the T287I increase in GABA sensitivity got less extreme.

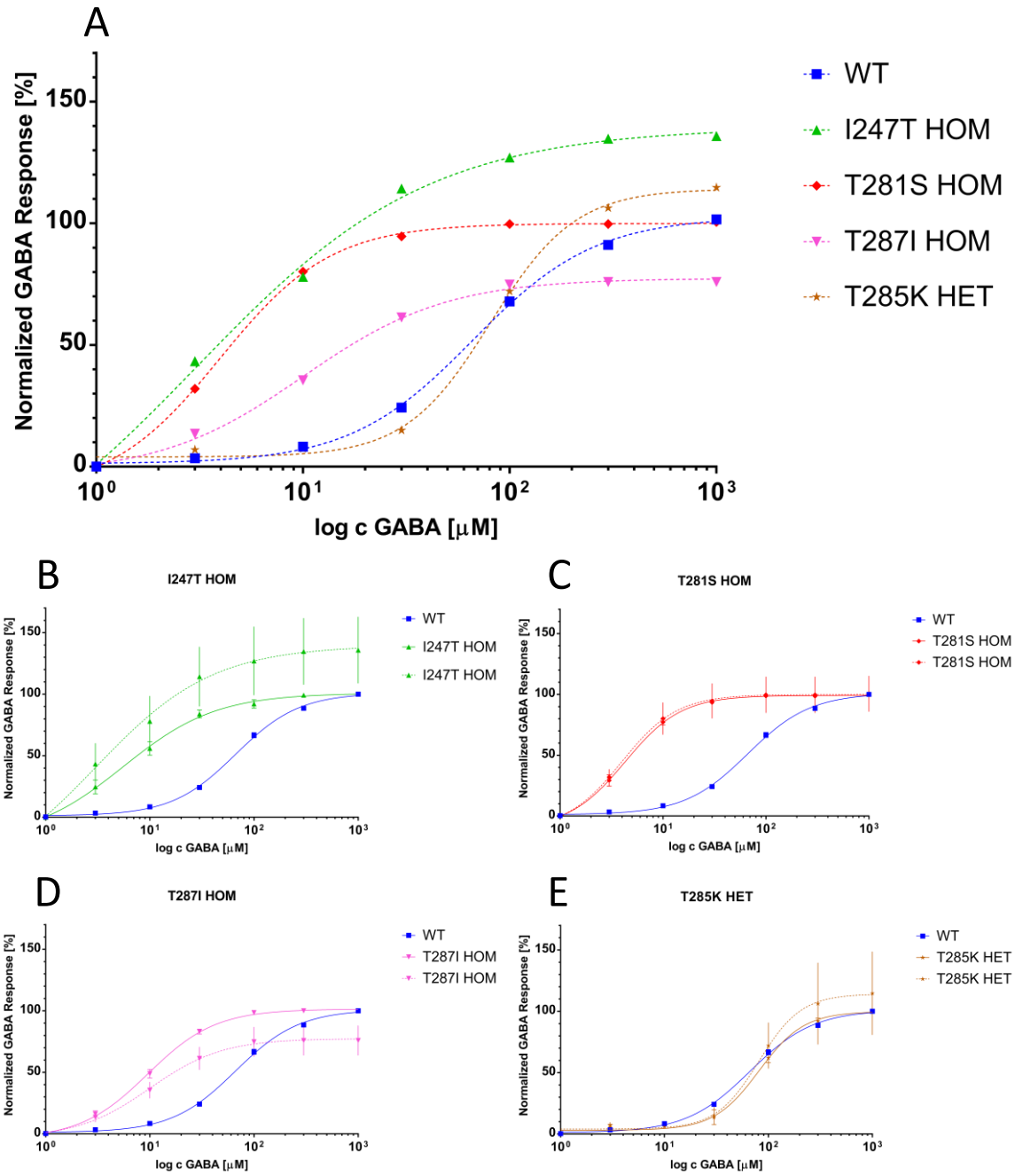

Figure 24. GABA sensitivity DRCs calculated from current responses to subsequent GABA application normalized to the average of maximum WT responses of the respective plate. Cells were recorded under the same conditions as described in Figure 23. DRCs from normalizing GABA current responses to the average of maximum WT responses of the respective plate are

represented as dotted lines. DRCs from normalizations to each cell's maximum response are depicted as continuous lines (not included in A.). Mean responses are shown as datapoints. To account for inherent noise, measured minimum responses were set to 0 for 1 µM GABA applications. **A.** gives an overview of all DRCs with the dotted line condition outlined above. SEM bars are not shown to retain clarity. **B.-E.** compare the two DRCs described above for the four respective variants. By definition, The two WT DRCs overlap and are depicted as a continuous line. SEM error bars for the dotted line are presented as a line, while SEM error bars for the straight line are presented as lines with ticks. The number of recorded cells corresponds to the information given in Table 20.

3.4.4 Summary of Electrophysiological Findings

To summarize, three variants (I247T, T281S, and T287I) did not show a significant difference in the amplitude of GABA-induced currents in response to a 1 mM GABA reference application compared to the WT channel. All three showed an increased sensitivity to GABA at lower concentrations, with a significantly lower EC_{50}.

One variant (T285K) did not show measurable currents with 1 mM GABA application, albeit with current amplitudes that were not significantly different from the WT responses when tested as a heteromeric channel by injecting a mix of WT and T285K RNA. Here, the DRC was comparable to that of the WT.

This summarizing information is presented in Table 21.

The ACMG classification considering these functional differences can be updated to 'pathogenic' due to fulfillment of the following criterion: well-established *in vitro* functional studies supportive of a damaging effect on the product (PS3).

Table 21. Summary of key functional results. The normalized maximum GABA response results are taken from the pooled analysis (Figure 20 and Table 17). For the GABA sensitivity plots, GABA responses were normalized to the maximum response for each cell (Figure 23 and Table 20). P-values were calculated using a non-parametric one-way ANOVA (Kruskal Wallis test) with Dunn's *post hoc* multiple comparison test, GoF: Gain-of-function, LoF: Loss-of-function,

ns = non-significant, HOM: homozygous recording condition (only variant subunit RNA injected), HET: heterozygous recording condition (1:1 variant and WT subunit RNA injected).

Variant	**Predicted effect**	**Measurement condition**	**Normalized maximum GABA response compared to WT (100%) [Median]**	**GABA sensitivity: Variant EC_{50} compared to WT EC_{50} (66.52 µM) [Best fit EC_{50}]**
I247T	GoF+LoF	HOM	ns, 125.80% (p>0.9999)	**GoF** 5.57 µM, 11.9-fold increase (p<0.0001)
T281S	GoF	HOM	ns, 95.03% (p>0.9999)	**GoF** 4.29 µM, 15.5-fold increase (p<0.0001)
T285K	LoF	HOM	Total **LoF** 0.49% (p<0.0001)	N/A
T285K	-	HET	ns, 121.3% (p>0.9999)	ns, 81.18 µM (p>0.9999)
T287I	GoF	HOM	ns, 52.17% (p=0.164)	**GoF** 9.58 µM, 6.9-fold increase (p<0.0001)

4 Discussion

4.1 Recapitulation of Research Goals

The primary goal of this study was to study *GABRB1* as a gene associated with genetic epilepsies, particularly DEEs. This was approached by examining the relationship between the electrophysiological features and the clinical phenotypes of the I247T, T281S, T285K, and T287I variants. Furthermore, the study aimed to compare the findings with previously reported *GABRB1* variants and corresponding variants in other $GABA_AR$ subunits.

4.2 Interpretation of Results

4.2.1 Genetic Evaluation

From analyzing the inheritance pattern as well as orthologs and paralogs and employing established scores for MAF, deleteriousness, conservation, and constraint, one can conclude that the four variants analyzed in this study likely cause functional alterations of $GABA_ARs$ which can sufficiently explain the DEE phenotypes of the variant carriers. This is due to the *de novo* character of the variants and the importance of the β1-subunit amino acids they affect.

Based on *in silico* analysis only, the predicted functional impact was least likely for the I247T variant, as it was the only variant for which the PPh2 HDIV score and the MTR score did not predict high deleteriousness and constraint, respectively. While I247 is highly conserved from nematodes to humans, it is weakly conserved among the different analyzed $GABA_AR$ subunits. This possibly implies limited functional relevance. Additionally, the modeling showed that while I247 is located at the beginning of M1 and transmembrane segments tend to be highly conserved (Maljevic et al. 2019b), it faces outwards, i.e., away from the pore, and a pathomechanistic explanation is less apparent than for T281, T285, and T287.

The latter three are all part of a TTVLTMTT motif fully conserved from nematodes to humans and in all $GABA_AR$ subunits that were evaluated. It is found towards the end of the M2 segment. The M2 segment of the five $GABA_AR$ subunits constitutes the primary segment facing inwards and composes the anion-pore

(Zhu et al. 2018). The modeling confirms that T281, T285, and T287 face inwards and might directly alter anion flux and, thereby, receptor function.

Lastly, more pathogenic variants have been reported in the molecular vicinity of this conserved motif than around the I247 area for other $GABA_AR$ subunits. This also hints at a higher functional relevance, as variants are more likely to cause phenotypic alterations and be clinically detected. Specific functional and clinical aspects of these variants will be discussed in sections 4.4 and 4.5.

4.2.2 Electrophysiological Recordings

The electrophysiological data of all four variants showed highly significant functional alterations for homozygous recording conditions. The outcome of the recordings can be classified into two categories. First, a complete LoF for T285K characterized by a total absence of measurable anion currents in response to the application of 1 mM GABA was observed. Second, a GoF characterized by a strong increase in GABA sensitivity by more than one order of magnitude compared to the WT for I247T, T281S, and T287I was shown. This strongly corroborates that the observed epileptic phenotypes are caused by the functional impairments attributed to the respective variants.

For the I247T, T281S, and T287I variants, no significant difference to the WT could be observed when comparing the normalized maximum current amplitudes in response to 1 mM GABA application. This was the case for all different conditions of injected RNAs.

One can conclude that these different compositions and total RNA amounts do not substantially influence the relative maximum GABA responses. One can also conclude that increases or reductions in maximum current response do not primarily pose the functional mechanism for altered receptor function for these variants.

Both 1:1:2 and 5:1:5 RNA injection conditions were tested for the following reasons. A 1:1:2 ratio has been established for compositions involving β-subunits and $GABA_AR$ recordings more generally (el Achkar et al. 2021; Hartiadi et al. 2016). Here, it is important to increase the fraction of γ2, with some studies

increasing it 5 or 10-fold, to reduce the number of binary αx-βx compositions forming and increase the probability of a more physiological αx-βx-γ2 composition (Boileau et al. 2002; Karim et al. 2013). Reducing the relative amount of β1, e.g., with a 5:1:5 ratio, aims to reduce the probability of β1 homomers forming (Garifulina et al. 2022). β1 homomers are known to be non-responsive to GABA and to spontaneously open (Krishek et al. 1996; Sigel et al. 1989). This caused problems during recordings for collaborators and was one key reason they aimed to control the $GABA_AR$ structure and configuration via concatenated pentamers (P. Ahring, N. Absalom, personal communication). Also, see section 4.8.1 for details.

The main functional alteration for I247T, T281S, and T287I was a significant increase in GABA sensitivity (11.9-fold for I247T, 15.5-fold for T281S, and 6.9-fold for T281S).

Several mechanisms have been proposed for causing GoF. For instance, it can be caused by increased receptor expression or altered channel properties (e.g., GABA potency, deactivation kinetics, opening probability, and duration, or tonically open channels) (Absalom et al. 2020; Janve et al. 2016; Maljevic et al. 2019b).

Little can be analyzed and interpreted for T285K based on this study's findings, as it was characterized by a complete lack of GABA response for the expression test application of 300 µM GABA. Many mechanisms have been proposed and shown to cause LoF, and without further functional analysis, explanation attempts about the nature of the T285K LoF remain speculative. For instance, alterations in channel gating (e.g., fast desensitization, slow activation onset), substantial GABA sensitivity reduction, or a reduction in channel surface expression (i.e., caused by intracellular trafficking defects, endoplasmic reticulum-associated degradation, or nonsense-mediated mRNA decay) have been proposed (Hernandez and Macdonald 2019; Hirose 2014; Maljevic et al. 2019b; Oyrer et al. 2018).

Due to the LoF in the homozygous recording condition, T285K was additionally recorded as a heterozygous condition. The heterozygous T285K condition

showed properties comparable to WT recordings for the normalized maximum GABA response, as well as the DRCs. Albeit this is hard to infer from *X. laevis* oocytes as a simple expression system, this is surprising and might suggest that the variant is causing haploinsufficiency rather than a dominant negative effect. However, it could also be explained by the fact that variant β1 subunits were not integrated into the heteropentamer, and only WT $GABA_AR$ were actually recorded.

The plausibility of haploinsufficiency as a mechanism is supported by the fact that a protein-truncating variant (c.424C>T:p.R142*) has been detected in a female individual with seizures starting in the first week of life, with otherwise very similar presentation to the studied individuals with missense variants (S. Weckhuysen, personal communication). The origin of this variant was presumed to be *de novo*. Functionally, its proximal location in the N-terminus makes non-sense-mediated decay an extremely likely outcome. Therefore, it was not included in the set of functionally studied variants.

Additionally, there is an inherited protein-truncating variant (c.343C>T:p.Q115*) in an individual with a GGE phenotype (S. Weckhuysen, personal communication). Importantly, haploinsufficiency has been previously reported in various *GABR*-genes, for instance, in *GABRA1-*, *GABRB3-*, or *GABRG2*-related seizure disorders with notable phenotypic heterogeneity (Johannesen et al. 2016; Papandreou et al. 2016; Warner et al. 2016).

4.3 Genotype-Phenotype Correlation

It has previously been shown that LoF and GoF variants segregate into two DEE groups with distinct characteristic clinical features for *GABRB3* (Absalom et al. 2022). The GoF cohort presented at a younger age (<6 months) and focal seizures at onset, higher risk of severe intellectual disability, microcephaly, hypotonia, multifocal interictal epileptic discharge (IED) in the EEG, focal seizures, and higher treatment resistance. In contrast, the LoF cohort presented at an older age (>6 months) with febrile seizures at onset, mild to moderate intellectual disability, generalized seizures, and generalized IED in the EEG. Given the congruency in this study's functional findings and previous findings

regarding single variants, it is interesting how these clinical findings correlate with the observed phenotypes and whether distinct clinical characteristics for GoF and LoF variants akin to *GABRB3* can be identified.

In short, all analyzed novel *GABRB1* individuals had *de novo* DEE variants with severe developmental delay, mostly normal MRI findings, hypotonia, and a seizure onset between the age of two and four months. Seizures were primarily dominated by tonic and focal-clonic seizures, except for the T281S individual, who had spasms. All were treatment-resistant except for the I247T individual, who was treated with VPA, VGB, CBZ, and nitrazepam.

Overall, the I247T individual had the least severe phenotype with the latest seizure onset (4 months) and, albeit being treatment-resistant during the first year, was the only one to become seizure-free within two years due to antiepileptic treatment. This aligns with the expectation that the variant was suspected to be least detrimental based on deleteriousness and constraint scores, paralog conservation, and its outwards-facing position in the M1 segment rather than the M2 pore-lining segment.

For *GABRB3* GoF variants, it has recently been shown that variants accelerating current decay kinetics lead to less severe phenotypes with later seizure onsets than those reducing desensitization at equilibrium (S. X. N. Lin et al. 2023). While it may initially seem like this could explain I247T being comparatively milder, the authors also conclude that the milder *GABRB3* variants are located in the coupling domain. However, I247T is located in the transmembrane region, which is associated with more severe phenotypes in *GABRB3*. Also, it shares similarities with the typically observed more severe phenotype, like movement disorders and migrating focal seizures.

At large, it is not possible to distinguish clinical features that differentiate the phenotypes of the T285K individuals compared to those of the I247T, T281S, and the limited information on the T287I individual. All are DEEs with largely similar characteristics, as previously summarized. When closely examining clinical characteristics, it remains hard to determine delineating features. Notably, one of the T285K individuals was the only individual with myoclonic seizures. Also, one

T285K individual only had mild hypotonia, which was more severe for the other individuals. However, there are also many similarities in the details between the T285K individuals and the other individuals, e.g., persistent treatment resistance and seizure onset at 2-3 months (like T281S and T287I bearing individuals), focal-clonic and migrating seizures (like I247T), or spasms and multifocal epileptic EEG activity (like T281S).

Ultimately, it must be concluded that no clear genotype-phenotype correlation can be established solely based on this study's findings. However, see section 4.10 on key forthcoming results revealing a T285K GoF component for additional discussion.

With the caveat that the number of reported individuals with *GABRB1* variants is too small to capture such dichotomy, these findings do not support a clear phenotypic difference between GoF and LoF *GABRB1* variants. The two LoF T285K individuals do not show any features that are reported as typical for *GABRB3* LoF individuals. Conversely, they show many clinical characteristics the study links to GoF variants, i.e., onset age <6 months, hypotonia, focal seizures, severe intellectual disability, and multifocal EEG elements. It is pertinent to note that *GABRB2* also did not show a clear genotype-phenotype pattern (el Achkar et al. 2021).

The discovery of three GoF variants (I247T, T281S, and T285K) and one LoF (T285K) in close proximity underlines that the variant-induced structural rearrangement of the $GABA_AR$ and particularly the M2 pore-forming region and its resulting functional alteration cannot be generalized but has to be individually determined for each variant.

Interestingly, due to the high conservation of the transmembrane segments across the Cys-loop superfamily (Hernandez et al. 2017; Hibbs and Gouaux 2011), these findings might not solely be of interest regarding $GABA_ARs$ but could potentially translate to, for instance, glycine, 5-HT_3 or nicotinic acetylcholine receptors.

4.4 Comparison to Other *GABRB1* Variants

4.4.1 The Functionally Characterized GABRB1 F246S Variant

Just one *GABRB1* variant has hitherto been functionally studied: 737T>C: p.Phe246Ser (Allen et al. 2013; Janve et al. 2016). This amino acid position is one position before the I247T variant studied here. The F246S variant stems from an individual who presented with focal cognitive seizures at 12 months, developing into IS at 35 months. He also experienced absences, atypical, atonic, and myoclonic seizures. The EEG showed hypsarrhythmia that later progressed to spike waves. The MRI was largely normal but revealed a thin *corpus callosum*. The individual displayed global delay, hypotonia, ataxia, as well as cortical visual impairment and regressed clinically after IS onset.

Functional studies of this variant were conducted via patch clamp in HEK 293T cells using whole-cell and single-channel techniques. Cell surface expression levels were measured via flow cytometry and did not show any reduction in α1, β3 or γ2L^{HA} subunits. In essence, current densities and current peak amplitudes only showed minor alterations. However, there were significant alterations in channel kinetics with a reduction in the current deactivation rate, a decrease in channel opening frequency, an increase in channel mean open time (3.75-fold), single channel burst duration (3.2-fold), and spontaneous channel openings. Modeling data revealed that the F246S variant caused structural rearrangements to the coupling zone domains, which propagated to the transmembrane domains (Janve et al. 2016; Miller and Aricescu 2014; Venkatachalan and Czajkowski 2012). Thus, it induced alterations of conserved domains that are important for translating GABA binding to proper channel gating. The authors hypothesized that an altered depolarizing drive could negatively impact circuit formation in CNS development due to effects on phasic inhibition and thus cause epileptic encephalopathy. Ultimately, classifying this as GoF or LoF is challenging, as the authors described GoF as well as LoF traits. A review classified the variant as partial LoF (Wei et al. 2017).

Comparing the phenotype of the *GABRB1* F246S carrier to this study's *GABRB1* I247T individual yields a mixed picture. Similarities include global developmental

delay, hypotonia, focal seizures, and the thin *corpus callosum* in MRI. Striking differences include onset age and EEG findings. Also, the F246S individual had atonic seizures, absences, and ataxia, while the I247T individual had tonic seizures, cyanosis, and. quadriplegia. As no GABA sensitivity (no DRC) analysis was conducted for the F246S variant and the more complex parameters cannot be analyzed in the TEVC *X. laevis* oocyte recordings for I247T, comparing the functional results remains inconclusive. The modeling data shows that variants in this region can perpetuate to cause large-scale structural rearrangements, which could plausibly translate to the I247T variant in this conserved region.

4.4.2 Not Functionally Characterized GABRB1 Variants

A few other reported variants have been shown or suggested to be linked to epilepsy. A c.1075G>A: p.Val359Ile (Z.-J. Lin et al. 2023) variant was linked to JME, thus presenting the first case linked to an IGE. The variant was paternally inherited (similar phenotype), onset age was 10 years with absences, myoclonic and generalized tonic-clonic seizures, generalized spike-slow wave EEG, and seizure freedom upon treatment with VPA.

Another c.1017G>C: Lys339Asn (Fernández-Marmiesse et al. 2019) variant was found in a treatment-refractory DEE individual with onset at seven months, microcephaly, and frontal brain atrophy, although it could not be confirmed to be *de novo*. The limited information available shows many similarities to the four investigated DEE variants.

Lastly, databases like NCBI ClinVar (Landrum et al. 2018) or the Epi25 WES Browser (Epi25 2019) offer insights into variants proposed as potentially pathogenic. For instance, Epi25 lists three variants in the DEE cohort of their public online database: c.1213C>T: p.Arg405Cys, c.1394A>G: p.Asn465Ser, c.766C>G: p.Leu256Val. They also list one that is not classified regarding epilepsy type: c.214A>G: Ile72Val. ClinVar lists another likely pathogenic DEE variant: c.157C>T: p.Arg53Trp. Most of these variants are in the less conserved linker region between the third and fourth transmembrane domains, and their relevance to the phenotype in the absence of functional validation remains to be clarified.

GABRB1 variants have not been prominently linked to pathologies outside of epileptology. One example includes linking variants in the M1 and M3 domains to increased alcohol consumption in mice by demonstrating spontaneous $GABA_AR$ channel openings and increases in GABA sensitivity through whole-cell voltage-clamp in brain slices (nucleus accumbens) and HEK293 cells, as well as single channel outside-out patch recordings in HEK293 cells (Anstee et al. 2013). However, the authors did not investigate potentially epileptogenic effects. Another study predicted required propofol dosages for individuals based on single nucleotide polymorphisms (SNPs) (Zheng et al. 2022).

Collating these findings with this study, one can conclude that DEEs seem to be the primary pathology associated with missense variants in *GABRB1*.

4.5 Comparison to Other $GABA_AR$ Subunit Variants

Various variants have been reported in *GABRA1-6*, *GABRB1-3*, *GABRG1-3,* and *GABRD* that relate to the *GABRB1* I247T, T281S, T285K, and T287I variants either by:

1. Corresponding in position and amino acid change.
2. Corresponding in position, but not amino acid change.
3. Being positioned closely adjacent to the position, likely in the same functional domain.

Functional findings and associated phenotypes of these variants are comprehensively displayed in Figure 15, Figure 16, Table 15, and Table 16, but will be more thoroughly discussed in the following sections.

4.5.1 Corresponding Variants in Position and Amino Acid Change

The clinical and functional data is collated from the publications quoted at the beginning of each paragraph.

No variants precisely corresponding to the T281S variant are available.

4.5.1.1 Corresponding to I247T

The following *GABRB2* variant is known *de novo* from two individuals and corresponds directly to the I247T variant: c.737T>C: p.Ile246Thr (el Achkar et al. 2021).

Both individuals had a treatment-resistant DEE with severe developmental delay, daily seizures, focal motor as well as generalized seizures. Seizure onset was between the age of two to five months. One individual was classified as a Lennox-Gastaut Syndrome (LGS)-like epilepsy syndrome, and the other as early myoclonic encephalopathy (EME)

Functional results from I246T recordings in *X. laevis* oocytes revealed reduced amplitudes of GABA-evoked currents as the primary finding. However, the DRC also indicated a GoF element with a higher GABA sensitivity than WT upon applying GABA concentrations of 0.01 to 10 µM (EC_{50} values [µM]: WT 80 ± 10 versus I246T 11 ± 3 ($p<0.0001$)). As physiological GABA concentrations during synaptic transmission are approximately 1 mM, the reduction in current amplitudes was suggested to be the primary epileptogenic mechanism, and the variant was classified as LoF.

Comparing these results to this study's findings reveals that the phenotypes are broadly comparable regarding epilepsy type, onset, seizure type, and many other clinical features. The GoF element with a significant increase in GABA sensitivity is well reflected in the data. However, a significant reduction in current amplitude as response to 1 mM GABA could not be observed. Conversely, the normalized response to 1 mM GABA was not significantly changed for the I247T variant. Concludingly, the shared increase in GABA sensitivity as a GoF element could cause the phenotypical similarity, while the LoF element might further aggravate the clinical condition for the *GABRB2* variant. Also, novel data (upcoming, currently unpublished) questions the relevance of reduced current amplitudes for pathogenicity (P. Ahring, personal communication).

4.5.1.2 Corresponding to T285K

One *GABRA2* and one *GABRB2* variant are known that correspond directly to the *GABRB1* T285K variant – *GABRA1*: c.875C>A: p.Thr292Lys (Butler et al. 2018) and *GABRB2*: c.851C>A: p.Thr284Lys (Hamdan et al. 2017).

The *GABRA2 de novo* T292K variant was carried by a DEE individual. The individual presented with seizure onset at 6 weeks, including tonic, tonic-clonic, myoclonic seizures, spasms, clustered partial seizures, severe developmental delay, microcephaly, central hypotonia, spasticity, and cerebral palsy. The condition was strongly treatment-resistant.

Functional results from T292K patch clamp recordings in HEK293T cells did not generate any GABA-evoked currents upon GABA applications at 0.3–3000 µM. The authors demonstrated that channel expression was reduced by 40% compared to the WT, and the variant led to tonically open channels with high leak currents, even without GABA application. Similar results concerning open channels and lack of GABA response were also shown for the artificial (i.e., not found in an individual) *GABRA2* T292W variant (labeled T265W there) (Ueno et al. 2000). This underlines the crucial role of this particular threonine in channel gating.

The *GABRB2 de novo* T284K variant was also carried by a DEE individual who presented with a myoclonic and tonic seizure onset on day 7. He showed severe global developmental delay and was diagnosed with EME. The condition was very treatment-resistant, and the individual passed away at the age of 17 days. No functional data are available.

These findings are congruent with clinical and functional data from this study. The tonic, tonic-clonic, and myoclonic seizures, severe developmental delay, and particularly treatment resistance are found in all individuals studied. This study also observed the total absence of GABA-evoked currents, suggesting that tonically open channels and reduced channel expression are key mechanistic explanations for why the total LoF in the *GABRB1* T285K variant was observed. However, also see section 4.10 on key forthcoming results revealing a T285K GoF component for additional discussion.

4.5.1.3 Corresponding to T287I

Variants that exactly correspond to the *GABRB1* T287I variant have been detected in *GABRA1* (c.881C>T: p.Thr294Ile (Lindy et al. 2018)), *GABRA4* (c.899C>T: p.Thr300Ile (Ahring et al. 2022b; Vogel et al. 2022), *GABRB3* (c.860C>T: p.Thr287Ile (Absalom et al. 2020; Absalom et al. 2022; Papandreou et al. 2016)) and *GABRD* (c.872C>T: p.Thr291Ile (Ahring et al. 2022a)).

No clinical or functional data is available on the *GABRA1* variant.

The *GABRA4 de novo* T300I variant was found as a somatic mosaic (17% of reads) that likely occurred at an early embryonic state. This likely explains the comparatively mild phenotype that was not classified as DEE. Seizure onset occurred at 3.5 years as clustered nocturnal focal rapidly generalizing frontal lobe motor seizures. The neurodevelopment showed a slight delay. The condition was initially treatment-resistant but ultimately controlled.

Functional results from *X. laevis* oocyte recordings revealed a 6-fold increase in maximum current amplitude, a 10-fold increase in GABA sensitivity, and an 18-fold increase in maximum estimated open probability. It also showed accelerated desensitization kinetics at higher GABA concentrations (>1 µM) but not at lower concentrations (<1 µM). The authors also showed a reduction in seizure-protective neurosteroid function. Due to α4's role in facilitating extrasynaptic long-lasting tonic inhibition at low GABA concentrations, the variant was classified as GoF based on the increases in sensitivity and current amplitudes despite the complex findings on changes in GABA concentration-dependent desensitization kinetics.

The individual carrying the *GABRB3 de novo* T287I variant was diagnosed with a treatment-resistant DEE. Seizure onset was at three months with focal tonic seizures. The individual suffered from a severe global developmental delay.

Functional results from *X. laevis* oocyte recordings reveal that while T287I does not alter absolute currents, deactivation kinetics, or estimated maximum open channel probability, it significantly increases the GABA sensitivity (EC_{50} values [µM]: WT: 69, versus T287I: 22, ($p<0.0001$)). While the previous findings stem

from a γ-β3-α1-β3-α1 construct (see sections 2.3.2 and 4.8.1 for more context), displaying a synaptic situation, T287I was also recorded in a γ-β3-α5-β3-α5 construct, mimicking mediation of extrasynaptic tonic currents. A 2-fold increase in GABA sensitivity was also shown here. The authors concluded a GoF mechanism. Further analyses in HEK293AD cells revealed reduced desensitization at equilibrium, aggravating the GoF trait (S. X. N. Lin et al. 2023).

Lastly, the *GABRD* T291I variant was discovered in a mother and her twin sons. Seizure onset was between one and four years with absences. Individuals had mild to moderate intellectual disability and developmental delay and continued to have daily treatment-resistant absences.

Functional data from *X. laevis* oocyte recordings show a large increase in the average maximum current amplitude in $(\alpha1)_2(\beta3)_2\delta$ (9-fold) and $(\alpha4)_2(\beta2)_2\delta$ (5-fold) receptors and an increase in GABA sensitivity in $(\alpha4)_2(\beta2)_2\delta$ (4-fold), but not in $(\alpha1)_2(\beta3)_2\delta$ receptors. This was attributed primarily to alterations in the gating efficiency, and the variant was classified as GoF.

Clinically, the *GABRB3* T287I individual displayed a severe DEE phenotype that was largely similar to the *GABRB1* T287I variant and additionally shared many features with the other three I247T, T281S, and T285K DEE variants. Comparing the findings regarding clinical phenotype for α and δ variants to the information known about the T287I individual is less straightforward and yields a mixed picture. Keeping in mind that *GABRA4* T300I was a mosaic, the findings were milder, whereas key features like neurodevelopmental delay and high treatment resistance prevailed. The *GABRD* T291I individuals also had milder phenotypes and absence seizures but also exhibited intractable daily seizures.

Functionally, it is striking that all studies concluded a GoF mechanism, which is congruent with this study's overall finding. While an increase in the average maximum current amplitude, like *GABRA4* T300I and *GABRD* T291I, this study also found the stark increase in GABA sensitivity that was reported for all three variants. Notably, the findings in *GABRB3*, which is most closely related to *GABRB1,* correspond closely to findings from this study, with the GABA sensitivity increase being the predominant GoF mechanism. They also observed

this with α5 units, which were also utilized for this study's recordings. This is further discussed in section 4.6. Overall, the findings underpin the locus as a functionally relevant variant hotspot.

4.5.2 Corresponding Variants in Position but not Amino Acid Change

No corresponding variants are available for I247T.

4.5.2.1 Corresponding to T281S

For T281S, three variants from two genes are known that correspond to this position but do not have the same amino acid change - *GABRB3*: c.841A>G: p.Thr281Ala and c.842C>T: p.Thr281Ile (Absalom et al. 2022) and *GABRG2*: c.929C>T: p.Thr310Ile (Yang et al. 2022).

For the two *GABRB3* variants, authors interestingly observed divergent DEE phenotypes that were explained by divergent outcomes in functional analysis. One showed a LoF, and the other showed a GoF. The GoF individual (T281A) had her seizure onset (focal, absences with frequent multifocal spikes in the EEG) at the age of less than a month, severe intellectual disability, and a treatment-resistant condition. In contrast, the LoF individual (T281I) had her seizure onset (febrile, occipital bilateral slow waves in EEG) at seven months, moderate intellectual disability, continued to have febrile, focal, and myoclonic seizures but became seizure-free upon treatment (PB, VPA, stiripentol). The classification in GoF and LoF was based on a 10.5-fold increase in GABA sensitivity for T281A and a 4-fold decrease for T281I, with no significant change in maximum current response observed. Further studies also revealed a significantly reduced desensitization at equilibrium for T281A (S. X. N. Lin et al. 2023). This illustrates how monogenic disease-causing diverging point mutations at the same amino acid position can cause a broad spectrum of phenotypes.

Only clinical data is available for the GABRG2 T310I variant. The phenotype appears mild. The individual presented with clustered febrile generalized tonic-clonic and myoclonic seizures at 8 months onset. Developmental progress was normal. LEV and VPA successfully achieved freedom from seizures.

Comparing these to the findings from this study, one can conclude that the clinical presentation of the *GABRG2* T310I individual does not match the *GABRB1* individual. However, this variant can be presumed to have a LoF effect as all hitherto functionally characterized *GABRG2* variants causing GEFS+ are LoF variants (Kang and Macdonald 2016). This fits with the findings in *GABRB3* T281I (LoF) and T281A (GoF) as well as this study's findings in T281S (GoF). The more severe phenotype of the *GABRB3* T281A GoF individual closely resembles the *GABRB1* individual, especially regarding the severe developmental delay, seizure characteristics, and resistance to treatment, whereas the T281I LoF is milder. Interestingly, this study also observed increased GABA sensitivity as the primary GoF mechanism. Together, these findings reflect the authors' main conclusion that GoF variants in *GABRB3* are associated with more severe phenotypes than LoF, and it can be observed that severe phenotypes are also associated with GoF in *GABRB1*.

4.5.2.2 Corresponding to T285K

For T285K, three variants from two genes are known that correspond to this position but do not have the same amino acid change – *GABRA1*: c.875C>T: p.Thr292Ile (Allen et al. 2013; Chen et al. 2022; Reyes-Nava et al. 2020) and c.875C>G: p.Thr292Ser (Chen et al. 2022) as well as *GABRA5*: c.896C>T: p.Thr299Ile (Charzewska et al. 2023).

The *GABRA5* T299I variant was found with maternal inheritance in an individual with epileptic seizures post-vaccination and ultimately classified as a variant of unknown significance (VUS) with no clinical or functional data available.

The first case of the *GABRA1* T292I variant was reported in a DS individual with no details available (Allen et al. 2013; Johannesen et al. 2016). A second individual with the same variant was reported that presented with seizure onset at three months and evolved into an intractable LGS with light-sensitive myoclonic epilepsy, EGTC, hypotonia, visual impairment, and developmental delay. This was in contrast to the treatment-resistant *GABRA1* T292S individual with severe neurodevelopmental delay, feeding difficulties, and visual impairment but no diagnosed somatic seizure activity.

When functionally compared in HEK293 cells, T292I reduced GABA sensitivity, decreased maximum response, and diminished single-channel open time and probability (LoF), whereas T292S increased GABA sensitivity without affecting maximal response and increased single-channel open time and probability (GoF). Also, the respective channel impairments could be largely reversed by applying thiocolchicoside for T292S and DZP plus verapamil for T292I. As previously shown for the *GABRB3* T281A and T281I variants, this underlines the wide spectrum of functional alterations and resulting clinical phenotypes that different point mutations at the same position can cause.

When comparing the clinical findings to this study's *GABRB1* T285K variant, it can be concluded that all encompassed a significant neurodevelopmental delay and were treatment-resistant. However, there were also significant differences with regard to light-sensitive seizures or lack of somatic seizures at all. Functionally, like T292I, this study also found a LoF but cannot make statements about the sensitivity or single-channel open time or probability. Also, these findings are not congruent with the tonically open channels that were previously discussed for the *GABRA2* T292K variant. As the authors showed, different point mutations at the same position can cause different functional alterations, and it is plausible that different LoF mechanisms can cause different phenotypes. Still, the *GABRB1* T285K phenotypes were more closely resembled by the T292I LoF than the T292S GoF variant.

4.5.2.3 Corresponding to T287I

For T287I, one recently discovered variant is known that corresponds to this position but does not have the same amino acid change - *GABRG1*: c.941C>A: p.T314K (Williams et al. 2022). For this variant, only clinical information is available. The phenotype can be classified as DEE. The individual suffered from global developmental delay, hypotonia, feeding difficulties, and had myoclonic seizure onset at 2.5 years. The EEG showed high amplitude generalized spike activity. LEV and CLB yielded seizure freedom. A priori, LoF, is the common disease mechanism in *GABRG2*-related epilepsies, although this is not functionally verified for this variant (Kang and Macdonald 2016). While

representing a DEE, it must be concluded that this phenotype is significantly milder than T287I.

4.5.3 Adjacent Variants in Transmembrane Domains

As previously described, the I247T variant is located in a highly conserved region right at the beginning of M1, whereas T281S, T285K, and T287I are located in a very highly conserved motif towards the end of M2. Missense burden analysis across all $GABA_AR$ subunits showed that M1 and especially M2 variants harbored particularly devastating outcomes (Maljevic et al. 2019b). This is backed by data for *GABRB1-3*, but also *GABRG1-3*, *GABRA1,* and *GABRA4-6* (el Achkar et al. 2021; Hernandez and Macdonald 2019) that highlight the mutation intolerance and absence of variants in M1 and M2 in control populations, thus implying high functional relevance.

Structural $GABA_AR$ studies reveal that the amino acid sidechains of the M2 domain from the five subunits surround the chloride channel pore and are crucial for receptor gating by causing the transition from closed to open state (Masiulis et al. 2019; Venkatachalan and Czajkowski 2012). Due to the fully conserved TTVLTMTT motif among *GABRA1-6*, *GABRB1-3*, *GABRG1-3,* and *GABRD* and a high degree of conservation in surrounding positions, the M2 region has been of significant interest.

For instance, detailed functional and modeling data of the DEE-associated *GABRB3* T288N variant (corresponds to *GABRB1* T288) showed that the threonine protrudes into the pore and causes perturbations reshaping, albeit restricted to the channel pore, altering its polarity and reducing the pore radius, thus resulting in a LoF (Hernandez et al. 2017). However, the authors' hypothesis that this would result in LoF mechanisms for other variants in the same region did not prove accurate. A functional characterization of DEE-associated *GABRB3* I280F, T281A, T281I, L284R, L284M, T287I, T288N, and L293H variants, some of which have been previously discussed, showed that every variant apart from T281I showed GoF traits characterized by a 2.8- to 17-fold increase in GABA sensitivity (Absalom et al. 2022). The authors acknowledged that M2's critical role in stabilizing $GABA_AR$ open and closed states can result in structural

rearrangements that cause GoF or LoF, although their data heavily suggested an over-representation in GoF.

For instance, GoF could be caused by greater flexibility of the alpha-helix to tilt into open conformation. LoF could be caused by channel pore occlusion by stabilizing the Leucine (L284) regarded to contain the channel gate.

Relatedly, other variants from the domain that have been functionally characterized add to this mixed picture. For instance, the DEE-associated *GABRD* I284T variant (corresponds to *GABRB1* I280) is a clear GoF due to effects on gating efficiency (Ahring et al. 2022a), but the also DEE-associated *GABRA2* L291V variant (corresponds to *GABRB1* L284) was a total LoF, with a stark reduction in current amplitudes (Maljevic et al. 2019a).

Less focus has so far been on variants in the M1 domain. One of the most thorough prior studies is elaborated on in section 4.4.1. Like M2, DEE-associated *GABRB3* variants in M1 can be GoF or LoF. For instance, Y245H, S254F, and L256Q showed a 1.7- to 3.0-fold increase, while Q249K showed a 3.4-fold decrease in GABA sensitivity, and P253L showed no difference (Absalom et al. 2022). A DS-associated *GABRA1* G251S variant (corresponds to G244 in *GABRB1*) was LoF, with a 5-fold reduction in GABA sensitivity and a 2.6-fold decrease in maximum amplitude (Carvill et al. 2014).

Overall, the GoF I247T variant fits into this mixed picture. While modeling data is needed, it can be hypothesized that, as shown for the *GABRB1* F246S variant, mutations at the start of or right before the M1 domain can cause modifications to the coupling zone domains that propagate to the transmembrane segments, resulting in GoF or LoF, based on the exact structural alteration.

Generally, compared to other regions, variants in the M1 and M2 segments were often linked with severe DEE phenotypes (el Achkar et al. 2021; Yang et al. 2020). Also, in *GABRB3*, GoF variants were linked to more severe DEE phenotypes than LoF (Absalom et al. 2022). Lastly, *GABRB3* variants in the M1 and M2 segments were linked to the most severe GoF phenotypes due to their influence on receptor desensitization (S. X. N. Lin et al. 2023).

4.6 Possible Causative Epilepsy Mechanism

To this end, it can be concluded that all variants analyzed in this study cause severe DEEs by causing either a LoF or GoF. This is in line with the literature finding many severe DEEs from variants in M1 and particularly M2 in other $GABA_AR$ subunits caused by LoF or GoF, dependent on the exact structural rearrangement of the receptor. The question remains: how do these LoF or GoF mechanisms lead to the observed epileptic phenotype?

Hitherto, LoF mechanisms have posed the predominant characteristic associated with $GABA_AR$ variants (Absalom et al. 2023; Maljevic et al. 2019b). While exact details remain unsolved, the proposed explanation is that a reduction of the $GABA_AR$-mediated inhibitory function leads to neuronal hyperexcitability, resulting in seizures (Baulac et al. 2001; Bianchi et al. 2002; Møller et al. 2017; Niturad et al. 2017; Orsini et al. 2018; Wei et al. 2017). Here, it is important to highlight the complex and intricate mechanisms by which GABAergic interneuron subclasses can influence the circuit-level excitation-inhibition balance across space and time (Cardin 2018; Tremblay et al. 2016).

The predominance of LoF mechanisms in epileptogenesis was recently challenged by the discovery of a multitude of epilepsy-associated *GABRD* and *GABRB3* GoF variants and considerations on how this can be reconciled with overall CNS hyperexcitability (Absalom et al. 2020; Absalom et al. 2022; Absalom et al. 2023; Ahring et al. 2022a). While the authors acknowledge that more detailed studies are required, they point to the complex role of δ-subunit-containing receptors and the GoF-caused increase in tonic inhibition in reducing or increasing neuronal activity based on neuronal subtype and excitability state in circuits associated with epilepsy (Bryson et al. 2020; Song et al. 2011). For β3, the authors highlight its role in early brain development where GABA acts as a major excitatory and depolarizing neurotransmitter and the resulting effect on neuronal circuit formation that was shown to include pro-convulsive states (Ben-Ari 2006; Fillman et al. 2010; Pavlov and Walker 2013). This is in line with a study showing that epilepsy-associated LoF variants associated with the GABA uptake transporter gene *SLC6A1* result in accumulating synaptic GABA, causing

activation of synaptic and extrasynaptic $GABA_AR$s and suggests these converge on the same pathogenic pathway (Mattison et al. 2018).

Similarly, not just GoF but also tonically open channels, potentially arising from the *GABRB1* T285K variant, could lead to pathologically high levels of depolarization signals altering tonic GABAergic currents important for proper brain development and thus inducing epileptic phenotypes. This general mechanism has hitherto been more widely acknowledged (Butler et al. 2018; Lee and Maguire 2014).

For β1, one can draw many parallels to β3, with both being widely expressed in developing and adult brains, although β1 expression begins somewhat later at around birth (Laurie et al. 1992). Both subunits are abundant in neuronal circuits strongly associated with seizure generation, where they mediate tonic (perisynaptic) and phasic (synaptic) inhibition, for instance, in the cortex, hippocampus, and thalamic reticular neurons (Hörtnagl et al. 2013). As crucial elements of human brain development and circuit formation, particularly hippocampal and cortical, continue postnatal (Stiles and Jernigan 2010; van Dyck and Morrow 2017), it can be hypothesized that similar effects as for β3 regarding control of neuronal proliferation, migration, integration, differentiation, and synaptic growth (Represa and Ben-Ari 2005) facilitate the formation of abnormal neuronal networks. Additionally, given that the reported *GABRB3* and the *GABRB1* GoF individuals had severe DEE phenotypes, this offers an explanation not only related to epileptic seizures but to the global developmental delay and intellectual disability more generally.

Ultimately, this study's findings prove that similar GoF scenarios exist for *GABR* genes outside of *GABRD* and *GABRB3* and contribute to underlining this paradigmatic shift in understanding $GABA_AR$-associated epileptogenesis.

4.7 Clinical Implications

The high complexity of $GABA_AR$-associated epileptogenesis and findings that different amino acid changes at the same position can lead to LoF or GoF mechanisms, taken together with the significant divergence in clinical

presentation, calls for a treatment approach that requires personalized precision medicine (Knowles et al. 2022; Krey et al. 2022).

The distinct functional mechanisms observed for the individuals carrying the I247T, T281S, and T287I GoF variants versus those carrying the T285K LoF variant suggest that distinct ASM treatment might be warranted. In contrast, the strong phenotypical similarities should caution against drawing strong conclusions for the proposed ASM regimen from this functional result alone (see section 4.10).

It was suggested that drugs increasing GABAergic inhibition, for instance, PB, VGB, neurosteroids, or benzodiazepines, should be avoided in individuals carrying GoF variants. This has been underlined by cases where treatment with VGB in a *GABRB3* GoF individual and PB and CZP in a *GABRA5* GoF variant aggravated the respective clinical condition (Absalom et al. 2020; Butler et al. 2018).

Also, limited data shows that sodium channel inhibitors (for instance, CBZ) can improve clinical outcomes in *GABRB3* GoF variants while partly worsening outcomes in *GABRB3* LoF variants (Absalom et al. 2022). Discussions among leading clinicians propose sodium channel inhibitors might be a promising treatment option for $GABA_AR$ GoF variants more generally (H. Lerche, personal communication). Notably, *SCN1A* GoF variants have been associated with a DEE phenotype very similar to the individuals in this study, which suggests potential functional parallels in pathogenicity and the efficacy of sodium channel inhibitors (Brunklaus et al. 2022).

Conversely, drugs increasing GABAergic tone can successfully be employed in individuals with LoF variants. Unfortunately, a lot of ASM involves increasing GABAergic inhibition, and pharmacological studies and drug discovery have seldom focused on medication decreasing GABAergic activity. Thus, current treatment options are limited to ASM, which utilizes other functional mechanisms but does not increase GABAergic tone, such as LEV, lamotrigine, or CBS. Novel substances, like negative allosteric $GABA_AR$ modulators, are greatly needed.

This study thus suggests that no substances that increase GABAergic inhibition should be prescribed in the individuals carrying the I247T, T281S, and T287I GoF variants.

The T281S individual is currently treated with LEV, which is favorable, and the I247T individual with CBZ and VPA. As VPA increases GABAergic inhibition (Safdar and Ismail 2023; Singh et al. 2021), one would, in theory, propose a change in the treatment regimen. However, the individual is currently seizure-free, so a change in the regimen is not acutely warranted.

No treatment information is available for the T287I individual.

The condition of the two individuals carrying the T285K variant is heavily treatment-resistant. Unfortunately, drugs increasing GABAergic inhibition, like benzodiazepines, have not improved the individuals' conditions, and treatment of the corresponding *GABRA2* T292K variant with PB, VGB, VPA, or CLB did not yield any improvement (Butler et al. 2018).

However, this study recommends trying more GABAergic substances. Also, it must be noted that the variant potentially inducing tonically open channels can plausibly result in allosteric modulators like benzodiazepines not working. $GABA_AR$ blockers like bicuculline or picrotoxin are only used in pharmacological studies, whereas flumazenil could pose a therapeutic option (Johnston 2013).

It should also be noted that the physiological dynamics will be more complex with WT and mutant receptors, as well as receptors not expressing β1 being affected by the drug. Substances like pyrazoloquinolinones that selectively modulate receptors containing β1 subunits pose a promising approach on the way to personalized precision therapy, although they are currently only used in pharmacological studies (Simeone et al. 2017). Novel substances that selectively modulate GABAergic currents at $GABA_ARs$ containing particular subunits more generally, as well as antisense oligonucleotide therapy, pose promising approaches for personalized precision medicine targeting $GABA_AR$ dysfunction (Absalom et al. 2023).

4.8 Limitations

4.8.1 Controlling the $GABA_AR$ Structure and Configuration

An inherent problem of injecting separate RNA strands, each encoding one subunit, is that due to the complex heteromeric structure of the $GABA_AR$, receptors of variable subunit types, ratios, and orientations can form (Liao et al. 2019). This complicates the accurate interpretation of resulting functional data. For instance, homomeric receptors (comprised of five times the same subunit) can form in theory. Heteromeric binary, ternary, or quaternary (i.e., comprised of two, three, or four subunit types, respectively) have been shown to exist physiologically, although not all theoretical combinations of the 19 subunit types are found in the brain (Olsen and Sieghart 2008). Knowing the exact subunit type, ratio, and orientation is important as ligand binding sites can typically be found at subunit interfaces, for instance, benzodiazepines at the α-γ interface and GABA at the β-α interface (Zhu et al. 2018).

A technique to control receptor arrangement and stoichiometry is subunit concatenation. This implies introducing a linker segment fusing the C-terminus and the N-terminus of subsequent subunits to express them as one. The modification at the cDNA level eliminates the respective stop codons. The subunits are then transcribed to the respective RNA and translated as one. Informed by modeling, linkers are designed to allow for appropriate protein folding. However, concerns have been raised that relate to proteolysis, linker length, loop-outs, effectively controlling counter- and counterclockwise assembly, and curtailing downstream signal-peptide sequences (Ericksen and Boileau 2007; Sigel et al. 2009).

Most concatenated constructs used in $GABA_AR$ research have consisted of dimeric or trimeric subunit assemblies (Baumann et al. 2001; Botzolakis et al. 2016; Im et al. 1995; Minier and Sigel 2004; Shu et al. 2012). While they pose an improvement compared to free subunit recordings in controlling structure and configuration, they do not offer a physiological condition and still have some limitations mentioned above, especially regarding clock- and counterclockwise orientation and multiple assembly possibilities.

To offer full control over assembly conditions, Ahring and colleagues proposed a variety of pentameric concatenated constructs in 2019 (Liao et al. 2019). Similar constructs were created for *GABRB1* (γ2-β1-α1-β1-α1) as it was originally intended to utilize these for the TEVC recordings in *X. laevis* oocytes (see section 2.3.2 for details). Unfortunately, this was conducted before the W117C and I429N variants were detected in the commercially attained *GABRB1* sequence (see section 0). This likely explains why the *X. laevis* TEVC oocyte recordings with the pentamer containing two alleged WT *GABRB1* sequences, like those of non-concatenated RNA injections derived from this *GABRB1*, did not yield any currents upon GABA application (data not shown). Unfortunately, it was not possible to repeat WT nor variant pentamer construct recordings with the corrected (C117W and N429I) *GABRB1* sequences, as finalizing the complex cloning process for the corrected pentamer was hindered by considerable time constraints.

However, our collaborators recorded various *GABRB1* variants in concatenated γ2-β1-α1-β1-α1 pentamers in the context of a joint follow-up study (see section 4.10).

4.8.2 TEVC Recording Conditions

To allow for an even more accurate and nuanced recording and plotting of GABA sensitivity DRCs, recordings could have included applications of lower GABA concentrations, i.e., 0.3, 0.1, 0.03, and 0.001 µM. However, this comes at the cost of longer recordings and exposure of the remaining oocytes to room temperature, increasing the risk of necrosis.

Also, homozygous conditions for I247T, T281S, and T287I should optimally have been supplemented by respective recordings of heterozygous conditions.

Lastly, all recordings were conducted in an α5β1γ2 composition. However, the modeling was done with α1 instead of α5 as this was the structural model available. As α1 is the most ubiquitous alpha-subunit, it would have been better suited to mimic this in recordings. However, initial pilot recordings yielded high leak currents in an α1β1γ2 composition, so α5 was ultimately selected, as it is still sufficiently expressed in the brain, and its usage is well-established in-house.

4.8.3 Validation and Quantification of Protein Expression

Another shortcoming of this study was that no Western Blots or other protein detection techniques were performed to verify and quantify $GABA_AR$ protein expression on the oocyte surface. This is especially relevant for the T285K variant, as the possibility remains that the total LoF was caused by methodological errors from variant cloning through RNA preparation to receptor expression and is not an inherent property of the variant.

As all the other variants yielded GABA currents, protein imaging was less relevant, albeit favorable, for them.

4.8.4 Eukaryotic and Neuronal Expression Systems

Although *X. laevis* oocytes are a well-established heterologous expression system for initial functional TEVC studies (Karim et al. 2013), they are not commonly used for more nuanced electrophysiological studies, like channel kinetics or rapid GABA application, which are often studied in HEK 293 cells for $GABA_AR$ variants (although outside-out patch clamp recordings of oocytes are possible). Such studies would be crucial for fully characterizing the GoF variants, for instance, with regard to desensitization. Also, oocytes do not offer physiological conditions like neurons. It would, for instance, be interesting to assess the expression of the T285K LoF variant via immunostaining and imaging or investigate synaptic transmission and plasticity.

4.9 Potential Further Research

The results of this study call for several potential follow-up studies.

This study could be improved by performing protein expression analyses, e.g., Western Blots, to verify $GABA_AR$ expression.

A thorough electrophysiological characterization via patch clamp that allows for fast GABA application, for instance, in a heterologous system like HEK 293T cells (Janve et al. 2016), could unveil the exact mechanisms causing the GoF or LoF. This could involve analyzing gating kinetics in an ultra-fast application system (Krampfl et al. 1998; Krampfl et al. 2005) for the GoF variants or the potentially tonically open channels in the T285K variant. The findings can then be compared

to previous analyses of the *GABRB1* F246S or *GABRA2* T292K variants (Butler et al. 2018; Janve et al. 2016).

Studies in a physiological, homologous expression system like neurons, for instance, in cultured hippocampal neurons, acute brain slices, or iPSC-derived neurons, would present the first of its kind in *GABRB1* variants and further contribute to establishing this as an epilepsy-associated gene. This allows for studying synaptic transmission, brain network effects, surface expression, and more thorough electrophysiological studies (Eugene et al. 2007).

An orthogonal step toward physiological human conditions includes establishing a mouse model, which could also be used for acute brain slices (Reid et al. 2013).

Indeed, as it was initially planned to select one or two variants based on initial functional *X. laevis* TEVC results and perform patch-clamp recordings in cultivated murine hippocampal neurons or HEK 293 cells, an appropriate pCMV6-*GABRB1* vector with an eGFP tag was successfully constructed (see section 2.3.3 and Figure 8). The N-terminal eGFP tag could potentially alter the protein structure, although previous testing of similarly structured β2 constructs showed fluorescence patterns suggestive of normal membrane localization (data not shown). Due to the time constraint, patch clamp experiments were not completed, but they would be valuable to conduct in the future.

Given the variety of outcomes in previous modeling work on structural rearrangements of the $GABA_AR$ and particularly the pore-region dependent on the exact variant, detailed modeling data for the four novel *GABRB1* variants could be crucial in unraveling how exactly the channel function is being altered. In the long term, protein structure prediction tools like AlphaFold (Jumper et al. 2021) could be employed to accurately predict GoF or LoF effects of specific variants, reducing the need for resource-consuming functional studies and allowing for timely individualized treatment proposals.

Aggregating clinical data on and functionally characterizing the remaining *GABRB1* variants that have been reported is crucial to fully understanding the epileptogenic role of *GABRB1*. Here, it would be particularly interesting to

compare if the *GABRB3* finding, linking LoF to milder DEE phenotypes and GoF to more severe DEE phenotypes, can be translated to *GABRB1* (Absalom et al. 2022). Moreover, for *GABRB3* GoF variants, a recent study differentiated two phenotype groups with distinct clinical characteristics based on different receptor desensitization properties. Variants that reduced desensitization at equilibrium were associated with more severe clinical outcomes, while variants accelerating current decay kinetics were associated with comparatively milder, albeit still severe, phenotypes (S. X. N. Lin et al. 2023). Investigating desensitization in mammalian cell lines might thus be promising to potentially further differentiate genotype-phenotype correlations in *GABRB1* GoF variants.

In conclusion, this study underpins the recent paradigmatic shift of acknowledging the role of $GABA_AR$ subunit GoF variants in epileptogenesis. This calls for network-level studies investigating how this apparent conundrum can be resolved.

As the ultimate goal is improving therapeutic options for individuals, complementing studies focused on personalizing medicines investigating the effects of previously discussed experimental or approved therapeutics like flumazenil, bicuculline, picrotoxin, pyrazoloquinolinones, VGB, benzodiazepines, antisense oligonucleotides, as well as novel and potentially superior drug candidates will be of great importance.

4.10 Forthcoming Results Revealing T285K Variant GoF Component

Based on the functional results gathered in this study, the previous discussion and conclusion treated the T285K variant as a total LoF.

However, as shown in a forthcoming manuscript (Millevert / Kan / Hanke (shared first authorship) et al., unpublished), collaborators A. S. H. Kan, M. Chebib and P. Ahring (all Brain and Mind Centre, School of Medical Sciences, Faculty of Medicine and Health, The University of Sydney, Sydney, New South Wales, Australia) conducted *X. laevis* TEVC recordings of concatenated γ2-β1*-α1-β1-α1 pentamers (where β1* is either a mutant β1 or a WT subunit, see section 2.3.2) for several *GABRB1* variants, including the I247T, T281S, T285K and T287I variants that were analyzed in this study. Notably, $GABA_ARs$ in the

concatenated pentamers contained one mutant β1 and one WT β1, while receptors in this study were recorded with two mutant β1 (referred to as homozygous condition) except for the T285K heterozygous recordings (i.e., half of the injected β1 RNA carried the variant).

Results for the I247T, T281S, and T287I recordings in concatenated pentamers mirrored the increase in GABA sensitivity GoF effect observed in this study.

However, our collaborators observed a very strong, almost 100-fold, increase in GABA sensitivity for the T285K variant without significant decreases in normalized peak current amplitude responses to 10 mM GABA, ultimately classifying the variant as GoF (data not shown). They also observed the receptors displaying constitutive activity.

Given the similarity between the T285K and I247T, T281S, and T287I DEE phenotypes, this observed GoF effect offers a crucial piece of information that allows for establishing a clear genotype-phenotype correlation between *GABRB1* GoF variants and severe DEE phenotypes, akin to as it was established for *GABRB3* (Absalom et al. 2022).

Similarly, the question arises: what caused the discrepancy between LoF results from this study and their GoF findings? Besides methodological errors, this could be explained by a stronger constitutive activity of receptors that carry two mutant β1 subunits than the concatenated pentamers that only carried one. This strong constitutive activity would cause the receptor to lack a current response to any GABA stimulus, as observed in this study and interpreted as LoF. Also, the variant can pose a mix of GoF and LoF effects, which are known to cause particularly severe DEE phenotypes, for instance, in *KCNA2* (Masnada et al. 2017).

Studies in homologous expression systems, like neurons, would allow insights into how $GABA_A$Rs assemble physiologically regarding β1 subunits carrying the T285K variant, given the artificial nature of concatenated pentamers. Accompanying electrophysiological studies could illuminate details of GoF and LoF mechanisms potentially involved in pathogenicity.

4.11 Final Remarks

Using *X. laevis* oocyte TEVC recordings, it was shown that the *GABRB1* variants I247T, T281S, T285K, and T287I, located in highly conserved regions and associated with severe DEEs, cause severe alterations in functional outcomes. T285K causes a total LoF with absence of GABA-evoked responses (however, our collaborators were subsequently able to show a T285K GoF effect; forthcoming manuscript, see section 4.10), and I247T, T281S, and T287I cause a GoF in the form of a 6.9 to 15.5-fold increase in GABA sensitivity. Thus, this study corroborates the causation between the genetic alteration and the observed phenotype that was already suggested by the variants' *de novo* occurrence and their localization in highly conserved $GABA_AR$ regions. With only one previous functional study available, this fully establishes *GABRB1* as a gene linked to epilepsy and severe developmental problems. While it was not possible to clearly establish a genotype-phenotype correlation based solely on findings in this study, supplementing this with our collaborators' GoF results for the T285K variant establishes a link between *GABRB1* GoF variants and severe DEEs and underpins the paradigmatic shift towards acknowledging the role of $GABA_AR$ subunit GoF variants in epileptogenesis. Currently, while sodium channel inhibitors should generally be attempted, the implications of these findings on clinical treatment remain limited and underline the future effort required to ultimately allow for personalized precision medicine, improving affected individuals' outcomes.

5 Summary

Severe epilepsies with developmental delay and intellectual disability are caused by variants in genes involved in neurotransmission. A rare cause includes epileptogenic variants in the subunits of the GABA receptor type A ($GABA_AR$), the mammalian brain's most important inhibitory ligand-gated ion channels.

This study presents four individuals with severe developmental and epileptic encephalopathies (DEEs), carrying three new variants in highly conserved regions of the *GABRB1* gene, encoding the ubiquitously expressed β1 subunit: c.740T>C:p.Ile247Thr, c.841A>T:p.Thr281Ser and c.854C>A:p.Thr285Lys. Including a previously reported DEE-associated variant, c.860C>T:p.Thr287Ile, this study assessed ortholog and paralog conservation, compared the variants to previously reported $GABA_AR$ subunit variants, assembled the respective bacterial vectors, synthesized and injected subunit mRNA, and functionally expressed mutant and wild-type channels *in vitro* in *X. laevis* oocytes. GABA responses were recorded via two-electrode voltage clamp recordings to assess the functional mechanisms that link the genetic findings and epileptic phenotypes.

T285K caused a total loss-of-function (LoF) with absence of GABA-evoked responses, while I247T, T281S, and T287I caused a gain-of-function (GoF) with a stark (6.9-15.5-fold) increase in GABA sensitivity. Collaborators later showed a strong (~100-fold) GABA sensitivity increase GoF effect for T285K. Supplementing this study's findings, this establishes a clear genotype-phenotype correlation between *GABRB1* GoF variants and severe DEEs, as previously shown for other $GABA_AR$ subunit variants, notably *GABRB3*.

With only one *GABRB1* variant previously functionally characterized, this fully establishes *GABRB1* as a gene linked to DEEs and epilepsy in general. This study's findings underpin the paradigmatic shift towards acknowledging the role of $GABA_AR$ GoF variants in epileptogenesis. This calls for further studies and a more nuanced view of the predominant explanation that LoF-induced reduction of $GABA_AR$-mediated neuronal inhibition causes hyperexcitability, resulting in epileptic seizures. With few therapeutic options available today, particularly for GoF patients, studies exploring novel treatment approaches are greatly needed.

6 Deutsche Zusammenfassung

Schwere Epilepsien mit Entwicklungsverzögerungen werden durch Mutationen in Genen verursacht, die an der Neurotransmission beteiligt sind. Eine seltene Ursache sind hierbei epileptogene Varianten in den Untereinheiten des GABA-Rezeptors Typ A ($GABA_AR$), einem der wichtigsten inhibitorischen, ligandengesteuerten Ionenkanäle des Gehirns.

Diese Studie präsentiert vier Individuen mit schweren entwicklungsbedingten und epileptischen Enzephalopathien (DEEs), die drei neue Varianten in hochkonservierten Regionen des *GABRB1*-Gens aufweisen, das für die ubiquitär exprimierte β1-Untereinheit kodiert: c.740T>C:p.Ile247Thr, c.841A>T:p.Thr281Ser und c.854C>A:p.Thr285Lys. Einschließlich einer zuvor beschriebenen DEE-assoziierten Variante, c.860C>T:p.Thr287Ile, wurden die Varianten hinsichtlich orthologer und paraloger Konservierung evaluiert, mit zuvor beschriebenen Varianten in $GABA_AR$-Untereinheiten verglichen, entsprechende bakterielle Vektoren kloniert, mRNA synthetisiert und injiziert und mutierte sowie Wildtyp-Kanäle *in vitro* in *X. laevis* Oozyten exprimiert. Mittels Zwei-Elektroden-Spannungsklemme wurden hiervon GABA-induzierte Ströme aufgezeichnet, um die funktionalen Mechanismen zwischen genetischem Befund und epileptischem Phänotyp zu evaluieren.

T285K verursachte einen totalen Funktionsverlust (LoF) mit Mangel an GABA-induzierten Strömen, wohingegen I247T, T281S und T287I einen Funktionsgewinn (GoF) mit starker Zunahme (6,9-15,5-facher Verstärkung) der GABA-Potenz vorwiesen. Kollaborationspartner zeigten später eine starke (~100-fache) Zunahme der GABA Potenz, entsprechend einem GoF für T285K. Ergänzend zu den Erkenntnissen dieser Studie, etabliert dies eine Genotyp-Phänotyp Korrelation zwischen *GABRB1* GoF-Varianten and schweren DEEs, wie sie bereits für Varianten in anderen $GABA_AR$ Untereinheiten, insbesondere *GABRB3* demonstriert wurde.

Bei nur einer zuvor funktionell charakterisierten *GABRB1*-Variante wurde *GABRB1* hierbei vollständig als ein mit DEEs und Epilepsie im Allgemeinen assoziiertem Gen etabliert. Die Ergebnisse dieser Studie untermauern den

Paradigmenwechsel hin zur Anerkennung der Rolle von $GABA_AR$ GoF-Varianten in der Epileptogenese. Dies impliziert, neben der Notwendigkeit weiterer Studien um diese Mechanismen zu untersuchen, eine nuanciertere Sichtweise der gängigen Erklärung, dass eine LoF-induzierte Reduktion der $GABA_AR$-vermittelten neuronalen Hemmung Übererregbarkeit verursacht, die zu epileptischen Anfällen führt. Insbesondere für GoF-Patienten sind aktuell wenige therapeutische Optionen verfügbar und Studien, die neue Behandlungsansätze erforschen, verbleiben dringend erforderlich.

7 References

Absalom, N. L., Liao, V. W. Y., Johannesen, K. M. H., Gardella, E., Jacobs, J., Lesca, G., Gokce-Samar, Z., Arzimanoglou, A., Zeidler, S., Striano, P., Meyer, P., Benkel-Herrenbrueck, I., Mero, I.-L., Rummel, J., Chebib, M., Møller, R. S. and Ahring, P. K. (2022). Gain-of-function and loss-of-function GABRB3 variants lead to distinct clinical phenotypes in patients with developmental and epileptic encephalopathies. Nat Commun *13*, 1822, doi:10.1038/s41467-022-29280-x.

Absalom, N. L., Liao, V. W. Y., Kothur, K., Indurthi, D. C., Bennetts, B., Troedson, C., Mohammad, S. S., Gupta, S., McGregor, I. S., Bowen, M. T., Lederer, D., Mary, S., De Waele, L., Jansen, K., Gill, D., Kurian, M. A., McTague, A., Møller, R. S., Ahring, P. K., Dale, R. C. and Chebib, M. (2020). Gain-of-function GABRB3 variants identified in vigabatrin-hypersensitive epileptic encephalopathies. Brain Commun *2*, fcaa162, doi:10.1093/braincomms/fcaa162.

Absalom, N. L., Lin, S. X. N., Liao, V. W. Y., Chua, H. C., Møller, R. S., Chebib, M. and Ahring, P. K. (2023). GABAA receptors in epilepsy: Elucidating phenotypic divergence through functional analysis of genetic variants. J Neurochem, doi:10.1111/jnc.15932.

Adzhubei, I. A., Schmidt, S., Peshkin, L., Ramensky, V. E., Gerasimova, A., Bork, P., Kondrashov, A. S. and Sunyaev, S. R. (2010). A method and server for predicting damaging missense mutations. Nat Methods *7*, 248–249, doi:10.1038/nmeth0410-248.

Ahring, P. K., Liao, V. W. Y., Gardella, E., Johannesen, K. M., Krey, I., Selmer, K. K., Stadheim, B. F., Davis, H., Peinhardt, C., Koko, M., Coorg, R. K., Syrbe, S., Bertsche, A., Santiago-Sim, T., Diemer, T., Fenger, C. D., Platzer, K., Eichler, E. E., Lerche, H., Lemke, J. R., Chebib, M. and Møller, R. S. (2022a). Gain-of-function variants in GABRD reveal a novel pathway for neurodevelopmental disorders and epilepsy. Brain *145*, 1299–1309, doi:10.1093/brain/awab391.

Ahring, P. K., Liao, V. W. Y., Lin, S., Absalom, N. L., Chebib, M. and Møller, R. S. (2022b). The de novo GABRA4 p.Thr300Ile variant found in a patient with early-onset intractable epilepsy and neurodevelopmental abnormalities displays gain-of-function traits. Epilepsia *63*, 2439–2441, doi:10.1111/epi.17358.

Allen, A. S., Berkovic, S. F., Cossette, P., Delanty, N., Dlugos, D., Eichler, E. E., Epstein, M. P., Glauser, T., Goldstein, D. B., Han, Y., Heinzen, E. L., Hitomi, Y., Howell, K. B., Johnson, M. R., Kuzniecky, R., Lowenstein, D. H., Lu, Y.-F., Madou, M. R. Z., Marson, A. G., Mefford, H. C., Nieh, S. E., O'Brien, T. J., Ottman, R., Petrovski, S., Poduri, A., Ruzzo, E. K., Scheffer, I. E., Sherr, E. H., Yuskaitis, C. J., Abou-Khalil, B., Alldredge, B. K., Bautista, J. F., Berkovic, S. F., Boro, A., Cascino, G. D., Consalvo,

D., Crumrine, P., Devinsky, O., Dlugos, D., Epstein, M. P., Fiol, M., Fountain, N. B., French, J., Friedman, D., Geller, E. B., Glauser, T., Glynn, S., Haut, S. R., Hayward, J., Helmers, S. L., Joshi, S., Kanner, A., Kirsch, H. E., Knowlton, R. C., Kossoff, E. H., Kuperman, R., Kuzniecky, R., Lowenstein, D. H., McGuire, S. M., Motika, P. V., Novotny, E. J., Ottman, R., Paolicchi, J. M., Parent, J. M., Park, K., Poduri, A., Scheffer, I. E., Shellhaas, R. A., Sherr, E. H., Shih, J. J., Singh, R., Sirven, J., Smith, M. C., Sullivan, J., Thio, L. L., Venkat, A., Vining, E. P. G., Allmen, G. K. V., Weisenberg, J. L., Widdess-Walsh, P. and Winawer, M. R. (2013). De novo mutations in epileptic encephalopathies. Nature *501*, 217–221, doi:10.1038/nature12439.

Anstee, Q. M., Knapp, S., Maguire, E. P., Hosie, A. M., Thomas, P., Mortensen, M., Bhome, R., Martinez, A., Walker, S. E., Dixon, C. I., Ruparelia, K., Montagnese, S., Kuo, Y.-T., Herlihy, A., Bell, J. D., Robinson, I., Guerrini, I., McQuillin, A., Fisher, E. M. C., Ungless, M. A., Gurling, H. M. D., Morgan, M. Y., Brown, S. D. M., Stephens, D. N., Belelli, D., Lambert, J. J., Smart, T. G. and Thomas, H. C. (2013). Mutations in the Gabrb1 gene promote alcohol consumption through increased tonic inhibition. Nat Commun *4*, 2816, doi:10.1038/ncomms3816.

Baulac, S., Huberfeld, G., Gourfinkel-An, I., Mitropoulou, G., Beranger, A., Prud'homme, J. F., Baulac, M., Brice, A., Bruzzone, R. and LeGuern, E. (2001). First genetic evidence of GABA(A) receptor dysfunction in epilepsy: a mutation in the gamma2-subunit gene. Nat Genet *28*, 46–48, doi:10.1038/ng0501-46.

Baumann, S. W., Baur, R. and Sigel, E. (2001). Subunit Arrangement of γ-Aminobutyric Acid Type A Receptors. J Biol Chem *276*, 36275–36280, doi:10.1074/jbc.M105240200.

Beghi, E. (2020). The Epidemiology of Epilepsy. Neuroepidemiology *54*, 185–191, doi:10.1159/000503831.

Ben-Ari, Y. (2002). Excitatory actions of gaba during development: the nature of the nurture. Nat Rev Neurosci *3*, 728–739, doi:10.1038/nrn920.

Ben-Ari, Y. (2006). Seizures beget seizures: the quest for GABA as a key player. Crit Rev Neurobiol *18*, 135–144, doi:10.1615/critrevneurobiol.v18.i1-2.140.

Berkovic, S. F., Howell, R. A., Hay, D. A. and Hopper, J. L. (1998). Epilepsies in twins: genetics of the major epilepsy syndromes. Ann Neurol *43*, 435–445, doi:10.1002/ana.410430405.

Berman, H. M., Westbrook, J., Feng, Z., Gilliland, G., Bhat, T. N., Weissig, H., Shindyalov, I. N. and Bourne, P. E. (2000). The Protein Data Bank. Nucleic Acids Res *28*, 235–242, doi:10.1093/nar/28.1.235.

Bianchi, M. T., Song, L., Zhang, H. and Macdonald, R. L. (2002). Two Different Mechanisms of Disinhibition Produced by GABAA Receptor Mutations Linked to Epilepsy in Humans. J Neurosci *22*, 5321–5327, doi:10.1523/JNEUROSCI.22-13-05321.2002.

Boileau, A. J., Baur, R., Sharkey, L. M., Sigel, E. and Czajkowski, C. (2002). The relative amount of cRNA coding for γ2 subunits affects stimulation by benzodiazepines in GABAA receptors expressed in Xenopus oocytes. Neuropharmacology *43*, 695–700, doi:10.1016/S0028-3908(02)00036-9.

Botzolakis, E. J., Gurba, K. N., Lagrange, A. H., Feng, H.-J., Stanic, A. K., Hu, N. and Macdonald, R. L. (2016). Comparison of γ-Aminobutyric Acid, Type A (GABAA), Receptor αβγ and αβδ Expression Using Flow Cytometry and Electrophysiology: Evidence for alternative subunit stoichiometries and arrangements. J Biol Chem *291*, 20440–20461, doi:10.1074/jbc.M115.698860.

Brunklaus, A., Feng, T., Brünger, T., Perez-Palma, E., Heyne, H., Matthews, E., Semsarian, C., Symonds, J. D., Zuberi, S. M., Lal, D. and Schorge, S. (2022). Gene variant effects across sodium channelopathies predict function and guide precision therapy. Brain *145*, 4275–4286, doi:10.1093/brain/awac006.

Bryson, A., Hatch, R. J., Zandt, B.-J., Rossert, C., Berkovic, S. F., Reid, C. A., Grayden, D. B., Hill, S. L. and Petrou, S. (2020). GABA-mediated tonic inhibition differentially modulates gain in functional subtypes of cortical interneurons. Proc Natl Acad Sci U S A *117*, 3192–3202, doi:10.1073/pnas.1906369117.

Burgess, R., Wang, S., McTague, A., Boysen, K. E., Yang, X., Zeng, Q., Myers, K. A., Rochtus, A., Trivisano, M., Gill, D., Consortium, E., Sadleir, L. G., Specchio, N., Guerrini, R., Marini, C., Zhang, Y.-H., Mefford, H. C., Kurian, M. A., Poduri, A. H. and Scheffer, I. E. (2019). The Genetic Landscape of Epilepsy of Infancy with Migrating Focal Seizures. Ann Neurol *86*, 821–831, doi:10.1002/ana.25619.

Butler, K. M., Moody, O. A., Schuler, E., Coryell, J., Alexander, J. J., Jenkins, A. and Escayg, A. (2018). De novo variants in GABRA2 and GABRA5 alter receptor function and contribute to early-onset epilepsy. Brain *141*, 2392–2405, doi:10.1093/brain/awy171.

Cardin, J. A. (2018). Inhibitory Interneurons Regulate Temporal Precision and Correlations in Cortical Circuits. Trends Neurosci *41*, 689–700, doi:10.1016/j.tins.2018.07.015.

Carvill, G. L., Weckhuysen, S., McMahon, J. M., Hartmann, C., Møller, R. S., Hjalgrim, H., Cook, J., Geraghty, E., O'Roak, B. J., Petrou, S., Clarke, A., Gill, D., Sadleir, L. G., Muhle, H., Spiczak, S. von, Nikanorova, M., Hodgson, B. L., Gazina, E. V., Suls, A., Shendure, J., Dibbens, L. M.,

Jonghe, P. D., Helbig, I., Berkovic, S. F., Scheffer, I. E. and Mefford, H. C. (2014). GABRA1 and STXBP1: Novel genetic causes of Dravet syndrome. Neurology *82*, 1245–1253, doi:10.1212/WNL.0000000000000291.

Catterall, W. A. (2018). Dravet Syndrome: A Sodium Channel Interneuronopathy. Curr Opin Physiol *2*, 42–50, doi:10.1016/j.cophys.2017.12.007.

Charzewska, A., Terczyńska, I., Lipiec, A., Mazurczak, T., Górka-Skoczylas, P., Szlendak, R., Kanabus, K., Tataj, R., Dawidziuk, M., Wojtaś, B., Gielniewski, B., Bal, J., Stawicka, E. and Hoffman-Zacharska, D. (2023). Genetic Risk Factors for Neurological Disorders in Children with Adverse Events Following Immunization: A Descriptive Study of a Polish Case Series. Int J Mol Sci *24*, 1117, doi:10.3390/ijms24021117.

Chen, W., Ge, Y., Lu, J., Melo, J., So, Y. W., Juneja, R., Liu, L. and Wang, Y. T. (2022). Distinct Functional Alterations and Therapeutic Options of Two Pathological De Novo Variants of the T292 Residue of GABRA1 Identified in Children with Epileptic Encephalopathy and Neurodevelopmental Disorders. Int J Mol Sci *23*, 2723, doi:10.3390/ijms23052723.

Chunn, L. M., Nefcy, D. C., Scouten, R. W., Tarpey, R. P., Chauhan, G., Lim, M. S., Elenitoba-Johnson, K. S. J., Schwartz, S. A. and Kiel, M. J. (2020). Mastermind: A Comprehensive Genomic Association Search Engine for Empirical Evidence Curation and Genetic Variant Interpretation. Front Genet *11:577152*, doi:10.3389/fgene.2020.577152.

ClinVar (2023). 2023 VCV000205523.2 - ClinVar - NCBI, , URL: https://www.ncbi.nlm.nih.gov/clinvar/variation/205523/ [Accessed May 2023].

Cossette, P., Liu, L., Brisebois, K., Dong, H., Lortie, A., Vanasse, M., Saint-Hilaire, J.-M., Carmant, L., Verner, A., Lu, W.-Y., Wang, Y. T. and Rouleau, G. A. (2002). Mutation of GABRA1 in an autosomal dominant form of juvenile myoclonic epilepsy. Nat Genet *31*, 184–189, doi:10.1038/ng885.

Crunelli, V. and Leresche, N. (2002). Childhood absence epilepsy: Genes, channels, neurons and networks. Nat Rev Neurosci *3*, 371–382, doi:10.1038/nrn811.

Cunningham, F., Allen, J. E., Allen, J., Alvarez-Jarreta, J., Amode, M. R., Armean, I. M., Austine-Orimoloye, O., Azov, A. G., Barnes, I., Bennett, R., Berry, A., Bhai, J., Bignell, A., Billis, K., Boddu, S., Brooks, L., Charkhchi, M., Cummins, C., Da Rin Fioretto, L., Davidson, C., Dodiya, K., Donaldson, S., El Houdaigui, B., El Naboulsi, T., Fatima, R., Giron, C. G., Genez, T., Martinez, J. G., Guijarro-Clarke, C., Gymer, A., Hardy, M.,

Hollis, Z., Hourlier, T., Hunt, T., Juettemann, T., Kaikala, V., Kay, M., Lavidas, I., Le, T., Lemos, D., Marugán, J. C., Mohanan, S., Mushtaq, A., Naven, M., Ogeh, D. N., Parker, A., Parton, A., Perry, M., Piližota, I., Prosovetskaia, I., Sakthivel, M. P., Salam, A. I. A., Schmitt, B. M., Schuilenburg, H., Sheppard, D., Pérez-Silva, J. G., Stark, W., Steed, E., Sutinen, K., Sukumaran, R., Sumathipala, D., Suner, M.-M., Szpak, M., Thormann, A., Tricomi, F. F., Urbina-Gómez, D., Veidenberg, A., Walsh, T. A., Walts, B., Willhoft, N., Winterbottom, A., Wass, E., Chakiachvili, M., Flint, B., Frankish, A., Giorgetti, S., Haggerty, L., Hunt, S. E., IIsley, G. R., Loveland, J. E., Martin, F. J., Moore, B., Mudge, J. M., Muffato, M., Perry, E., Ruffier, M., Tate, J., Thybert, D., Trevanion, S. J., Dyer, S., Harrison, P. W., Howe, K. L., Yates, A. D., Zerbino, D. R. and Flicek, P. (2022). Ensembl 2022. Nucleic Acids Res *50*, D988–D995, doi:10.1093/nar/gkab1049.

Davydov, E. V., Goode, D. L., Sirota, M., Cooper, G. M., Sidow, A. and Batzoglou, S. (2010). Identifying a high fraction of the human genome to be under selective constraint using GERP++. PLoS Comput Biol *6*, e1001025, doi:10.1371/journal.pcbi.1001025.

De Vivo, D. C., Trifiletti, R. R., Jacobson, R. I., Ronen, G. M., Behmand, R. A. and Harik, S. I. (1991). Defective Glucose Transport across the Blood-Brain Barrier as a Cause of Persistent Hypoglycorrhachia, Seizures, and Developmental Delay. New Engl J Med *325*, 703–709, doi:10.1056/NEJM199109053251006.

Dean, M., Lucas-Derse, S., Bolos, A., O'Brien, S. J., Kirkness, E. F., Fraser, C. M. and Goldman, D. (1991). Genetic mapping of the beta 1 GABA receptor gene to human chromosome 4, using a tetranucleotide repeat polymorphism. Am J Hum Genet *49*, 621–626.

Dewey, F. E., Murray, M. F., Overton, J. D., Habegger, L., Leader, J. B., Fetterolf, S. N., O'Dushlaine, C., Van Hout, C. V., Staples, J., Gonzaga-Jauregui, C., Metpally, R., Pendergrass, S. A., Giovanni, M. A., Kirchner, H. L., Balasubramanian, S., Abul-Husn, N. S., Hartzel, D. N., Lavage, D. R., Kost, K. A., Packer, J. S., Lopez, A. E., Penn, J., Mukherjee, S., Gosalia, N., Kanagaraj, M., Li, A. H., Mitnaul, L. J., Adams, L. J., Person, T. N., Praveen, K., Marcketta, A., Lebo, M. S., Austin-Tse, C. A., Mason-Suares, H. M., Bruse, S., Mellis, S., Phillips, R., Stahl, N., Murphy, A., Economides, A., Skelding, K. A., Still, C. D., Elmore, J. R., Borecki, I. B., Yancopoulos, G. D., Davis, F. D., Faucett, W. A., Gottesman, O., Ritchie, M. D., Shuldiner, A. R., Reid, J. G., Ledbetter, D. H., Baras, A. and Carey, D. J. (2016). Distribution and clinical impact of functional variants in 50,726 whole-exome sequences from the DiscovEHR study. Science *354*, aaf6814, doi:10.1126/science.aaf6814.

Dibbens, L. M. (2004). GABRD encoding a protein for extra- or peri-synaptic GABAA receptors is a susceptibility locus for generalized epilepsies. Hum Mol Genet *13*, 1315–1319, doi:10.1093/hmg/ddh146.

el Achkar, C. M., Harrer, M., Smith, L., Kelly, M., Iqbal, S., Maljevic, S., Niturad, C. E., Vissers, L. E. L. M., Poduri, A., Yang, E., Lal, D., Lerche, H., Møller, R. S. and Olson, H. E. (2021). Characterization of the GABRB2 associated neurodevelopmental disorders. Ann Neurol *89*, 573–586, doi:10.1002/ana.25985.

Epi25 (2019). Ultra-Rare Genetic Variation in the Epilepsies: A Whole-Exome Sequencing Study of 17,606 Individuals. Am J Hum Genet *105*, 267–282, doi:https://doi.org/10.1016/j.ajhg.2019.05.020.

Ericksen, S. S. and Boileau, A. J. (2007). Tandem couture. Mol Neurobiol *35*, 113–127, doi:10.1007/BF02700627.

Eugene, E., Depienne, C., Baulac, S., Baulac, M., Fritschy, J. M., Guern, E. L., Miles, R. and Poncer, J. C. (2007). GABA(A) receptor gamma 2 subunit mutations linked to human epileptic syndromes differentially affect phasic and tonic inhibition. J Neurosci *27*, 14108–14116, doi:10.1523/JNEUROSCI.2618-07.2007.

Fernández-Marmiesse, A., Roca, I., Díaz-Flores, F., Cantarín, V., Pérez-Poyato, M. S., Fontalba, A., Laranjeira, F., Quintans, S., Moldovan, O., Felgueroso, B., Rodríguez-Pedreira, M., Simón, R., Camacho, A., Quijada, P., Ibanez-Mico, S., Domingno, M. R., Benito, C., Calvo, R., Pérez-Cejas, A., Carrasco, M. L., Ramos, F., Couce, M. L., Ruiz-Falcó, M. L., Gutierrez-Solana, L. and Martínez-Atienza, M. (2019). Rare Variants in 48 Genes Account for 42% of Cases of Epilepsy With or Without Neurodevelopmental Delay in 246 Pediatric Patients. Front Neurosci *13:1135*, doi:10.3389/fnins.2019.01135.

Fillman, S. G., Duncan, C. E., Webster, M. J., Elashoff, M. and Weickert, C. S. (2010). Developmental co-regulation of the β and γ GABAA receptor subunits with distinct α subunits in the human dorsolateral prefrontal cortex. Int J Dev Neurosci *28*, 513–519, doi:10.1016/j.ijdevneu.2010.05.004.

Fisher, R. S., Acevedo, C., Arzimanoglou, A., Bogacz, A., Cross, J. H., Elger, C. E., Engel, J., Forsgren, L., French, J. A., Glynn, M., Hesdorffer, D. C., Lee, B. I., Mathern, G. W., Moshé, S. L., Perucca, E., Scheffer, I. E., Tomson, T., Watanabe, M. and Wiebe, S. (2014). ILAE Official Report: A practical clinical definition of epilepsy. Epilepsia *55*, 475–482, doi:10.1111/epi.12550.

Garifulina, A., Friesacher, T., Stadler, M., Zangerl-Plessl, E.-M., Ernst, M., Stary-Weinzinger, A., Willam, A. and Hering, S. (2022). β subunits of GABAA receptors form proton-gated chloride channels: Insights into the molecular basis. Commun Biol *5*, 784, doi:10.1038/s42003-022-03720-2.

Guerrini, R., Balestrini, S., Wirrell, E. C. and Walker, M. C. (2021). Monogenic Epilepsies. Neurology *97*, 817–831, doi:10.1212/WNL.0000000000012744.

Guerrini, R., Conti, V., Mantegazza, M., Balestrini, S., Galanopoulou, A. S. and Benfenati, F. (2023). Developmental and epileptic encephalopathies: from genetic heterogeneity to phenotypic continuum. Physiol Rev *103*, 433–513, doi:10.1152/physrev.00063.2021.

Gutierrez, A., Khan, Z. U. and Blas, A. D. (1994). Immunocytochemical localization of gamma 2 short and gamma 2 long subunits of the GABAA receptor in the rat brain. J Neurosci *14*, 7168–7179, doi:10.1523/JNEUROSCI.14-11-07168.1994.

Hamdan, F. F., Myers, C. T., Cossette, P., Lemay, P., Spiegelman, D., Laporte, A. D., Nassif, C., Diallo, O., Monlong, J., Cadieux-Dion, M., Dobrzeniecka, S., Meloche, C., Retterer, K., Cho, M. T., Rosenfeld, J. A., Bi, W., Massicotte, C., Miguet, M., Brunga, L., Regan, B. M., Mo, K., Tam, C., Schneider, A., Hollingsworth, G., FitzPatrick, D. R., Donaldson, A., Canham, N., Blair, E., Kerr, B., Fry, A. E., Thomas, R. H., Shelagh, J., Hurst, J. A., Brittain, H., Blyth, M., Lebel, R. R., Gerkes, E. H., Davis-Keppen, L., Stein, Q., Chung, W. K., Dorison, S. J., Benke, P. J., Fassi, E., Corsten-Janssen, N., Kamsteeg, E.-J., Mau-Them, F. T., Bruel, A.-L., Verloes, A., Ounap, K., Wojcik, M. H., Albert, D. V. F., Venkateswaran, S., Ware, T., Jones, D., Liu, Y.-C., Mohammad, S. S., Bizargity, P., Bacino, C. A., Leuzzi, V., Martinelli, S., Dallapiccola, B., Tartaglia, M., Blumkin, L., Wierenga, K. J., Purcarin, G., O'Byrne, J. J., Stockler, S., Lehman, A., Keren, B., Nougues, M.-C., Mignot, C., Auvin, S., Nava, C., Hiatt, S. M., Bebin, M., Shao, Y., Scaglia, F., Lalani, S. R., Frye, R. E., Jarjour, I. T., Jacques, S., Boucher, R.-M., Riou, E., Srour, M., Carmant, L., Lortie, A., Major, P., Diadori, P., Dubeau, F., D'Anjou, G., Bourque, G., Berkovic, S. F., Sadleir, L. G., Campeau, P. M., Kibar, Z., Lafreniere, R. G., Girard, S. L., Mercimek-Mahmutoglu, S., Boelman, C., Rouleau, G. A., Scheffer, I. E., Mefford, H. C., Andrade, D. M., Rossignol, E., Minassian, B. A. and Michaud, J. L. (2017). High Rate of Recurrent De Novo Mutations in Developmental and Epileptic Encephalopathies. Am J Hum Genet *101*, 664–685, doi:10.1016/j.ajhg.2017.09.008.

Hartiadi, L. Y., Ahring, P. K., Chebib, M. and Absalom, N. L. (2016). High and low GABA sensitivity α4β2δ GABAA receptors are expressed in Xenopus laevis oocytes with divergent stoichiometries. Biochem Pharmacol *103*, 98–108, doi:10.1016/j.bcp.2015.12.021.

Hedrich, U. B. S., Lauxmann, S., Wolff, M., Synofzik, M., Bast, T., Binelli, A., Serratosa, J. M., Martínez-Ulloa, P., Allen, N. M., King, M. D., Gorman, K. M., Zeev, B. B., Tzadok, M., Wong-Kisiel, L., Marjanovic, D., Rubboli, G., Sisodiya, S. M., Lutz, F., Ashraf, H. P., Torge, K., Yan, P., Bosselmann, C., Schwarz, N., Fudali, M. and Lerche, H. (2021). 4-Aminopyridine is a promising treatment option for patients with gain-of-

function KCNA2-encephalopathy. Sci Transl Med *13*, eaaz4957, doi:10.1126/scitranslmed.aaz4957.

Hernandez, C. C. and Macdonald, R. L. (2019). A structural look at GABAA receptor mutations linked to epilepsy syndromes. Brain Res *1714*, 234–247, doi:10.1016/j.brainres.2019.03.004.

Hernandez, C. C., XiangWei, W., Hu, N., Shen, D., Shen, W., Lagrange, A. H., Zhang, Y., Dai, L., Ding, C., Sun, Z., Hu, J., Zhu, H., Jiang, Y. and Macdonald, R. L. (2019). Altered inhibitory synapses in de novo GABRA5 and GABRA1 mutations associated with early onset epileptic encephalopathies. Brain *142*, 1938–1954, doi:10.1093/brain/awz123.

Hernandez, C. C., Zhang, Y., Hu, N., Shen, D., Shen, W., Liu, X., Kong, W., Jiang, Y. and Macdonald, R. L. (2017). GABA A Receptor Coupling Junction and Pore GABRB3 Mutations are Linked to Early-Onset Epileptic Encephalopathy. Sci Rep *7*, 15903, doi:10.1038/s41598-017-16010-3.

Hibbs, R. E. and Gouaux, E. (2011). Principles of activation and permeation in an anion-selective Cys-loop receptor. Nature *474*, 54–60, doi:10.1038/nature10139.

Hirose, S. (2014). Mutant GABA(A) receptor subunits in genetic (idiopathic) epilepsy. Prog Brain Res *213*, 55–85, doi:10.1016/B978-0-444-63326-2.00003-X.

Hörtnagl, H., Tasan, R. O., Wieselthaler, A., Kirchmair, E., Sieghart, W. and Sperk, G. (2013). Patterns of mRNA and protein expression for 12 GABAA receptor subunits in the mouse brain. Neuroscience *236*, 345–372, doi:10.1016/j.neuroscience.2013.01.008.

Im, W. B., Pregenzer, J. F., Binder, J. A., Dillon, G. H. and Alberts, G. L. (1995). Chloride Channel Expression with the Tandem Construct of α6-β2 GABAA Receptor Subunit Requires a Monomeric Subunit of α6 or γ2. J Biol Chem *270*, 26063–26066, doi:10.1074/jbc.270.44.26063.

Ioannidis, N. M., Rothstein, J. H., Pejaver, V., Middha, S., McDonnell, S. K., Baheti, S., Musolf, A., Li, Q., Holzinger, E., Karyadi, D., Cannon-Albright, L. A., Teerlink, C. C., Stanford, J. L., Isaacs, W. B., Xu, J., Cooney, K. A., Lange, E. M., Schleutker, J., Carpten, J. D., Powell, I. J., Cussenot, O., Cancel-Tassin, G., Giles, G. G., MacInnis, R. J., Maier, C., Hsieh, C.-L., Wiklund, F., Catalona, W. J., Foulkes, W. D., Mandal, D., Eeles, R. A., Kote-Jarai, Z., Bustamante, C. D., Schaid, D. J., Hastie, T., Ostrander, E. A., Bailey-Wilson, J. E., Radivojac, P., Thibodeau, S. N., Whittemore, A. S. and Sieh, W. (2016). REVEL: An Ensemble Method for Predicting the Pathogenicity of Rare Missense Variants. Am J Hum Genet *99*, 877–885, doi:10.1016/j.ajhg.2016.08.016.

Ishii, A., Kang, J.-Q., Schornak, C. C., Hernandez, C. C., Shen, W., Watkins, J. C., Macdonald, R. L. and Hirose, S. (2017). A de novo missense mutation of GABRB2 causes early myoclonic encephalopathy. J Med Genet *54*, 202–211, doi:10.1136/jmedgenet-2016-104083.

Janve, V. S., Hernandez, C. C., Verdier, K. M., Hu, N. and Macdonald, R. L. (2016). Epileptic encephalopathy de novo GABRB mutations impair gamma-aminobutyric acid type A receptor function. Ann Neurol *79*, 806–825, doi:10.1002/ana.24631.

Jauss, R.-T., Schließke, S. and Jamra, R. A. (2022). Routine Diagnostics Confirm Novel Neurodevelopmental Disorders. Genes-Basel *13*, doi:10.3390/genes13122305.

Johannesen, K., Marini, C., Pfeffer, S., Moller, R. S., Dorn, T., Niturad, C. E., Gardella, E., Weber, Y., Sondergard, M., Hjalgrim, H., Nikanorova, M., Becker, F., Larsen, L. H. G., Dahl, H. A., Maier, O., Mei, D., Biskup, S., Klein, K. M., Reif, P. S., Rosenow, F., Elias, A. F., Hudson, C., Helbig, K. L., Schubert-Bast, S., Scordo, M. R., Craiu, D., Djemie, T., Hoffman-Zacharska, D., Caglayan, H., Helbig, I., Serratosa, J., Striano, P., Jonghe, P. D., Weckhuysen, S., Suls, A., Muru, K., Talvik, I., Talvik, T., Muhle, H., Borggraefe, I., Rost, I., Guerrini, R., Lerche, H., Lemke, J. R., Rubboli, G. and Maljevic, S. (2016). Phenotypic spectrum of GABRA1: From generalized epilepsies to severe epileptic encephalopathies. Neurology *87*, 1140–1151, doi:10.1212/WNL.0000000000003087.

Johnston, G. A. (2013). Advantages of an antagonist: bicuculline and other GABA antagonists. Brit J Pharmacol *169*, 328–336, doi:10.1111/bph.12127.

Jumper, J., Evans, R., Pritzel, A., Green, T., Figurnov, M., Ronneberger, O., Tunyasuvunakool, K., Bates, R., Žídek, A., Potapenko, A., Bridgland, A., Meyer, C., Kohl, S. A. A., Ballard, A. J., Cowie, A., Romera-Paredes, B., Nikolov, S., Jain, R., Adler, J., Back, T., Petersen, S., Reiman, D., Clancy, E., Zielinski, M., Steinegger, M., Pacholska, M., Berghammer, T., Bodenstein, S., Silver, D., Vinyals, O., Senior, A. W., Kavukcuoglu, K., Kohli, P. and Hassabis, D. (2021). Highly accurate protein structure prediction with AlphaFold. Nature *596*, 583–589, doi:10.1038/s41586-021-03819-2.

Kang, J.-Q. and Macdonald, R. L. (2016). GABRG2 Mutations Associated with a spectrum of epilepsy syndromes from Generalized Absence Epilepsy to Dravet syndrome. JAMA Neurol *73*, 1009–1016, doi:10.1001/jamaneurol.2016.0449.

Karczewski, K., Francioli, L., Tiao, G., Cummings, B., Alföldi, J., Wang, Q., ... and MacArthur, D. (2020). The mutational constraint spectrum quantified from variation in 141,456 humans. Nature *581*, 434–443, doi:https://doi.org/10.1038/s41586-020-2308-7.

Karim, N., Wellendorph, P., Absalom, N., Johnston, G. A. R., Hanrahan, J. R. and Chebib, M. (2013). Potency of GABA at human recombinant GABAA receptors expressed in Xenopus oocytes: a mini review. Amino Acids *44*, 1139–1149, doi:10.1007/s00726-012-1456-y.

Knowles, J. K., Helbig, I., Metcalf, C. S., Lubbers, L. S., Isom, L. L., Demarest, S., Goldberg, E. M., George, A. L., Lerche, H., Weckhuysen, S., Whittemore, V., Berkovic, S. F. and Lowenstein, D. H. (2022). Precision medicine for genetic epilepsy on the horizon: Recent advances, present challenges, and suggestions for continued progress. Epilepsia *63*, 2461–2475, doi:10.1111/epi.17332.

Kodera, H., Ohba, C., Kato, M., Maeda, T., Araki, K., Tajima, D., Matsuo, M., Hino-Fukuyo, N., Kohashi, K., Ishiyama, A., Takeshita, S., Motoi, H., Kitamura, T., Kikuchi, A., Tsurusaki, Y., Nakashima, M., Miyake, N., Sasaki, M., Kure, S., Haginoya, K., Saitsu, H. and Matsumoto, N. (2016). De novo GABRA1 mutations in Ohtahara and West syndromes. Epilepsia *57*, 566–573, doi:10.1111/epi.13344.

Koko, M., Krause, R., Sander, T., Bobbili, D. R., Nothnagel, M., May, P., Lerche, H., and Epi25 Collaborative (2021). Distinct gene-set burden patterns underlie common generalized and focal epilepsies. EBioMedicine *72*, 103588, doi:10.1016/j.ebiom.2021.103588.

Krampfl, K., Lepier, A., Jahn, K., Franke, C. and Bufler, J. (1998). Molecular modulation of recombinant rat α1β2γ2 GABAA receptor channels by diazepam. Neurosci Lett *256*, 143–146, doi:10.1016/S0304-3940(98)00767-8.

Krampfl, K., Maljevic, S., Cossette, P., Ziegler, E., Rouleau, G. A., Lerche, H. and Bufler, J. (2005). Molecular analysis of the A322D mutation in the GABA receptor alpha-subunit causing juvenile myoclonic epilepsy. Eur J Neurosci *22*, 10–20, doi:10.1111/j.1460-9568.2005.04168.x.

Krey, I., Platzer, K., Esterhuizen, A., Berkovic, S. F., Helbig, I., Hildebrand, M. S., Lerche, H., Lowenstein, D., Møller, R. S., Poduri, A., Sadleir, L., Sisodiya, S. M., Weckhuysen, S., Wilmshurst, J. M., Weber, Y., Lemke, J. R., Berkovic, S. F., Cross, J. H., Helbig, I., Lerche, H., Lowenstein, D., Mefford, H. C., Perucca, P., Tan, N. C. K., Caglayan, H., Helbig, K., Singh, G., Weber, Y. and Weckhuysen, S. (2022). Current practice in diagnostic genetic testing of the epilepsies. Epileptic Disord *24*, 765–786, doi:10.1684/epd.2022.1448.

Krishek, B. J., Moss, S. J. and Smart, T. G. (1996). Homomeric beta 1 gamma-aminobutyric acid A receptor-ion channels: evaluation of pharmacological and physiological properties. Mol Pharmacol *49*, 494–504.

Lal, D., May, P., Perez-Palma, E., Samocha, K. E., Kosmicki, J. A., Robinson, E. B., Møller, R. S., Krause, R., Nürnberg, P., Weckhuysen, S., De

Jonghe, P., Guerrini, R., Niestroj, L. M., Du, J., Marini, C., Balling, R., Barisic, N., Baulac, S., Caglayan, H., Craiu, D. C., De Jonghe, P., Depienne, C., Guerrini, R., Helbig, I., Hjalgrim, H., Hoffman-Zacharska, D., Jähn, J., Klein, K. M., Koeleman, B. P. C., Komarek, V., Krause, R., Leguern, E., Lehesjoki, A.-E., Lemke, J. R., Lerche, H., Linnankivi, T., Marini, C., May, P., Muhle, H., Pal, D. K., Palotie, A., Rosenow, F., Schubert-Bast, S., Selmer, K., Serratosa, J. M., Stephani, U., Štěrbová, K., Striano, P., Suls, A., Talvik, T., von Spiczak, S., Weber, Y. G., Weckhuysen, S., Zara, F., Ware, J. S., Kurki, M., Gormley, P., Tang, S., Wu, S., Biskup, S., Poduri, A., Neubauer, B. A., Koeleman, B. P. C., Helbig, K. L., Weber, Y. G., Helbig, I., Majithia, A. R., Palotie, A., Daly, M. J., and EuroEPINOMICS-RES Consortium (2020). Gene family information facilitates variant interpretation and identification of disease-associated genes in neurodevelopmental disorders. Genome Med *12*, 28, doi:10.1186/s13073-020-00725-6.

Landrum, M. J., Lee, J. M., Benson, M., Brown, G. R., Chao, C., Chitipiralla, S., Gu, B., Hart, J., Hoffman, D., Jang, W., Karapetyan, K., Katz, K., Liu, C., Maddipatla, Z., Malheiro, A., McDaniel, K., Ovetsky, M., Riley, G., Zhou, G., Holmes, J. B., Kattman, B. L. and Maglott, D. R. (2018). ClinVar: improving access to variant interpretations and supporting evidence. Nucleic Acids Res *46*, D1062–D1067, doi:10.1093/nar/gkx1153.

Laurie, D. J., Wisden, W. and Seeburg, P. H. (1992). The distribution of thirteen GABAA receptor subunit mRNAs in the rat brain. III. Embryonic and postnatal development. J Neurosci *12*, 4151–4172, doi:10.1523/JNEUROSCI.12-11-04151.1992.

Lee, V. and Maguire, J. (2014). The impact of tonic GABAA receptor-mediated inhibition on neuronal excitability varies across brain region and cell type. Front Neural Circuits *8*, 3, doi:10.3389/fncir.2014.00003.

Liao, V. W. Y., Chua, H. C., Kowal, N. M., Chebib, M., Balle, T. and Ahring, P. K. (2019). Concatenated γ-aminobutyric acid type A receptors revisited: Finding order in chaos. J Gen Physiol *151*, 798–819, doi:10.1085/jgp.201812133.

Lien, E., Våtevik, A. K., Østern, R., Haukanes, B. I. and Houge, G. (2016). A second patient with a De Novo *GABRB1* mutation and epileptic encephalopathy: Letter to the Editor. Ann Neurol *80*, 311–312, doi:10.1002/ana.24699.

Lin, S. X. N., Ahring, P. K., Keramidas, A., Liao, V. W. Y., Møller, R. S., Chebib, M. and Absalom, N. L. (2023). Correlations of receptor desensitization of gain-of-function GABRB3 variants with clinical severity. Brain awad285, doi:10.1093/brain/awad285.

Lin, Z.-J., Li, B., Lin, P.-X., Song, W., Yan, L.-M., Meng, H. and He, N. (2023). Clinical application of trio-based whole-exome sequencing in idiopathic generalized epilepsy. Seizure, doi:10.1016/j.seizure.2023.02.011.

Lindy, A. S., Stosser, M. B., Butler, E., Downtain-Pickersgill, C., Shanmugham, A., Retterer, K., Brandt, T., Richard, G. and McKnight, D. A. (2018). Diagnostic outcomes for genetic testing of 70 genes in 8565 patients with epilepsy and neurodevelopmental disorders. Epilepsia *59*, 1062–1071, doi:10.1111/epi.14074.

Luscher, B., Fuchs, T. and Kilpatrick, C. L. (2011). GABAA Receptor Trafficking-Mediated Plasticity of Inhibitory Synapses. Neuron *70*, 385–409, doi:10.1016/j.neuron.2011.03.024.

Maljevic, S., Keren, B., Aung, Y. H., Forster, I. C., Mignot, C., Buratti, J., Lafitte, A., Freihuber, C., Rodan, L. H., Bergin, A., Hubert, L., Poirier, K., Munnich, A., Besmond, C., Hauser, N., Miller, R., McWalter, K., Nabbout, R., Héron, D., Leguern, E., Depienne, C., Petrou, S. and Nava, C. (2019a). Novel GABRA2 variants in epileptic encephalopathy and intellectual disability with seizures. Brain *142*, e15, doi:10.1093/brain/awz079.

Maljevic, S., Møller, R. S., Reid, C. A., Perez-Palma, E., Lal, D., May, P. and Lerche, H. (2019b). Spectrum of GABAA receptor variants in epilepsy. Curr Opin Neurol *32*, 183–190, doi:10.1097/WCO.0000000000000657.

Marini, C., Scheffer, I. E., Nabbout, R., Suls, A., De Jonghe, P., Zara, F. and Guerrini, R. (2011). The genetics of Dravet syndrome. Epilepsia *52*, 24–29, doi:10.1111/j.1528-1167.2011.02997.x.

Masiulis, S., Desai, R., Uchański, T., Serna Martin, I., Laverty, D., Karia, D., Malinauskas, T., Zivanov, J., Pardon, E., Kotecha, A., Steyaert, J., Miller, K. W. and Aricescu, A. R. (2019). GABAA receptor signalling mechanisms revealed by structural pharmacology. Nature *565*, 454–459, doi:10.1038/s41586-018-0832-5.

Masnada, S., Hedrich, U. B. S., Gardella, E., Schubert, J., Kaiwar, C., Klee, E. W., Lanpher, B. C., Gavrilova, R. H., Synofzik, M., Bast, T., Gorman, K., King, M. D., Allen, N. M., Conroy, J., Ben Zeev, B., Tzadok, M., Korff, C., Dubois, F., Ramsey, K., Narayanan, V., Serratosa, J. M., Giraldez, B. G., Helbig, I., Marsh, E., O'Brien, M., Bergqvist, C. A., Binelli, A., Porter, B., Zaeyen, E., Horovitz, D. D., Wolff, M., Marjanovic, D., Caglayan, H. S., Arslan, M., Pena, S. D. J., Sisodiya, S. M., Balestrini, S., Syrbe, S., Veggiotti, P., Lemke, J. R., Møller, R. S., Lerche, H. and Rubboli, G. (2017). Clinical spectrum and genotype–phenotype associations of KCNA2-related encephalopathies. Brain *140*, 2337–2354, doi:10.1093/brain/awx184.

Mattison, K. A., Butler, K. M., Inglis, G. A. S., Dayan, O., Boussidan, H., Bhambhani, V., Philbrook, B., da Silva, C., Alexander, J. J., Kanner, B. I. and Escayg, A. (2018). SLC6A1 variants identified in epilepsy patients reduce γ-aminobutyric acid transport. Epilepsia *59*, e135–e141, doi:10.1111/epi.14531.

May, P., Girard, S., Harrer, M., Bobbili, D. R., Schubert, J., Wolking, S., Becker, F., Lachance-Touchette, P., Meloche, C., Gravel, M., Niturad, C. E., Knaus, J., Kovel, C. D., Toliat, M., Polvi, A., Iacomino, M., Guerrero-Lopez, R., Baulac, S., Marini, C., Thiele, H., Altmuller, J., Jabbari, K., Ruppert, A.-K., Jurkowski, W., Lal, D., Rusconi, R., Cestele, S., Terragni, B., Coombs, I. D., Reid, C. A., Striano, P., Caglayan, H., Siren, A., Everett, K., Moller, R. S., Hjalgrim, H., Muhle, H., Helbig, I., Kunz, W. S., Weber, Y. G., Weckhuysen, S., Jonghe, P. D., Sisodiya, S. M., Nabbout, R., Franceschetti, S., Coppola, A., Vari, M. S., Trenite, D. K.-N., Baykan, B., Ozbek, U., Bebek, N., Klein, K. M., Rosenow, F., Nguyen, D. K., Dubeau, F., Carmant, L., Lortie, A., Desbiens, R., Clement, J.-F., Cieuta-Walti, C., Sills, G. J., Auce, P., Francis, B., Johnson, M. R., Marson, A. G., Berghuis, B., Sander, J. W., Avbersek, A., McCormack, M., Cavalleri, G. L., Delanty, N., Depondt, C., Krenn, M., Zimprich, F., Peter, S., Nikanorova, M., Kraaij, R., Rooij, J. van, Balling, R., Ikram, M. A., Uitterlinden, A. G., Avanzini, G., Schorge, S., Petrou, S., Mantegazza, M., Sander, T., LeGuern, E., Serratosa, J. M., Koeleman, B. P. C., Palotie, A., Lehesjoki, A.-E., Nothnagel, M., Nurnberg, P., Maljevic, S., Zara, F., Cossette, P., Krause, R. and Lerche, H. (2018). Rare coding variants in genes encoding GABAA receptors in genetic generalised epilepsies: an exome-based case-control study. Lancet Neurol *17*, 699–708, doi:10.1016/S1474-4422(18)30215-1.

McTague, A., Howell, K. B., Cross, J. H., Kurian, M. A. and Scheffer, I. E. (2016). The genetic landscape of the epileptic encephalopathies of infancy and childhood. Lancet Neurol *15*, 304–316, doi:10.1016/S1474-4422(15)00250-1.

Mefford, H. C. (2018). Expanding role of GABAA receptors in generalised epilepsies. Lancet Neurol *17*, 657–658, doi:10.1016/S1474-4422(18)30252-7.

Meira, I. D., Romao, T. T., Prado, H. J. P. do, Kruger, L. T., Pires, M. E. P. and Conceicao, P. O. da (2019). Ketogenic Diet and Epilepsy: What We Know So Far. Front Neurosci *13*, 5, doi:10.3389/fnins.2019.00005.

Miller, P. S. and Aricescu, A. R. (2014). Crystal structure of a human GABAA receptor. Nature *512*, 270–275, doi:10.1038/nature13293.

Minier, F. and Sigel, E. (2004). Techniques: Use of concatenated subunits for the study of ligand-gated ion channels. Trends Pharmacol Sci *25*, 499–503, doi:10.1016/j.tips.2004.07.005.

Möhler, H. (2006). GABAA Receptors in Central Nervous System Disease: Anxiety, Epilepsy, and Insomnia. J Recept Sig Transd *26*, 731–740, doi:10.1080/10799890600920035.

Møller, R. S., Wuttke, T. V., Helbig, I., Marini, C., Johannesen, K. M., Brilstra, E. H., Vaher, U., Borggraefe, I., Talvik, I., Talvik, T., Kluger, G., Francois, L. L., Lesca, G., de Bellescize, J., Blichfeldt, S., Chatron, N., Holert, N., Jacobs, J., Swinkels, M., Betzler, C., Syrbe, S., Nikanorova, M., Myers, C. T., Larsen, L. H. G., Vejzovic, S., Pendziwiat, M., von Spiczak, S., Hopkins, S., Dubbs, H., Mang, Y., Mukhin, K., Holthausen, H., van Gassen, K. L., Dahl, H. A., Tommerup, N., Mefford, H. C., Rubboli, G., Guerrini, R., Lemke, J. R., Lerche, H., Muhle, H. and Maljevic, S. (2017). Mutations in GABRB3: From febrile seizures to epileptic encephalopathies. Neurology *88*, 483–492, doi:10.1212/WNL.0000000000003565.

Mueller, A. L., Chesnut, R. M. and Schwartzkroin, P. A. (1983). Actions of GABA in developing rabbit hippocampus: an in vitro study. Neurosci Lett *39*, 193–198, doi:10.1016/0304-3940(83)90076-9.

Mullen, S. A. and Scheffer, I. E. (2009). Translational Research in Epilepsy Genetics: Sodium Channels in Man to Interneuronopathy in Mouse. Arch Neurol *66*, doi:10.1001/archneurol.2008.559.

NCBI Nucleotide Database (2019). *Homo sapiens gamma-aminobutyric acid type A receptor beta1 subunit (GABRB1), mRNA*, URL: http://www.ncbi.nlm.nih.gov/nuccore/NM_000812.3 [Accessed April 2023].

Nemecz, Á., Prevost, M. S., Menny, A. and Corringer, P.-J. (2016). Emerging Molecular Mechanisms of Signal Transduction in Pentameric Ligand-Gated Ion Channels. Neuron *90*, 452–470, doi:10.1016/j.neuron.2016.03.032.

Niturad, C. E. (2016). *GABAergic mechanisms in epilepsy and contribution of the ClC-2 chloride channel to neuronal excitability*. Dissertation zur Erlangung des Grades eines Doktors der Naturwissenschaften, Eberhard Karls Universität Tübingen.

Niturad, C. E., Lev, D., Kalscheuer, V. M., Charzewska, A., Schubert, J., Lerman-Sagie, T., Kroes, H. Y., Oegema, R., Traverso, M., Specchio, N., Lassota, M., Chelly, J., Bennett-Back, O., Carmi, N., Koffler-Brill, T., Iacomino, M., Trivisano, M., Capovilla, G., Striano, P., Nawara, M., Rzonca, S., Fischer, U., Bienek, M., Jensen, C., Hu, H., Thiele, H., Altmuller, J., Krause, R., May, P., Becker, F., Balling, R., Biskup, S., Haas, S. A., Nurnberg, P., Gassen, K. L. I. van, Lerche, H., Zara, F., Maljevic, S. and Leshinsky-Silver, E. (2017). Rare GABRA3 variants are associated with epileptic seizures, encephalopathy and dysmorphic features. Brain *140*, 2879–2894, doi:10.1093/brain/awx236.

Olsen, R. W. and Sieghart, W. (2008). International Union of Pharmacology. LXX. Subtypes of γ-Aminobutyric AcidA Receptors: Classification on the Basis of Subunit Composition, Pharmacology, and Function. Update. Pharmacol Rev *60*, 243–260, doi:10.1124/pr.108.00505.

OriGene (2020). 2020 GABA A Receptor beta 1 (GABRB1) (NM_000812) Human Tagged ORF Clone – RC205166 | OriGene, , URL: https://www.origene.com/catalog/cdna-clones/expression-plasmids/rc205166/gaba-a-receptor-beta-1-gabrb1-nm_000812-human-tagged-orf-clone [Accessed April 2023].

Orsini, A., Zara, F. and Striano, P. (2018). Recent advances in epilepsy genetics. Neurosci Lett *667*, 4–9, doi:10.1016/j.neulet.2017.05.014.

Oyrer, J., Maljevic, S., Scheffer, I. E., Berkovic, S. F., Petrou, S. and Reid, C. A. (2018). Ion Channels in Genetic Epilepsy: From Genes and Mechanisms to Disease-Targeted Therapies. Pharmacol Rev *70*, 142–173, doi:10.1124/pr.117.014456.

Papandreou, A., McTague, A., Trump, N., Ambegaonkar, G., Ngoh, A., Meyer, E., Scott, R. H. and Kurian, M. A. (2016). GABRB3 mutations: a new and emerging cause of early infantile epileptic encephalopathy. Dev Med Child Neurol *58*, 416–420, doi:10.1111/dmcn.12976.

Parrini, E., Marini, C., Mei, D., Galuppi, A., Cellini, E., Pucatti, D., Chiti, L., Rutigliano, D., Bianchini, C., Virdò, S., De Vita, D., Bigoni, S., Barba, C., Mari, F., Montomoli, M., Pisano, T., Rosati, A., Clinical Study Group and Guerrini, R. (2017). Diagnostic Targeted Resequencing in 349 Patients with Drug-Resistant Pediatric Epilepsies Identifies Causative Mutations in 30 Different Genes. Hum Mutat *38*, 216–225, doi:10.1002/humu.23149.

Pavlov, I. and Walker, M. C. (2013). Tonic GABA(A) receptor-mediated signalling in temporal lobe epilepsy. Neuropharmacology *69*, 55–61, doi:10.1016/j.neuropharm.2012.04.003.

Pettersen, E. F., Goddard, T. D., Huang, C. C., Meng, E. C., Couch, G. S., Croll, T. I., Morris, J. H. and Ferrin, T. E. (2021). UCSF ChimeraX: Structure visualization for researchers, educators, and developers. Protein Sci *30*, 70–82, doi:10.1002/pro.3943.

Phulera, S., Zhu, H., Yu, J., Claxton, D. P., Yoder, N., Yoshioka, C. and Gouaux, E. (2018). Cryo-EM structure of the benzodiazepine-sensitive α1β1γ2S tri-heteromeric GABAA receptor in complex with GABA. Elife *7*, e39383, doi:10.7554/eLife.39383.

Reid, C. A., Kim, T., Phillips, A. M., Low, J., Berkovic, S. F., Luscher, B. and Petrou, S. (2013). Multiple molecular mechanisms for a single GABAA mutation in epilepsy. Neurology *80*, 1003–1008, doi:10.1212/WNL.0b013e3182872867.

Rentzsch, P., Witten, D., Cooper, G. M., Shendure, J. and Kircher, M. (2019). CADD: predicting the deleteriousness of variants throughout the human genome. Nucleic Acids Res *47*, D886–D894, doi:10.1093/nar/gky1016.

Represa, A. and Ben-Ari, Y. (2005). Trophic actions of GABA on neuronal development. Trends Neurosci *28*, 278–283, doi:10.1016/j.tins.2005.03.010.

Reyes-Nava, N. G., Yu, H.-C., Coughlin, C. R., II, Shaikh, T. H. and Quintana, A. M. (2020). Abnormal expression of GABAA receptor subunits and hypomotility upon loss of gabra1 in zebrafish. Biol Open *9*, bio051367, doi:10.1242/bio.051367.

Richards, S., Aziz, N., Bale, S., and others (2015). Standards and guidelines for the interpretation of sequence variants: a joint consensus recommendation of the American College of Medical Genetics and Genomics and the Association for Molecular Pathology. Genet Med *17*, 405–423, doi:https://doi.org/10.1038/gim.2015.30.

Safdar, A. and Ismail, F. (2023). A comprehensive review on pharmacological applications and drug-induced toxicity of valproic acid. Saudi Pharm J *31*, 265–278, doi:10.1016/j.jsps.2022.12.001.

Saitsu, H., Kato, M., Mizuguchi, T., Hamada, K., Osaka, H., Tohyama, J., Uruno, K., Kumada, S., Nishiyama, K., Nishimura, A., Okada, I., Yoshimura, Y., Hirai, S., Kumada, T., Hayasaka, K., Fukuda, A., Ogata, K. and Matsumoto, N. (2008). De novo mutations in the gene encoding STXBP1 (MUNC18-1) cause early infantile epileptic encephalopathy. Nat Genet *40*, 782–788, doi:10.1038/ng.150.

Sallard, E., Letourneur, D. and Legendre, P. (2021). Electrophysiology of ionotropic GABA receptors. Cell Mol Life Sci *78*, 5341–5370, doi:10.1007/s00018-021-03846-2.

Samocha, K. E., Kosmicki, J. A., Karczewski, K. J., O'Donnell-Luria, A. H., Pierce-Hoffman, E., MacArthur, D. G., Neale, B. M. and Daly, M. J. (2017). Regional missense constraint improves variant deleteriousness prediction. bioRxiv 148353, doi:10.1101/148353.

Scheffer, I. E., Berkovic, S., Capovilla, G., Connolly, M. B., French, J., Guilhoto, L., Hirsch, E., Jain, S., Mathern, G. W., Moshe, S. L., Nordli, D. R., Perucca, E., Tomson, T., Wiebe, S., Zhang, Y.-H. and Zuberi, S. M. (2017). ILAE classification of the epilepsies: Position paper of the ILAE Commission for Classification and Terminology. Epilepsia *58*, 512–521, doi:10.1111/epi.13709.

Scheuber, P. S. (2023). *Elektrophysiologische Charakterisierung Epilepsie-assoziierter Defekte im GABRA3 Gen*. Dissertation zur Erlangung des Doktorgrades der Medizin, Eberhard Karls Universität Tübingen.

Sequeira, A., Shen, K., Gottlieb, A. and Limon, A. (2019). Human brain transcriptome analysis finds region- and subject-specific expression signatures of GABAAR subunits. Commun Biol *2*, 153, doi:10.1038/s42003-019-0413-7.

Shu, H.-J., Bracamontes, J., Taylor, A., Wu, K., Eaton, M. M., Akk, G., Manion, B., Evers, A. S., Krishnan, K., Covey, D. F., Zorumski, C. F., Steinbach, J. H. and Mennerick, S. (2012). Characteristics of concatemeric GABAA receptors containing α4/δ subunits expressed in Xenopus oocytes. Br J Pharmacol *165*, 2228–2243, doi:10.1111/j.1476-5381.2011.01690.x.

Sieghart, W. (1995). Structure and pharmacology of gamma-aminobutyric acidA receptor subtypes. Pharmacol Rev *47*, 181–234.

Sigel, E., Baur, R., Malherbe, P. and Möhler, H. (1989). The rat β1 -subunit of the GABAA receptor forms a picrotoxin-sensitive anion channel open in the absence of GABA. FEBS Letters *257*, 377–379, doi:10.1016/0014-5793(89)81576-5.

Sigel, E., Kaur, K. H., Lüscher, B. P. and Baur, R. (2009). Use of concatamers to study GABAA receptor architecture and function: application to δ-subunit-containing receptors and possible pitfalls. Biochem Soc T *37*, 1338–1342, doi:10.1042/BST0371338.

Sigel, E. and Steinmann, M. E. (2012). Structure, Function, and Modulation of GABAA Receptors*. Journal of Biological Chemistry *287*, 40224–40231, doi:10.1074/jbc.R112.386664.

Simeone, X., Siebert, D. C. B., Bampali, K., Varagic, Z., Treven, M., Rehman, S., Pyszkowski, J., Holzinger, R., Steudle, F., Scholze, P., Mihovilovic, M. D., Schnürch, M. and Ernst, M. (2017). Molecular tools for GABAA receptors: High affinity ligands for β1-containing subtypes. Sci Rep *7*, 5674, doi:10.1038/s41598-017-05757-4.

Singh, D., Gupta, S., Verma, I., Morsy, M. A., Nair, A. B. and Ahmed, A.-S. F. (2021). Hidden pharmacological activities of valproic acid: A new insight. Biomed Pharmacother *142*, 112021, doi:10.1016/j.biopha.2021.112021.

Singh, N. A., Charlier, C., Stauffer, D., DuPont, B. R., Leach, R. J., Melis, R., Ronen, G. M., Bjerre, I., Quattlebaum, T., Murphy, J. V., McHarg, M. L., Gagnon, D., Rosales, T. O., Peiffer, A., Anderson, V. E. and Leppert, M. (1998). A novel potassium channel gene, KCNQ2, is mutated in an inherited epilepsy of newborns. Nat Genet *18*, 25–29, doi:10.1038/ng0198-25.

Song, I., Savtchenko, L. and Semyanov, A. (2011). Tonic excitation or inhibition is set by GABA(A) conductance in hippocampal interneurons. Nat Commun *2*, 376, doi:10.1038/ncomms1377.

Stiles, J. and Jernigan, T. L. (2010). The Basics of Brain Development. Neuropsychol Rev *20*, 327–348, doi:10.1007/s11065-010-9148-4.

Suls, A., Jaehn, J. A., Kecskés, A., Weber, Y., Weckhuysen, S., Craiu, D. C., Siekierska, A., Djémié, T., Afrikanova, T., Gormley, P., von Spiczak, S., Kluger, G., Iliescu, C. M., Talvik, T., Talvik, I., Meral, C., Caglayan, H. S., Giraldez, B. G., Serratosa, J., Lemke, J. R., Hoffman-Zacharska, D., Szczepanik, E., Barisic, N., Komarek, V., Hjalgrim, H., Møller, R. S., Linnankivi, T., Dimova, P., Striano, P., Zara, F., Marini, C., Guerrini, R., Depienne, C., Baulac, S., Kuhlenbäumer, G., Crawford, A. D., Lehesjoki, A.-E., de Witte, P. A. M., Palotie, A., Lerche, H., Esguerra, C. V., De Jonghe, P., Helbig, I., Hendrickx, R., Holmgren, P., Stephani, U., Muhle, H., Pendiziwiat, M., Appenzeller, S., Selmer, K., Brilstra, E., Koeleman, B., Rosenow, F., Leguern, E., Sterbova, K., Magdalena, B., Rodica, G., Arsene, O. T., Diana, B., Guerrero-Lopez, R., Ortega, L., Todorova, A. P., Kirov, A. V., Robbiano, A., Arslan, M., Yiş, U. and Ivanović, V. (2013). De Novo Loss-of-Function Mutations in CHD2 Cause a Fever-Sensitive Myoclonic Epileptic Encephalopathy Sharing Features with Dravet Syndrome. The American Journal of Human Genetics *93*, 967–975, doi:10.1016/j.ajhg.2013.09.017.

Syrbe, S., Hedrich, U. B. S., Riesch, E., Djémié, T., Müller, S., Møller, R. S., Maher, B., Hernandez-Hernandez, L., Synofzik, M., Caglayan, H. S., Arslan, M., Serratosa, J. M., Nothnagel, M., May, P., Krause, R., Löffler, H., Detert, K., Dorn, T., Vogt, H., Krämer, G., Schöls, L., Mullis, P. E., Linnankivi, T., Lehesjoki, A.-E., Sterbova, K., Craiu, D. C., Hoffman-Zacharska, D., Korff, C. M., Weber, Y. G., Steinlin, M., Gallati, S., Bertsche, A., Bernhard, M. K., Merkenschlager, A., Kiess, W., Gonzalez, M., Züchner, S., Palotie, A., Suls, A., De Jonghe, P., Helbig, I., Biskup, S., Wolff, M., Maljevic, S., Schüle, R., Sisodiya, S. M., Weckhuysen, S., Lerche, H. and Lemke, J. R. (2015). De novo loss- or gain-of-function mutations in KCNA2 cause epileptic encephalopathy. Nat Genet *47*, 393–399, doi:10.1038/ng.3239.

Taliun, D., Harris, D. N., Kessler, M. D., Carlson, J., Szpiech, Z. A., Torres, R., Taliun, S. A. G., Corvelo, A., Gogarten, S. M., Kang, H. M., Pitsillides, A. N., LeFaive, J., Lee, S., Tian, X., Browning, B. L., Das, S., Emde, A.-K., Clarke, W. E., Loesch, D. P., Shetty, A. C., Blackwell, T. W., Smith, A. V., Wong, Q., Liu, X., Conomos, M. P., Bobo, D. M., Aguet, F., Albert, C., Alonso, A., Ardlie, K. G., Arking, D. E., Aslibekyan, S., Auer, P. L., Barnard, J., Barr, R. G., Barwick, L., Becker, L. C., Beer, R. L., Benjamin, E. J., Bielak, L. F., Blangero, J., Boehnke, M., Bowden, D. W., Brody, J. A., Burchard, E. G., Cade, B. E., Casella, J. F., Chalazan, B., Chasman, D. I., Chen, Y.-D. I., Cho, M. H., Choi, S. H., Chung, M. K., Clish, C. B., Correa, A., Curran, J. E., Custer, B., Darbar, D., Daya, M., de Andrade, M., DeMeo, D. L., Dutcher, S. K., Ellinor, P. T., Emery, L. S., Eng, C., Fatkin, D., Fingerlin, T., Forer, L., Fornage, M., Franceschini, N., Fuchsberger, C., Fullerton, S. M., Germer, S., Gladwin, M. T., Gottlieb, D. J., Guo, X., Hall, M. E., He, J., Heard-Costa, N. L., Heckbert, S. R.,

Irvin, M. R., Johnsen, J. M., Johnson, A. D., Kaplan, R., Kardia, S. L. R., Kelly, T., Kelly, S., Kenny, E. E., Kiel, D. P., Klemmer, R., Konkle, B. A., Kooperberg, C., Köttgen, A., Lange, L. A., Lasky-Su, J., Levy, D., Lin, X., Lin, K.-H., Liu, C., Loos, R. J. F., Garman, L., Gerszten, R., Lubitz, S. A., Lunetta, K. L., Mak, A. C. Y., Manichaikul, A., Manning, A. K., Mathias, R. A., McManus, D. D., McGarvey, S. T., Meigs, J. B., Meyers, D. A., Mikulla, J. L., Minear, M. A., Mitchell, B. D., Mohanty, S., Montasser, M. E., Montgomery, C., Morrison, A. C., Murabito, J. M., Natale, A., Natarajan, P., Nelson, S. C., North, K. E., O'Connell, J. R., Palmer, N. D., Pankratz, N., Peloso, G. M., Peyser, P. A., Pleiness, J., Post, W. S., Psaty, B. M., Rao, D. C., Redline, S., Reiner, A. P., Roden, D., Rotter, J. I., Ruczinski, I., Sarnowski, C., Schoenherr, S., Schwartz, D. A., Seo, J.-S., Seshadri, S., Sheehan, V. A., Sheu, W. H., Shoemaker, M. B., Smith, N. L., Smith, J. A., Sotoodehnia, N., Stilp, A. M., Tang, W., Taylor, K. D., Telen, M., Thornton, T. A., Tracy, R. P., Van Den Berg, D. J., Vasan, R. S., Viaud-Martinez, K. A., Vrieze, S., Weeks, D. E., Weir, B. S., Weiss, S. T., Weng, L.-C., Willer, C. J., Zhang, Y., Zhao, X., Arnett, D. K., Ashley-Koch, A. E., Barnes, K. C., Boerwinkle, E., Gabriel, S., Gibbs, R., Rice, K. M., Rich, S. S., Silverman, E. K., Qasba, P., Gan, W., Papanicolaou, G. J., Nickerson, D. A., Browning, S. R., Zody, M. C., Zöllner, S., Wilson, J. G., Cupples, L. A., Laurie, C. C., Jaquish, C. E., Hernandez, R. D., O'Connor, T. D. and Abecasis, G. R. (2021). Sequencing of 53,831 diverse genomes from the NHLBI TOPMed Program. Nature *590*, 290–299, doi:10.1038/s41586-021-03205-y.

Tanaka, M., Olsen, R. W., Medina, M. T., Schwartz, E., Alonso, M. E., Duron, R. M., Castro-Ortega, R., Martinez-Juarez, I. E., Pascual-Castroviejo, I., Machado-Salas, J., Silva, R., Bailey, J. N., Bai, D., Ochoa, A., Jara-Prado, A., Pineda, G., Macdonald, R. L. and Delgado-Escueta, A. V. (2008). Hyperglycosylation and reduced GABA currents of mutated GABRB3 polypeptide in remitting childhood absence epilepsy. Am J Hum Genet *82*, 1249–1261, doi:10.1016/j.ajhg.2008.04.020.

The UniProt Consortium (2019). UniProt: a worldwide hub of protein knowledge. Nucleic Acids Res *47*, D506–D515, doi:10.1093/nar/gky1049.

Traynelis, J., Silk, M., Wang, Q., Berkovic, S., Liu, L., Ascher, D., ... and Petrovski, S. (2017). Optimizing genomic medicine in epilepsy through a gene-customized approach to missense variant interpretation. Genome Res *27*, 1715–1729, doi:https://doi.org/10.1101/gr.226589.117.

Tremblay, R., Lee, S. and Rudy, B. (2016). GABAergic Interneurons in the Neocortex: From Cellular Properties to Circuits. Neuron *91*, 260–292, doi:10.1016/j.neuron.2016.06.033.

Ueno, S., Lin, A., Nikolaeva, N., Trudell, J. R., Mihic, S. J., Harris, R. A. and Harrison, N. L. (2000). Tryptophan scanning mutagenesis in TM2 of the GABAA receptor α subunit: effects on channel gating and regulation by ethanol. Br J Pharmacol *131*, 296–302, doi:10.1038/sj.bjp.0703504.

van Dyck, L. I. and Morrow, E. M. (2017). Genetic control of postnatal human brain growth. Curr Opin Neurol *30*, 114–124, doi:10.1097/WCO.0000000000000405.

Venkatachalan, S. P. and Czajkowski, C. (2012). Structural Link between γ-Aminobutyric Acid Type A (GABAA) Receptor Agonist Binding Site and Inner β-Sheet Governs Channel Activation and Allosteric Drug Modulation. J Biol Chem *287*, 6714–6724, doi:10.1074/jbc.M111.316836.

Vogel, F. D., Krenn, M., Westphal, D. S., Graf, E., Wagner, M., Leiz, S., Koniuszewski, F., Augé-Stock, M., Kramer, G., Scholze, P. and Ernst, M. (2022). A de novo missense variant in GABRA4 alters receptor function in an epileptic and neurodevelopmental phenotype. Epilepsia *63*, e35–e41, doi:10.1111/epi.17188.

Wallace, R. H., Marini, C., Petrou, S., Harkin, L. A., Bowser, D. N., Panchal, R. G., Williams, D. A., Sutherland, G. R., Mulley, J. C., Scheffer, I. E. and Berkovic, S. F. (2001). Mutant GABAA receptor γ2-subunit in childhood absence epilepsy and febrile seizures. Nat Genet *28*, 49–52, doi:10.1038/ng0501-49.

Warner, T. A., Shen, W., Huang, X., Liu, Z., Macdonald, R. L. and Kang, J.-Q. (2016). Differential molecular and behavioural alterations in mouse models of GABRG2 haploinsufficiency versus dominant negative mutations associated with human epilepsy. Hum Mol Genet *25*, 3192–3207, doi:10.1093/hmg/ddw168.

Wei, F., Yan, L.-M., Su, T., He, N., Lin, Z.-J., Wang, J., Shi, Y.-W., Yi, Y.-H. and Liao, W.-P. (2017). Ion Channel Genes and Epilepsy: Functional Alteration, Pathogenic Potential, and Mechanism of Epilepsy. Neurosci Bull *33*, 455–477, doi:10.1007/s12264-017-0134-1.

Williams, A., Cooney, E., Segal, G., Narayanan, S., Morand, M. and Agadi, S. (2022). GABRG1 variant as a potential novel cause of epileptic encephalopathy, hypotonia, and global developmental delay. Am J Med Genet A *188*, 3546–3549, doi:10.1002/ajmg.a.62969.

Yang, Y., Niu, X., Cheng, M., Zeng, Q., Deng, J., Tian, X., Wang, Y., Yu, J., Shi, W., Wu, W., Ma, J., Li, Y., Yang, X., Zhang, X., Jia, T., Yang, Z., Liao, J., Sun, Y., Zheng, H., Sun, S., Sun, D., Jiang, Y. and Zhang, Y. (2022). Phenotypic Spectrum and Prognosis of Epilepsy Patients With GABRG2 Variants. Front Mol Neurosci *15:809163*, doi:10.3389/fnmol.2022.809163.

Yang, Y., Xiangwei, W., Zhang, X., Xiao, J., Chen, J., Yang, X., Jia, T., Yang, Z., Jiang, Y. and Zhang, Y. (2020). Phenotypic spectrum of patients with GABRB2 variants: from mild febrile seizures to severe epileptic encephalopathy. Dev Med Child Neurol *62*, 1213–1220, doi:10.1111/dmcn.14614.

Zhang, L. and Liu, X. (2022). Clinical phenotype and genotype of children with GABAA receptor α1 subunit gene-related epilepsy. Front Neurol *13:941054*, doi:10.3389/fneur.2022.941054.

Zheng, Z., Xue, F., Wang, H., He, Y., Zhang, L., Ma, W., Zhang, C., Guan, Y., Ye, F., Wen, Y., Li, X., Huang, M., Huang, W., Wang, Z. and Li, J. (2022). A single nucleotide polymorphism-based formula to predict the risk of propofol TCI concentration being over 4 μg mL−1 at the time of loss of consciousness. Pharmacogenomics J *22*, 109–116, doi:10.1038/s41397-021-00263-3.

Zhu, S., Noviello, C. M., Teng, J., Walsh, R. M., Kim, J. J. and Hibbs, R. E. (2018). Structure of a human synaptic GABAA receptor. Nature *559*, 67–72, doi:10.1038/s41586-018-0255-3.

8 Declaration of Authorship

Deutsch:

Die Arbeit wurde am Zentrum für Neurologie/Hertie-Institut für klinische Hirnforschung in der Abteilung Neurologie mit Schwerpunkt Epileptologie unter Betreuung von Prof. Dr. med. Holger Lerche, Dr. rer. nat. Ulrike Hedrich-Klimosch und Dr. rer. nat. Mahmoud Koko Musa durchgeführt.

Die Konzeption der Studie erfolgte in Zusammenarbeit mit Prof. Dr. med. Holger Lerche, Dr. rer. nat. Ulrike Hedrich-Klimosch und Dr. rer. nat. Mahmoud Koko Musa.

Sämtliche Versuche wurden nach Einarbeitung durch die Labormitglieder Dr. rer. nat. Ulrike Hedrich-Klimosch und Dr. rer. nat. Mahmoud Koko Musa von mir eigenständig durchgeführt. Die bioinformatischen Analysen und strukturelle Modellierung wurden zusammen mit Dr. rer. nat. Mahmoud Koko Musa durchgeführt.

Die statistische Auswertung erfolgte nach Beratung durch Dr. rer. nat. Ulrike Hedrich-Klimosch, Dr. rer. nat. Mahmoud Koko Musa und Emilio Pardo Gonzalez durch mich.

Ich versichere, das Manuskript selbständig verfasst zu haben und keine weiteren als die von mir angegebenen Quellen verwendet zu haben.

English:

The work was performed at the Center of Neurology/Hertie Institute for Clinical Brain Research in the Department of Neurology and Epileptology under the supervision of Prof. Dr. med. Holger Lerche, Dr. rer. nat. Ulrike Hedrich-Klimosch and Dr. rer. nat. Mahmoud Koko Musa.

The study was designed in collaboration with Prof. Dr. med. Holger Lerche, Dr. rer. nat. Ulrike Hedrich-Klimosch and Dr. rer. nat. Mahmoud Koko Musa.

All experiments were performed independently by me after training by the laboratory members Dr. rer. nat. Ulrike Hedrich-Klimosch and Dr. rer. nat. Mahmoud Koko Musa. The bioinformatic analyses and structural modeling were performed together with Dr. rer. nat. Mahmoud Koko Musa.

I performed statistical analysis after consultation with Dr. rer. nat. Ulrike Hedrich-Klimosch, Dr. rer. nat. Mahmoud Koko Musa and Emilio Pardo Gonzalez.

I certify that I have written the manuscript independently and have not used any sources other than those I indicated.

Washington, D.C., den 18.01.2025

Moritz Sebastian Hanke

9 Acknowledgments

First and foremost, I would like to thank Prof. Holger Lerche for providing the exciting opportunity for me to pursue my thesis at his Lab at the Dept. for Neurology and Epileptology.

I would also like to thank Dr. Ulrike Hedrich-Klimosch for using her experience to provide kind guidance throughout the project.

Additionally, I would like to thank Ana Fulgencio Maisch, Betül Uysal, Carolin Fischer, Filip Rosa, Hannah Schwarz, Heidi Löffler, Johanna Krüger, Niklas Schwarz, Nikolas Layer, Simone Seiffert, and the rest of the Lerche Lab for providing a great and helpful research environment. I would also like to thank Emilio Pardo Gonzalez for being an epicenter of good mood and providing guidance on the statistical analysis, even after he left the Lab. Additionally, I'd like to thank Maryam Erfanian Omidvar for continuing this project.

I'd also like to thank all collaborators from around the world for providing data, knowledge, and resources for this project. I'd particularly like to thank Prof. Philip K. Ahring for spotting the two variants in the original construct – this was extremely crucial for the project.

I'd like to thank the IZKF Promotionskolleg (Medical Faculty, University of Tübingen) for providing funding and guidance. Also, I want to thank the Hertie Institute for Clinical Brain Research for an excellent research environment.

I would especially like to thank Pauline Scheuber for being an awesome Lab partner and becoming a close friend in the process. I am very grateful for that.

Most importantly, I would like to thank Mahmoud Koko Musa for everything – from showing me how to make an agarose gel to teaching me not to worry too much. Listing all of it here would take too long. You are a true hero and a legend.

Lastly, I would like to thank my friends, particularly Leon, Dominik, Laurenz, Joschka, Bjarne, and Tim, as well as my family – my Sister Franzi, my Mum Gabi, and my Dad Thomas – for continuously supporting me through the process and inoculating me with the perseverance required to complete this thesis.